ABSTRACT

Title of Document: MULTI-SCALE MECHANICAL CHARACTERIZATION AND MODELING OF HIERARCHICALLY-STRUCTURED MATERIALS: SYNTHETIC NANO-ENHANCED POLYMERS AND NATURAL PALMETTO WOOD

Alan Lawrence Gershon,
Doctor of Philosophy, 2009

Directed By: Professor Hugh A. Bruck,
Department of Mechanical Engineering

The development of hierarchical structure in synthetic materials is a new approach to enhancing multifunctional properties in a manner that is similar to natural materials. One means for achieving hierarchical structure is to add nanoscale ingredients to polymers that can either self-assemble in a “bottom-up” approach or can be added to polymer with microscale reinforcement through engineered-assembly in a “top-down” approach. In order to better understand synthetic hierarchical structures developed through the nano-enhancement of polymers and those occurring in natural materials, multi-scale characterization techniques and models are developed to elucidate the structure-property relationship due to hierarchical structure, and the control of

this relationship through processing in synthetic materials. A combinatorial approach is applied for rapid characterization of the processing-structure-property relationships that develop in nano-enhanced thermoplastic polymers associated with the hierarchical structure that forms from a combination of dispersed, agglomerated, and percolated nanoscale ingredients. A new approach to multi-scale mechanical characterization and modeling using microtensile testing and nanomechanical characterization of the mechanical properties for these hierarchically-structured materials is developed, as well as for the formation of hierarchical structures in epoxies and carbon fiber – epoxy composites through nano-enhancement. This characterization is used with Rule-of-Mixtures formulations to develop new multi-scale models that can predict macroscale properties from the hierarchical structure. Furthermore, it is possible to characterize the “degree of dispersion” in the hierarchical structure and the control of this structure through processing conditions such as sonication. The incorporation of melt annealing is also applied to hierarchically-structured thermoplastics in order to control properties through relaxation of fiber orientation in the microstructure. After establishing the multi-scale mechanical characterization approach, it is utilized to characterize and model the effects of nano-enhancement on curing kinetics in hierarchically-structured adhesives in order to understand the evolution of adhesion between the epoxy and nanoscale ingredient. In addition, this approach is exploited to characterize and model mechanical behavior in a naturally-occurring hierarchically-structured material, palmetto

wood. This knowledge serves as biological inspiration to guide further development of synthetic hierarchically-structured materials.

MULTI-SCALE MECHANICAL CHARACTERIZATION AND MODELING OF HIERARCHICALLY-STRUCTURED MATERIALS: SYNTHETIC NANO-ENHANCED POLYMERS AND NATURAL PALMETTO WOOD

By

Alan Lawrence Gershon

Dissertation submitted to the Faculty of the Graduate School of the
University of Maryland, College Park, in partial fulfillment
of the requirements for the degree of
Doctor of Philosophy
2009

Advisory Committee:
Dr. H.A. Bruck, Associate Professor of Mechanical Engineering, Chair
Dr. D.I. Bigio, Associate Professor of Mechanical Engineering
Dr. R.M. Briber, Professor and Chair of Materials Science & Engineering
Dr. A. Dasgupta, Professor of Mechanical Engineering
Dr. S.K. Gupta, Professor of Mechanical Engineering

Dedication

To the pursuit of knowledge and the preservation of imagination.

Imagination is more important than knowledge. For while knowledge defines all we currently know and understand, imagination points to all we might yet discover and create.

-Albert Einstein

Acknowledgements

First and foremost, I would like to express a deep gratitude and appreciation to Dr. Bruck for all of his guidance. Without his direction, encouragement and support through all my research efforts, this dissertation would not have been possible.

I am fortunate to have a very supportive family; without them I would not have been able to embark on this journey of scholarship – thank you Grandma, Savta, Mom, Dad, Eric, Alyssa, Mati, Maxi, Nim, Orli, Leeat, Sue, Robert, Anthony, Bill, Abbe, Debby, Maira, Shailee and Namir (I consider you all a part of my family).

I would also like to thank my colleagues Wojciech, Arun, Dan, Arvind, Nikolaos, Cardone and Cristallo for their assistance, suggestions and oft needed distractions both in and out of the lab.

In addition, I would like to thank the interns and undergraduate students that have helped me to complete myriad tasks and experiments. Thank you Shea, Christian, Mohammad, Marie and Dominik.

Finally, I would like to thank all of my friends who were always there to celebrate as well as commiserate with me throughout my academic career. You know who you are.

Table of Contents

List of Tables

List of Figures

List of Acronyms

ABS .....Acrylonitrile-butadiene-styrene
AFM .....Atomic Force Microscope or Atomic Force Microscopy
ASTM .....American Society for Testing and Materials
BAM .....Bridge Amplifier
CG .....Compositional Gradient
CMF .....Carbon Microfiber
CNC .....Computer Numerical Controlled
CNF .....Carbon Nanofiber
CNT .....Carbon Nanotube
DIC .....Digital Image Correlation
DMA .....Dynamic Mechanical Analysis
DSC .....Differential Scanning Calorimeter
FEA .....Finite Element Analysis
FFT .....Fast Fourier Transform
FRP .....Fiber Reinforced Polymer
GPa .....Gigapascal
HIPS .....High Impact Polystyrene
LDPE .....Low Density Polyethylene
MOR .....Modulus of Rupture
MPa .....Megapascal
MWCNT .....Multi-walled Carbon Nanotube
NASA .....National Aeronautics and Space Administration
PC .....Polycarbonate
PE .....Polyethylene
PEEK .....Polyetheretherketones
PEI .....Polyetherimide
PMMA .....Poly-(methyl methacrylate)
PP .....Polypropylene
PPS .....Polyphenylene sulfide
PS .....Polystyrene
PVA .....Poly(vinyl alcohol)
ROM .....Rule-of-Mixtures
RVD .....Residence Volume Distribution
SEM .....Scanning Electron Microscope or Scanning Electron Microscopy
SHPB .....Split Hopkinson Pressure Bar
SWNT .....Single-walled carbon nanotube
TA .....Thermal Analysis
TEM .....Transmission Electron Microscope or Transmission Electron Microscopy
TGA .....Thermogravimetric Analysis
TSE .....Twin Screw Extruder or Twin Screw Extrusion

Chapter 1 Introduction

1.1 Motivation for hierarchically-structured polymer composites

With the current focus on nanotechnology, it has become possible to engineer composite materials at the smallest length scales using nanostructured ingredients to control the distribution of properties and interaction of different material phases at the nanoscale [Berv05, Kuba06, Zhon04]. As a result, the development of advanced composite materials can now focus on the integration of various multi-scale ingredients in order to enhance the performance of these novel materials; see Figure 1.1. In this manner, certain properties of these composite materials, such as thermal conductivity and increased strength, can be tailored beyond the limitations of current microscale technology [Veed06]. Though it has now become possible to create hierarchically-structured polymer composites, it is increasingly necessary to determine how to process a wide variety of ingredients, such as polymers, Carbon Nanotubes (CNTs) Carbon Nanofibers (CNFs) and Carbon Microfibers (CMFs), to enhance many aspects of a material's performance – leading to multifunctional materials.

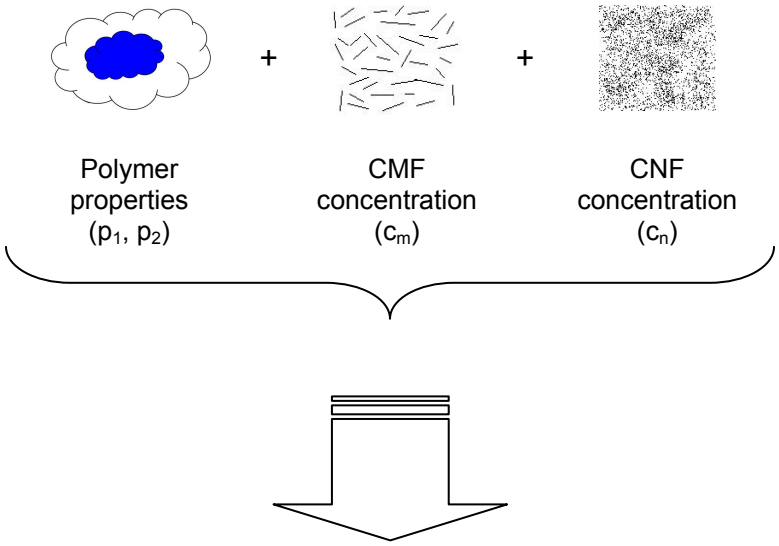

Figure 1.1. Processing diagram for multifunctional structures consisting of hierarchically-structured composites using a 'bottom-up' approach.

One critical question in the development of hierarchically-structured polymer composites involves the length scales and compositions at which the behavior of the composite material will transition and affect the performance of the structure. In nature, biological materials such as wood organize simple organic building blocks like collagen molecules at various length scales (i.e., hierarchical structure) to maximize the strength (MOR as high as 130 MPa), toughness (as high as 10 kJ), impact resistance (hammer drop heights of over 2 meters), and fatigue life (30 million cycles at 50% static strength) of these materials using the minimum amount of mass (ρ as low as 0.33 g/cc) [Gree99]. This balance of properties has made wood a valuable structural material in applications such as marine structures (i.e., ship hulls, masts, etc.). However, it has proven difficult to achieve similar balances in polymer composites made from

synthetic materials, such as fiberglass, with microscale glass fibers embedded in epoxy, where the chemical dissimilarities and microscale interfaces produce lower binding energies than biological counterparts resulting in lower impact resistance, strength, toughness, and fatigue life [Bruc02a]. Defining transition length scales and compositions will make it possible to understand how it is possible to overcome these limitations and yield mechanical properties similar or superior to biological counterparts through this "*bottom-up"* or *self-assembly* approach to creating hierarchically-structured materials.

Another method of creating hierarchically-structured materials involves the "*top-down"* or *engineered-assembly* of combining microscale and nanoscale ingredients with polymers to generate composite structures. In the top-down approach, materials with different length scales can also be integrated to create a hierarchical microstructure. For example, instead of mixing microscale and nanoscale ingredients as per Figure 1.1, pre-fabricated materials consisting of microscale and nanoscale ingredients are assembled. One of the simplest cases is to take microfiber polymer composite layers and join them using adhesives enhanced with nanofiber fillers (i.e., nano-enhanced adhesives) to form a hierarchically-structured polymer composite laminate. If the microfiber polymer composite layers are of different thicknesses or orientations, than a graded or multilayer length scale can be added to the hierarchical structure. Furthermore, it is possible to embed an electronic component, such as a polymer battery, to enhance multifunctionality while increasing the complexity of the hierarchical structure [Thom04, Thom06].

Understanding transition length scales and compositions will impact advanced numerical modeling tools being used in the design of hierarchically-structured polymer composites. The materials modeling community has demonstrated that it is possible to use complex numerical tools at each length scale to achieve hierarchically-structured "materials by design" with experimentally verified property enhancement, such as a twofold increase in strength, over conventional counterparts [Olso97]. However, these numerical tools require a variety of experimentally intensive data in order to understand the physics that is involved across the range of length scales. It has also been limited to designing metals, such as steel, and has not been as extensively developed for polymer composites where existing modeling techniques have focused on numerical micromechanics approaches, such as Self Consistent Schemes, Finite Element Analyses, and Generalized Method of Cells [Abou91]. Therefore, in order to extend these approaches to developing hierarchically-structured polymer composite "materials by design", it is necessary to experimentally characterize how physical properties of composites vary across length scales and compositions.

1.2 Research issues

To enhance the development of hierarchically-structured polymer composites, it is necessary to begin understanding transition length scales and compositions in hierarchically-structured polymer composites. Of particular interest is the failure resistance of the structure when subjected to mechanical

loading events, where certain critical distributions of nanoscale and microscale ingredients relative to the loading event may enhance resistance. Once characterized, these effects must be used to develop new models relating length scales and compositions to physical properties.

As previously mentioned, there are two basic approaches to creating hierarchically-structured polymer composites: *top-down* and *bottom-up*. The challenge has been to understand how these structures can be controlled in the case of bottom-up (e.g., dispersion effects), and in the case of top-down the challenge has been determining optimal polymer composite formulations and electronic components that are amenable to assembly at different length scales (e.g., effects of nano-fillers on adhesives and methods for integrating electronic components). Therefore, both approaches need to be investigated in more detail in order to develop fundamental processing-structure-property relationships that govern hierarchically-structured composites.

While there has been extensive dynamic and static testing of FRPs, there is not much data available on hierarchically-structured polymer composites that can elucidate on how different compositions respond to mechanical loading, and how to design the materials to enhance their mechanical properties [Hodg00, Sier01]. Therefore, fundamental experiments must be designed and conducted using model hierarchically-structured specimens that provide insight into the response to mechanical loading for both the “top down” and “bottom up” approaches. Through these experiments it is possible to elucidate on the property part of the processing-structure-property relationship and to understand

the impact on the multifunctional properties and/or performance associated with them. Furthermore, this work can be extended to the characterization and modeling of the structure-property relationship in biological materials with hierarchical structure which will lead to the design of biologically-inspired polymer composites using either the “top-down” or “bottom-up” approach.

1.2.1 Nanoscale constituents for enhancement of Fiber Reinforced Polymers (FRPs): *Top-down*

Fiber reinforced polymers are generally created through a process that impregnates a group of microscale fibers with a polymer. There are many ways to accomplish this, but all of the methods combine the two (or more) materials. This “top down” approach to creating a material is modified here to enhance the properties of conventional FRPs through the addition of a nanoscale constituent to the polymer that will be encapsulating the microscale fibers.

A fiber reinforced polymer is a composite material comprising a polymer matrix reinforced with fibers, which geometrically may be either continuous or short. Chemically, the fibers are usually E-glass, carbon, or aramid (Kevlar®); the polymer is usually an epoxy, vinylester or polyester thermosetting polymer or a thermoplastic like polypropylene (PP), Nylon, polyphenylene sulfide (PPS), polyetheretherketones (PEEK), polycarbonate (PC), and polyetherimide (PEI). FRPs are frequently used in the aerospace, automotive, marine, and construction industries [Jone98]. In many of these applications, the traditional Experimental Mechanics research interests have focused on characterizing and modeling the degradation of the composite properties due to exposure to hazardous

environmental elements (e.g., salt water), delamination due to weak interlaminar shear strength in laminated constructions, fiber-matrix debonding, and dynamic fracture/wave propagation [Bruc02b, Cost05, Kim03, Maso97, Whit93]. For example, osmotic pressure from swelling stresses due to non-uniform water uptake can induce a loss of load transfer in short fiber composites, the fiber-matrix interfacial strength can be enhanced by waviness or surface roughness of the fiber, the dynamic and static interlaminar shear stress can be reduced by reducing the difference in fiber angle between laminates, and the dynamic stress intensity factor will increase with time due to wave reflections and tunneling; see Figure 1.2 and Figure 1.3.

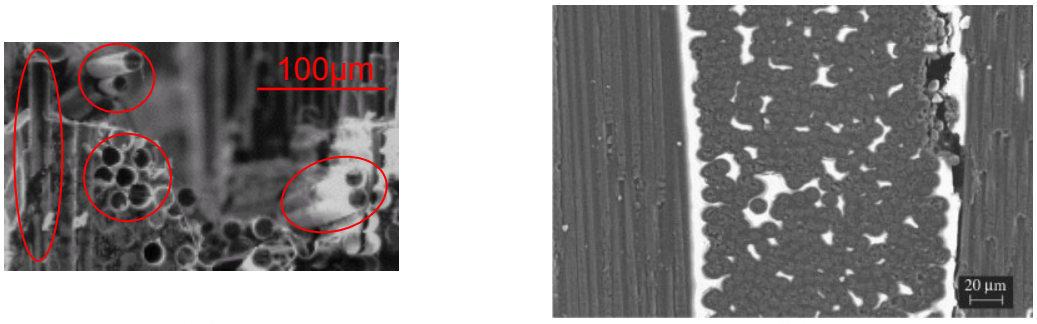

(a) (b)

Figure 1.2. (a) The regions circled in red depict fiber-matrix debonding [Kim03]. (b) Delamination at the interface of a wet carbon fiber/epoxy laminate (2.6% moisture content) [Cost05].

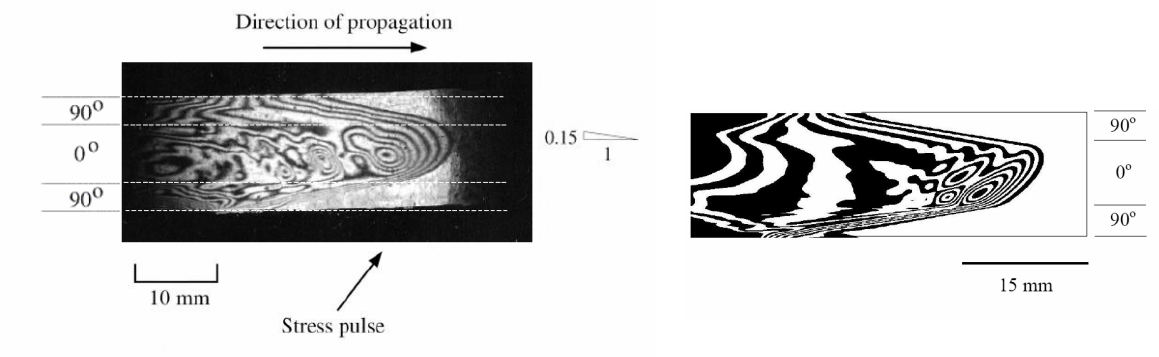

(a) (b)

Figure 1.3. (a) Dynamic Moiré fringe field from stress wave propagating in laminated microfiber-reinforced composite, (b) Numerical FEA prediction for non-planar impact. [Bruc02b]

1.2.2 Agglomeration, percolation, and dispersion in nano-enhanced polymers: *Bottom-up,*

Hierarchical structures can form from the bottom-up through the degree of interaction between nanoscale ingredients. When there is no interaction, the ingredients are considered *dispersed*. At a certain point, as the wt. % of a nanoscale ingredient is increased, a 3 dimensional interconnected network will also be formed in a sample with sufficient dispersion that is considered *percolated*. At this point, the nano-enhanced polymer material displays a significant change in certain properties such as electrical conductivity. If this percolation is not continuous throughout the material but is highly localized, then it is considered *agglomerated*. The formation of a hierarchical microstructure consisting of agglomerated, percolated, and dispersed nanoscale ingredients is an example of the “bottom up” method of creating a composite material with multifunctional properties, in this case electrical and mechanical. Both the degree of dispersion and concentration of nanoscale ingredients play a role in

the formation of the hierarchical structure, and the ability to control these parameters is of paramount importance for the proper growth of the hierarchical structure. With poor dispersion, the concentration at which a hierarchical structure forms will be higher, as can be seen in Figure 1.4.

At this plateau concentration, an interconnected network is formed that responds elastically over long timescales, *and* displays an increase in the electrical conductivity of the composite by ***20 orders of magnitude*** – nearly 1 S/m (Siemens per meter). [Kota07a, Kota07b]. The resulting nano-enhanced polymers have been characterized through electrical conductivity measurements and melt rheology. Using both melt rheology and electrical conductivity measurements, in conjunction with scanning electron microscopy (SEM) images, the presence of a continuous network of MWCNTs appears at particle concentrations exceeding 2 vol.% MWCNTs in PS.

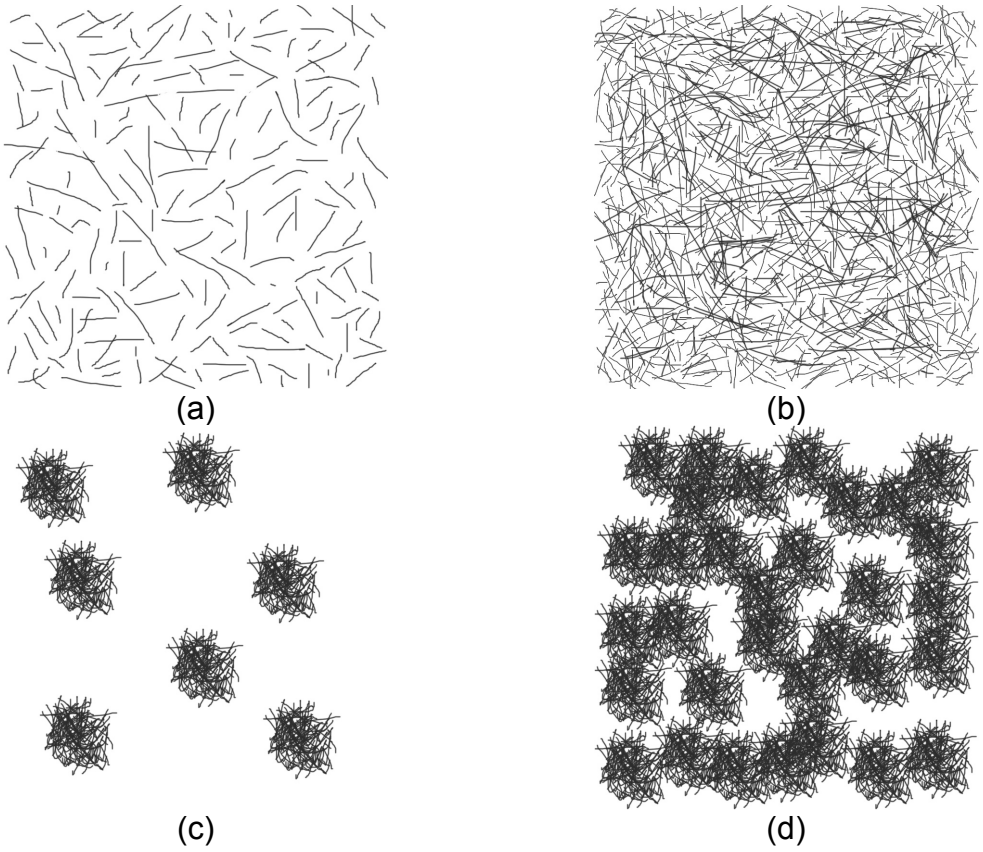

Figure 1.4. Representations of different distributions and concentrations of nanoscale ingredients in nano-enhanced polymers:
(a) Low concentration, good distribution – no interconnected network
(b) Medium concentration, good distribution – interconnected network
(c) Low concentration, poor distribution – no interconnected network
(d) High concentration, poor distribution – interconnected network

The amount of the continuous network present in the PS/MWCNT composite can be quantified by measuring electrical conductivity data at several concentrations of MWCNT, β. The change in electrical conductivity with concentration of MWCNTs has been associated with a proposed *degree of percolation*, $\overline{C}(\beta)$, developed using a conventional power-law formula with and without a percolation threshold. To predict the properties of these nano-enhanced polymers with continuous networks, the PS/MWCNT composite is treated as a combination of two distinct phases: the *continuous network phase*

consisting of a pseudo-solid like network of percolated MWCNTs, and a *continuous polymer phase reinforced by non-interacting MWCNTs*. The proposed degree of percolation is then used to quantify the distribution of MWCNTs in each phase, and is then used in a new Rule-of-Mixtures formulation for the storage modulus, $G'(\beta, \overline{C}(\beta), \omega)$, and the loss modulus, $G''(\beta, \overline{C}(\beta), \omega)$ seen in Figure 1.5, to predict the properties of the continuous phase consisting of percolated MWCNTs and the continuous reinforced polymer phase from the experimental melt rheology data. The properties of the continuous phase of percolated MWCNTs, seen in Figure 1.6, are indicative of a scaffold-like microstructure with an elastic behavior at lower frequencies and viscoplastic behavior at higher frequencies, most likely due to a stick-slip friction mechanism at the interface of the percolated MWCNTs.

Using a similar Rule-of-Mixtures modeling approach employing concepts related to the degree of dispersion that is employed for nano-enhanced thermoplastics, it will be possible to predict the effects of processing on the behavior of an epoxy based (thermoset) hierarchically-structured material. Furthermore, from a Rule-of-Mixtures perspective, the ability to conduct stress across the hierarchical structured formed by agglomerated, dispersed, and percolated nanostructures can substantially enhance mechanical properties in a linear sense (upper bound), as opposed to an inverse sense (lower bounds) associated with perfectly dispersed nanostructures. Also, a multi-scale modeling and characterization approach will be needed in order to understand the

processing-structure-property relationship that evolves in "bottom-up" hierarchically-structured materials.

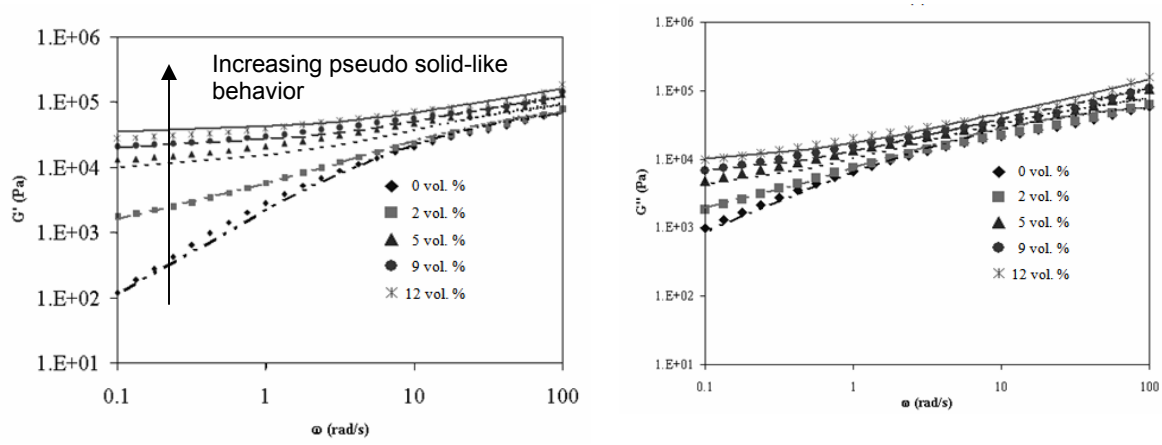

(a) (b)

Figure 1.5. Increasing pseudo solid-like behavior in (a) storage modulus, $G'(\beta, \overline{C}(\beta), \omega)$, and (b) loss modulus, $G''(\beta, \overline{C}(\beta), \omega)$, due to increasing degree of percolation, $\overline{C}(\beta)$, with increasing solids loading, β [Kota07b].

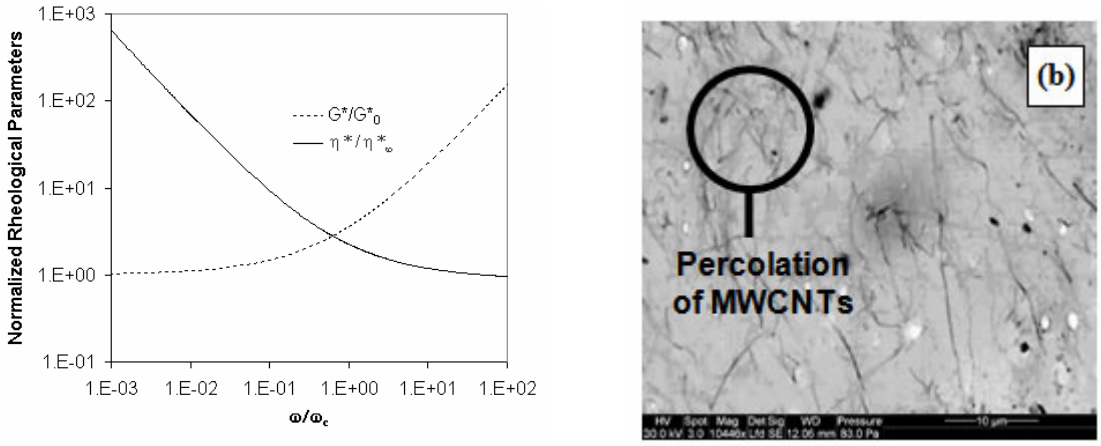

(a) (b)

Figure 1.6. (a) Normalized magnitude of rheological properties (complex modulus, G*, and complex viscosity, η*) associated with (b), the continuous phase formed by percolation of MWCNTs (SEM image) [Kota07b].

1.3 Research objectives

In order to address the research issues that have been discussed, the following has been investigated:

1.3.1 Processing of hierarchically-structured polymer composites

For this portion of the research effort, both a bottom-up and top-down approach will be pursued to understand processing-structure relationships in hierarchically-structured polymer composites. In the bottom-up approach, the following methods will be pursued:

1. Thermoplastics with CNFs mixed in twin screw and thermally-annealed
2. Thermoplastics with CNFs and CMFs mixed in solvent process
3. Thermosets with CNFs mixed in mechanically with ultrasonication
4. Thermosets with microfiber fillers and CNTs mixed in mechanically

For method 1, Polystyrene (PS) will be used as a model thermoplastic matrix material and then CNFs will be used to create the hierarchical structure in a combinatorial approach based on graded compositions obtained with the twin-screw extrusion mixing process. The hierarchical structure that is formed will be modified via thermal annealing after mixing. For method 2, PS will be dissolved in a solvent and then CNFs and CMFs added to create the hierarchical structure. For method 3, a thermoset adhesive, West system 105, will be investigated by mechanical mixing of CNFs into the adhesive with ultrasonic control over the hierarchical structure to form a nano-enhanced adhesive. For method 4, a

thermoset adhesive with microfibers, Hysol 9309.2, will have CNTs mechanically mixed in with ultrasonic and curing control over the hierarchical structure.

In the top-down approach, the PS with CNFs in the bottom-up approach will be used with pre-fabricated carbon microfiber layers to form the hierarchical structure. Alternatively, the nano-enhanced West system 105 adhesives will also be used to create a hierarchical microstructure.

1.3.2 Multi-scale characterization of hierarchically-structured polymer composites

After fabricating the hierarchically-structured polymer composites, the resulting structure-property relationships will be investigated at multiple length scale using various combinations of the following approaches:

1. Microtensile testing
2. Nanomechanical testing
3. Three point bend testing
4. Dynamic Mechanical Analysis
5. Quasi-static and dynamic compression

For 1, the focus will be on the small batch sizes and graded compositions associated with the solvent and combinatorial processing of the PS with CNFs, the West System 105 with CNFs, and the Hysol 9309.2 with CNTs in order to understand the effects of composition on the change in tensile properties associated with the hierarchical structure. For 2, the hierarchical structure will be probed in more detail for the PS with CNFs and the Hysol 9309.2 with CNTs in order to develop a “multi-scale” model of the structure-property relationship. For

3, the top-down hierarchically-structured polymer composites will be characterized in order to understand the effects of the structure on the failure mechanisms of the composites. For 4, DMA is used both at the nanoscale and macroscale with the Hysol 9309.2 with CNTs in order to characterizing curing effects on the hierarchical structure. For 5, the PS with CNFs and CMFs will be investigated to determine strain-rate effects on the response of the hierarchical structure. Finally, SEM and optical microscopy is extensively used to characterize the hierarchical structure in the polymer composites.

1.3.3 Natural hierarchically-structured materials

As a final objective of this dissertation, an enhanced understanding of hierarchical structure in natural materials is pursued as a basis for future development of "biologically inspired polymer composites". For this effort, the palmetto tree, the State Tree of South Carolina, is used as a model material. The palmetto tree has a historical basis for investigation since it was used during the Revolutionary and Civil wars as protection against cannon fire [Barb02]. The microtensile test is used to understand the mechanical response of individual microfibers in the hierarchical structure. Strain-rate sensitivity of failure mechanisms are characterized at the macroscale using three-point bend and Charpy impact testing. A prototype biologically-inspired hierarchically-structured polymer composite based on the knowledge obtained from the palmetto wood is fabricated using a top-down approach, and then tested to understand the

mechanical benefits that can be obtained using hierarchical-structure in synthetic materials.

1.4 Dissertation outline

In the following chapters of this dissertation, the methods used to address the above objectives and the results obtained will be presented focusing on hierarchical structures synthetically developed through the nano-enhancement of polymers and naturally occurring in palmetto wood. In particular, multi-scale characterization techniques and models are developed for understanding the structure-property relationship due to hierarchical structure, and the control of this relationship through processing in synthetic materials.

Chapter 2 contains a review of the state of the art for hierarchically-structured materials and nano-enhanced polymers. While providing a detailed review of the research conducted to understand processing-structure-property relationships, it also delineates the challenges in characterizing and modeling these relationships in various polymers. Chapter 3 describes the materials used in this work, their physical properties, as well as the experimental methods used to process and characterize the structure, microstructure, and properties of the hierarchically-structured nano-enhanced polymers. Chapter 4 describes a combinatorial approach for rapidly characterizing processing-structure-property relationships that develop in nano-enhanced thermoplastic polymers with hierarchical structures. Chapter 5 presents and discusses in detail a new approach to multi-scale mechanical characterization and modeling using

microtensile testing and nanomechanical characterization of the mechanical properties for these hierarchically-structured materials, as well as the development of hierarchical structures in epoxies and carbon fiber - epoxy composites through nano-enhancement. Chapter 6 expresses the insights achieved by the incorporation of melt annealing in controlling the properties of these hierarchically-structured materials through relaxation of fiber orientation in the microstructure.

After establishing the multi-scale mechanical characterization approach, Chapter 7 considers the application of this approach to understanding the effects of nano-enhancement on curing kinetics in hierarchically-structured adhesives. Chapter 8 further investigates the application of this approach to understanding and modeling mechanical behavior in a naturally-occurring hierarchically-structured material, palmetto wood. This understanding can serve as biological inspiration to guide further development of the synthetic hierarchically-structured materials in this dissertation. Finally, Chapter 9 summarizes the scientific and technical contributions of this work and presents the research issues that have potential for future investigation.

Chapter 2 Related work

Limited work has been conducted on the processing-structure-property relationship in hierarchically-structured materials. A great deal more work has been conducted on the nano-enhancement of polymers (i.e., polymer nano-enhanced polymers), that serves as a basis for creating hierarchical structure in polymers. Therefore, this chapter will first review processes for creating nano-enhanced polymers - in particular melt mixing and solvent processing - that can be used to create hierarchically-structured polymers. Then, a discussion of hierarchical structure that occur naturally and that have been attempted synthetically using nano-enhanced polymers will be discussed. Finally, attempts to control multifunctional properties of nano-enhanced polymers are reviewed. In each of these reviews, research challenges will be identified that this dissertation will address.

2.1 Melt mixing of nano-enhanced polymers

Melt mixing of thermoplastic polymers with CNTs/CNFs using conventional processing techniques such as extrusion compounding is particularly attractive due to its speed and the accessibility of this process in the plastics industry. Even so, there is still much to learn about the ability of CNTs/CNFs to endure the high magnitude of shear rates experienced in this process, as well as about the determination of processing parameters that should be used in this process in order to obtain materials with isotropic dispersion of

CNTs/CNFs. The process of extrusion compounding is extensively used in industry, and a very convenient melt mixing technique. Extrusion compounding is generally used to generate the polymer composite pellets with microscale fillers used in production processes such as injection molding. However, mixing nanoscale fillers with the polymer melt is more difficult than that of microscale fillers due to their strong tendency to agglomerate.

Mahfuz et al. [Mahf06] dry mixed Nylon6 and MWCNTs and extruded in a single screw extruder with heat stabilization to generate continuously drawn composite filaments. Pötschke et al. [Pöts04] and Sennet et al. [Senn03], in two different research efforts, compounded polycarbonate (PC) with MWCNTs in a DACA co-rotating, intermeshing, conical twin screw microcompounder at 50-80 rpm at 250-265°C to examine the effects of draw rate on the microstructure and properties of the resulting composites. Andrews et al. [Andr02] conducted an extensive study to examine the electrical, microstructural, mechanical and rheological properties of composites of polystyrene (PS), polypropylene (PP), and acrylonitrile-butadiene-styrene (ABS) with MWCNTs and CNFs by processing them using a Haake Polylab shear mixer. Kashiwagi et al. [Kash02] prepared composites of polypropylene (PP) with MWCNTs using a Haake Polylab shear mixer at 190°C and a screw speed of 20 rpm. The melt underwent mixing for 30 min to investigate the thermal stability and flame retardant properties. Sandler et al. [Sand99] dispersed MWCNTs in an epoxy by high rate mixing (2000 rpm), employing a dissolver disk for 1 hour. They also investigated the effects of increasing shear force by increasing the resin viscosity through

cooling during processing. Ferguson et al. [Ferg98] employed a Buss Kneader for primary compounding, followed by injection molding to create composites of CNTs with various thermoplastics.

Melt mixing of polymer-CNF composites to study their properties and microstructures has also been widely reported in the literature. For example, small quantities of premixed polypropylene and CNFs were supplied to a Haake Rheocord 90 twin screw extruder and extruded at a screw speed of 20 rpm followed by pelletization and fiber spinning [Kuma02] to study the form, structure and mechanical properties of the resulting composites.

Unlike solvent processing, melt mixing is beneficial because it can be a continuous process, eliminating batch to batch inconsistencies. In addition, melt mixing is a process that does not use solvents, which could possibly act as contaminants at the polymer-filler interfaces. In this dissertation, melt mixing is used to create hierarchically-structured polymer composites with thermoplastic polymer matrices.

2.2 Solvent processing of nano-enhanced thermoplastics

Solvent processing (also known as solution blending) utilizes solvents to reduce the viscosity of a polymer in order to facilitate mixing and dispersion of fillers, such as CNFs, in order to create a nano-enhanced polymer. The solvent can also act as a dispersant to enhance dispersion of the fillers. There are four major steps involved in solvent processing: (1) disperse the fillers in a solvent in order to deagglomerate them and create a suspension, (2) mix the solvent/filler

suspension with the polymer (at room temperature or elevated temperature), and (3) recover the polymer/filler mixture by removal of the solvent via non-solvent extraction in order to precipitate out the filler coated by the polymer from the solvent, and (4) evaporation or vacuum-assisted filtering of the solvent/non-solvent solution.

For nano-enhanced polymers, there have been several variations of three of these major steps in order to obtain nano-enhanced polymers with different microstructures and associated properties. In one example involving single-walled carbon nanotubes (SWNTs), a versatile coagulation method was developed by Du et al. [Du03] involving sonication of SWNTs, which was followed by mixing and stirring with poly-(methyl methacrylate) (PMMA) solution. During recovery by addition of the non-solvent, the precipitating polymer chains entrap the SWNTs, thereby preventing them from bundling. Another method for recovery was also pursued by cooling the suspension. Using polyethylene (PE), a PE-SWNT suspension was heated to supersaturate the solution with the polymer; precipitation was then induced through cooling [Du03]. When using slow solvent evaporation during processing, nanoscale fillers will tend to agglomerate nullifying the dispersive effects of the solvent. In order to circumvent this issue, there have been efforts to reduce evaporation time by placing the polymer-CNT suspension on a rotating substrate (spin-casting) [Dela99] or dropping the polymer-CNT suspension on a hot substrate (drop-casting) [Beno01].

Solvent processing has also been used with both thermoset and thermoplastic polymers. Biercuk et al. [Bier02] dissolved epoxy in a well dispersed, ultrasonicated SWNT suspension, which was then evaporated and cured to form a "nano-enhanced" adhesive. Safadi et al. [Safa02] and Watts et al. [Watt01] added multi-walled carbon nanotubes (MWCNTs) to a PS solution dissolved in toluene to make nano-enhanced adhesives by both film-casting and spin-casting.

Although many solvents tend to be quite unstable and carcinogenic, more stable and benign aqueous solutions have been employed for certain polymers. An aqueous poly(vinyl alcohol) (PVA) solution was mixed with an electrostatically stabilized dispersion of CNTs in water and cast to form a nano-enhanced polymer film [Shaf99]. Qian et al. [Qian00] made use of a simple solvent evaporation method assisted by high energy sonication to prepare PS-MWCNT composite films. The solvent processing of polymer-CNF composites is also not unprecedented, where Yang et al. [Yang04] and Zhang et al. [Zhan06] have prepared PS-CNF composites using toluene, sonication, and magnetic stirring.

Solvent processing has proven to be a simple, yet versatile lab scale, batch process for preparing the nano-enhanced polymers. However, to my knowledge, solvent processing has yet to be used for creating hierarchically-structured polymer composites. Therefore, in this dissertation, a model polymer with microscale and nanoscale fillers will be used to create a hierarchically-structured polymer composite via solvent processing.

2.3 Synthetically developed and naturally occurring hierarchically-structured materials

Nature is rife with systems whose mechanical properties far surpass those achieved using synthetic materials with present technologies [Vinc91]. This occurs due to the fact that organisms are able to produce composite materials that are organized in terms of composition and structure, containing both inorganic and organic components in complex structures that are hierarchically organized at the nano-, micro-, and meso-scales. Additionally, the multi-scale structure of biological materials, such as wood, lead to multifunctionality, and their structure can serve as templates for the design of hierarchically-structured polymer composites as can be seen in Figure 2.1 and Figure 2.2 [Srin91, Baer92]. Some examples of this multifunctionality in biological materials can be found in Table 2.1.

Biological Material	Multifunctionality
Bone	Structural support for body
	Blood cell formation
Chitin-based exoskeleton in arthropods	Attachment for muscles
	Environmental protection
	Water barrier
Sea spicules	Light transmission
	Structural support
Tree roots	Anchoring
	Nutrient transport

Table 2.1. Examples of multifunctional biological materials

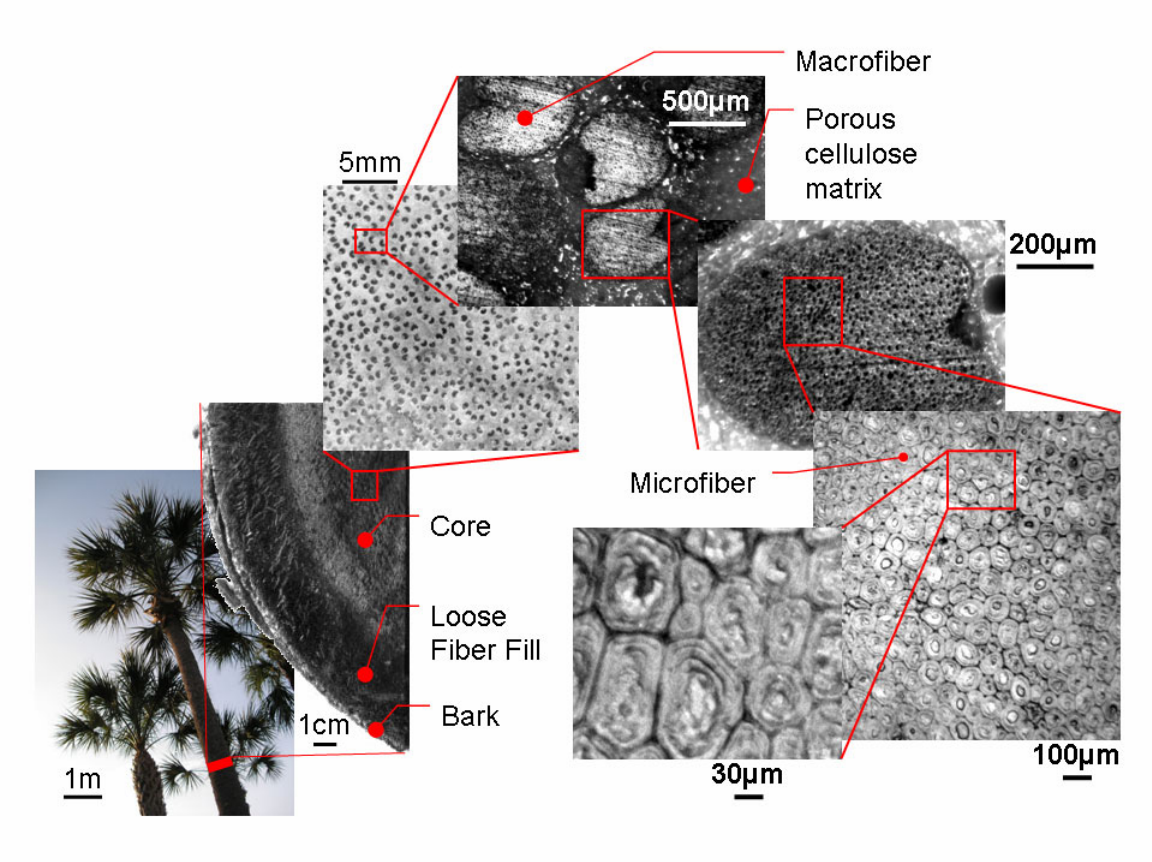

Figure 2.1. The multi-scale structure of wood that can serve as template for the design of hierarchically-structured polymer composites. Images obtained with a digital camera or through optical microscopy.

One of the defining features of the rigid biological systems that comprise a significant fraction of the structural biological materials is the existence of two components: a mineral and an organic component. The intercalation of these components can occur at the nano-, micro-, or meso-scale and often takes place at more than one dimensional scale [Meye06]. A well known example of this type of natural composite material is nacre, or mother of pearl. Nacre's constituents are 95% aragonite, which is one form of the mineral calcium carbonate, and 5% organic proteins and polysaccharides [Bart07, Sari95].

These materials are arranged in a brick and mortar type fashion, as can be seen in Figure 2.2 at the 10^{-4} meter length scale.

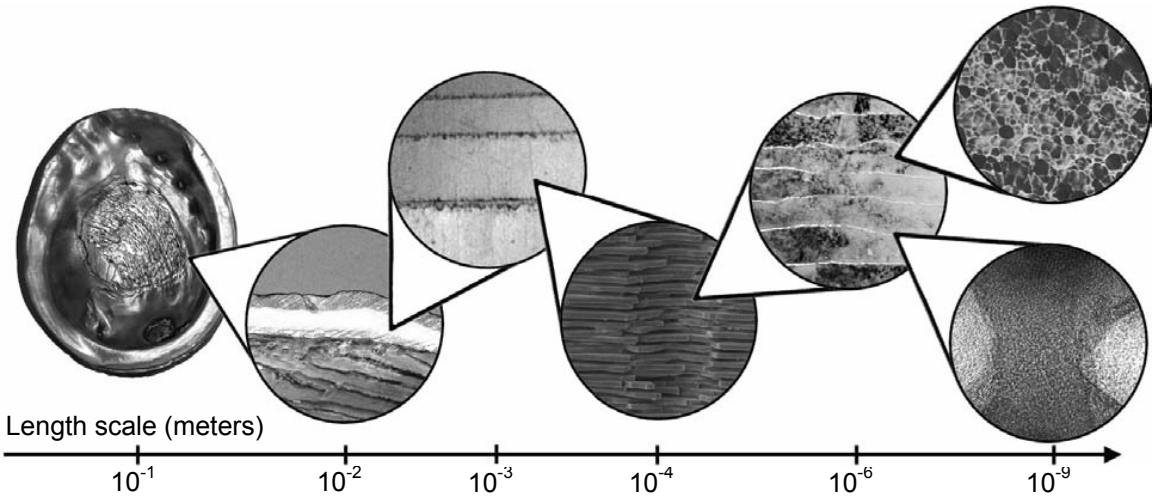

Figure 2.2. Nacre is a common example of a natural composite material. Here, the hierarchical structure is visible at various length scales [Bart07].

In Figure 2.1 and Figure 2.2, structure can be seen at several different length scales. The core wood of the palmetto tree seen in Figure 2.1 is a composite of macrofibers in a porous cellular matrix. These macrofibers are approximately 500μm in diameter, and are in turn composed of microfibers. The microfibers are approximately 60μm in diameter, and are also structured. The microfibers consist of concentric cylinders that are approximately 10μm thick.

The nacre of the red abalone shell seen in Figure 2.2 is also hierarchically-structured. The nacre is made up of 0.5μm thick layers of aragonite 'bricks'. These 5-8 μm diameter polygonal 'bricks' are held together by a 30nm thick 'mortar' of organic proteins and polysaccharides. The 'bricks' themselves are comprised of aragonite nanograins. [Bart07]

The mechanical properties displayed by these natural composites are a consequence of assembled substructures that support and reinforce the next, higher level architecture.

Although nano-enhanced polymers are continuing to evolve toward improved properties for materials applications, consider the extent to which synthetic nanoparticle-filled polymer materials can be directed to assemble into hierarchically ordered nano-enhanced polymers – similar to what can be found in nature in the abalone nacre or the palmetto wood. The construction of such complex structures remains a challenge but will lead to materials with new functionalities. Essential to meeting this challenge is establishing guidelines for process optimization, discovering assembly methods that yield a desired structure, and understanding structure-property relationships to predict the performance of a given architecture. With this knowledge available, nanoparticle/polymer mixtures hold promise for the fabrication of hierarchically ordered materials that have tailored structures and functionalities that span multiple length scales and dimensions [Bala06].

The greatest stumbling block to the large-scale production and commercialization of nano-enhanced polymers is the dearth of cost effective methods for controlling the dispersion of the nanoparticles in polymeric hosts. The nanoscale particles typically aggregate, which negates any benefits associated with structure in the nanoscale dimension. There is a critical need for establishing processing techniques that are effective on the nanoscale yet are applicable to macroscopic processing. [Bala06]

The absence of structure-property relationships presents a significant impediment to a more extensive use of nano-enhanced polymers, and especially hierarchically-structured nano-enhanced polymers. Research in this area is in its infancy, having begun in earnest over the past ten years. Because of this, there is a dearth of information, specifically in terms of properties of these materials [Ajay03].

Some work in this field has been accomplished, including work with carbon nanotube reinforced epoxies [Alla02, Gojn04, Gojn05, Seyh07, Zhou07, Zhou08], and functionalizing carbon fibers with carbon nanotubes for composites [Kepp08], but the properties of nano-enhanced polymers are not established [Esaw07]. There is still a lack of well defined processing – structure – property relationships that will greatly help in the design of new composite materials to be addressed in this dissertation through multi-scale characterization of both synthetic and natural hierarchically-structure materials.

2.4 Combinatorial approach to composite materials processing

Over the last decade academic and industrial scientists have become increasingly interested in modifying the properties of polymers by adding nanoscale fillers to form nano-enhanced polymers. With the increasing significance of nano-enhanced polymers [Breu04], it has become important to rapidly and accurately characterize the processing-structure-property relationships in these novel materials. The composites community has shown a great deal of interest specifically in carbon nanotubes (CNTs) and carbon

nanofibers (CNFs) because they exhibit extraordinary electrical and mechanical properties and can therefore be exploited in the development of a new generation of composite materials [Boko07]. However, effectively processing these nanoscale fillers with various polymer matrices to produce new ultra-strong composite materials has proven to be a daunting challenge [Cole06].

A thorough investigation of the entire parametric domain to optimize the mechanical properties of nano-enhanced polymers, especially when using expensive nanoscale fillers, can be very protracted, challenging, and financially prohibitive. Combinatorial materials science provides methodologies to address these issues [Xian95, Davi99, Engs00, Amis02, Nyde02, Poty05] through the use of methodical, continuous experimental approaches that are able to rapidly produce and characterize a wide range of materials without batch-to-batch variation, e.g. varying degrees of crystallinity in amorphous polymer. Specifically, continuous compositional gradients are well suited for prompt and inexpensive investigation of effects resulting from processing conditions [Gilm03, Gilm04], such as the dispersion of nanoscale fillers. The compositional gradients also assist in quickly and accurately determining the effect of composition on material properties over the entire domain of interest with high compositional resolution. Furthermore, it is possible to significantly reduce the amount of expensive nanoscale fillers that is needed to characterize processing-structure-property relationships, as compared to batch-processed composites where a minimum amount of filler is needed for processing and characterization at each

composition and where numerous batches are needed to statistically quantify batch-to-batch variations [Kota08a].

Because of its continuous nature, the TSE process is ideally suited for producing polymer blends and composites with continuous compositional gradients [Sand03a]. This is accomplished by operating a twin screw extruder at one steady condition, and then dynamically changing the proportion of ingredients to produce a new formulation that results in the extrudate gradually changing from one composition to another.

The gradual change in composition is due to the inherent back mixing that occurs in the extruder. So, even though an abrupt change has occurred in the proportion of ingredients, the output from the extruder exhibits a gradual change in the composition. Thus, the continuous nature of the process is especially well suited to combinatorially produce nano-enhanced polymers [Xian95, Amis02, Poty05]. A batch process, such as solvent processing, is incapable of producing such a gradual change in composition because any dynamic change in the proportion of ingredients would be homogenized into the entire batch during the mixing process.

The use of extruders for producing compositional gradients has only recently become of interest. Gilman et al. [Sand03a, Gilm03, Nyde02] produced extruded composites of Nylon6 or PS and purified organic clay filler in order to study the effects of the filler on the polymer via the compositional gradients (CGs) to prove that a single experiment could provide samples for either in situ or a posteriori characterization over a compositional domain of interest. This the

main advantage of using compositional gradients over batch mixes for combinatorial processing, since it significantly reduces the batch-to-batch variation and the time consumed in producing samples over a range of compositions. Potyrailo et al. [Poty03] have also used a combinatorial extrusion system to generate polymeric CGs with two different material systems: (a) PP with model additives, and (b) PC with a titanium dioxide filler. Gallant et al. demonstrated that a TSE could be used as a new combinatorial approach to investigate burning rate effects in composite solid propellants [Gall06].

One challenge in using the TSE to produce CGs for combinatorial processing of polymer composites is to rapidly characterize the gradient in the extrudate. Eidelman et al. [Eide04] used an elaborate Fourier transform infrared microspectroscopy technique to monitor the reflection-transmission spectra and relate it back to the composition. Potyrailo et al. [Poty03] characterized the CGs in situ using an optical probe signal to track changes in color of the blend. Gallant et al. used the addition of a small quantity of dye to the polymer when a change was made in the proportion of ingredients in order to create a subtle color gradient that correlated directly with the composition gradient [Gall04].

While certain combinations of polymers and fillers are amenable to these techniques, it is not necessarily suitable for fillers such as CNFs and over all composition ranges. For example, all of the non-destructive in situ characterization approaches developed so far with optical probes are limited to low loadings of the filler in the composite. As the loading of the filler increases in the polymer, especially for a dark-colored filler like CNF, the optical probes tend

to saturate and reach a limit of detection rendering it incapable of detecting any further changes in composition. Therefore, it is not always possible to use in situ characterization for CG characterization. Kota et al. used a posteriori techniques like TGA to characterize the gradient by direct decomposition of selected portions of the CG in order to determine composition and reconstruct the CG to validate the use of Resident Volume Distributions in convolution integrals as a means of rapidly predicting the gradient architecture [Kota08a]. In this dissertation, a method for using the TSE as a combinatorial approach to characterize processing-structure-property relationships in hierarchically-structured polymer composites will be developed.

2.5 Control of multifunctional properties through hierarchical structure

Another interest in developing nano-enhanced polymers is the control of multifunctional properties. For example, electrically conductive nanoparticles, such as multi walled carbon nanotubes (MWCNTs) and carbon nanofibers (CNFs), have been of particular interest because they have the potential to enhance the electrical conductivity of polymers [Baug02, Moni06]. The combination of high conductivity resulting from the presence of these particles with the flexibility and ease of processing polymers is a highly desirable combination. Materials with such unique and intriguing properties are apt to enable new applications, such as lightweight radiation shields for use by NASA in spacecraft [Dalt03, Rama03, Smit04]. As such, many groups have investigated

polymer-MWCNT as well as polymer-CNF nano-enhanced polymers, and impressive conductivities have been reported. For example, conductivities on the order of 1 S/m have been obtained with loadings of just 2 wt. % of multi-walled MWCNTs [Pöts03, Pöts04] or 5 wt. % of CNFs [Loza01].

The polymer-MWCNT/CNF composites that have been previously studied have typically been prepared at a laboratory scale, often employing solvent-processing procedures or *in situ* polymerization techniques since these are appropriate methodologies for small sample sizes [Dalm05, Du04, Du05, Gojn06, Kota07a, Moni06, Sand03b, Stép02]. However, is it possible to produce these same materials on a much larger scale using conventional polymer processing techniques such as single- or twin-screw extrusion, compression or injection molding, or melt spinning? One line of research in this dissertation arose out of attempts to make polymer-MWCNT/CNF nano-enhanced polymers via twin-screw extrusion. Surprisingly, the conductivities of extruded samples were very low. In fact, an examination of relevant literature demonstrates that a rather wide range of conductivity values have been obtained, sometimes much lower than might be expected for a given particle loading [Alig07, Khar04, McNa05, Moni06, Pöts03, Pöts04]. These differences can generally be attributed to the wide range of processing methods and conditions used by different authors. It is clear that processing affects conductivity as well as other material properties. In light of this realization, the control of properties in nano-enhanced polymers through hierarchical structure is of increased interest.

A simple way to recover the electrical conductivities of polymer-MWCNT/CNF nano-enhanced polymers following extrusion is through the melt annealing the materials at a temperature exceeding the glass transition temperature (T_g) of the polymer. The annealing step is shown to increase the room temperature conductivity by several orders of magnitude in some cases. Systematic effects on conductivity are observed as a function of annealing temperature and annealing time. When the material is annealed, the particle distribution becomes more isotropic compared to the aligned fibers of the as-processed material. Due to this random orientation, the connectivity of the fibers throughout the composite increases. However, this connectivity can also result in a change in the mechanical behavior due to the reorientation of the fibers. This dissertation explores both the mechanism for the control of electrical properties in polymer-MWCNT/CNF nano-enhanced polymers and the resulting effect it has on the mechanical properties of the polymer-CNF system.

Chapter 3 Materials and methods

Samples were made using several different materials over the course of this work. In section 3.1, different materials used in this research will be discussed. The methods by which these materials were tested will be discussed in section 3.2.

3.1 Materials used in this work

3.1.1 Nano-enhanced High Impact Polystyrene (HIPS): *Bottom-up*

The nano-enhanced HIPS used in this work was made by Arun Kota for his Ph.D. research [Kota07d]. Here, the ingredients and methods used to create the materials will be reviewed.

In order to produce the nano-enhanced polymers used in this research, a model nanoscale filler and a compatible polymer matrix were chosen that are appropriate for use in a Twin Screw Extruder (TSE). PR-19 grade Carbon Nanofibers (CNFs) were obtained from Applied Sciences and used as nanoscale filler due to their availability and reasonable cost. A high-strength thermoplastic, high impact polystyrene (HIPS) was obtained from Nova Chemicals and used as the polymer matrix due to its earlier utilization in work on establishing the processing-structure relationships in nano-enhanced polymers [Kota07a, Kota07c, Kota08a, Kota08b].

A 28 mm screw diameter Werner and Pfleiderer co-rotating, intermeshing TSE was used with a slit die (25 mm wide x 1 mm high) to produce the nano-

enhanced polymers. Feeders fed both CNFs and HIPS by weight into the TSE system as shown in Figure 3.1. The extruder was operated at a screw speed of 200 rpm and operating temperatures were 210°C for all five barrel zones and 165°C at the die. Two different methods were employed in the production of materials: combinatorial and steady-state. In the case of the combinatorial material, 0.2 lb/hr of CNFs were step fed into a 1.8 lb/hr steady flow of the HIPS melt and the HIPS-CNF composite that resulted from this transient response was a compositional gradient ranging from 0 to 10 wt. % CNFs. An example of this 0 to 10 wt. % compositionally-graded extrudate can be seen in Figure 3.2. It is also possible to see alignment of the CNFs in the direction of the compositional gradient due to shear in the flow of the extrudate through a slit die. This alignment is visible in the SEM micrograph of the extrudate cross-section in Figure 3.2. In the case of the steady-state material, the extrudate resulting from a steady-state response to 0.2 lb/hr of CNFs being step fed into a 1.8 lb/hr steady flow of the HIPS melt and the HIPS-CNF composite was collected. The steady-state response occurs after the transition from 0 to maximum wt. % has completed. Steady-state HIPS-CNF composites were prepared at 1, 3, 5, 7 and 10 weight percent CNFs by varying the HIPS and CNF feed rates such that the total flow rate was 2 lb/h.

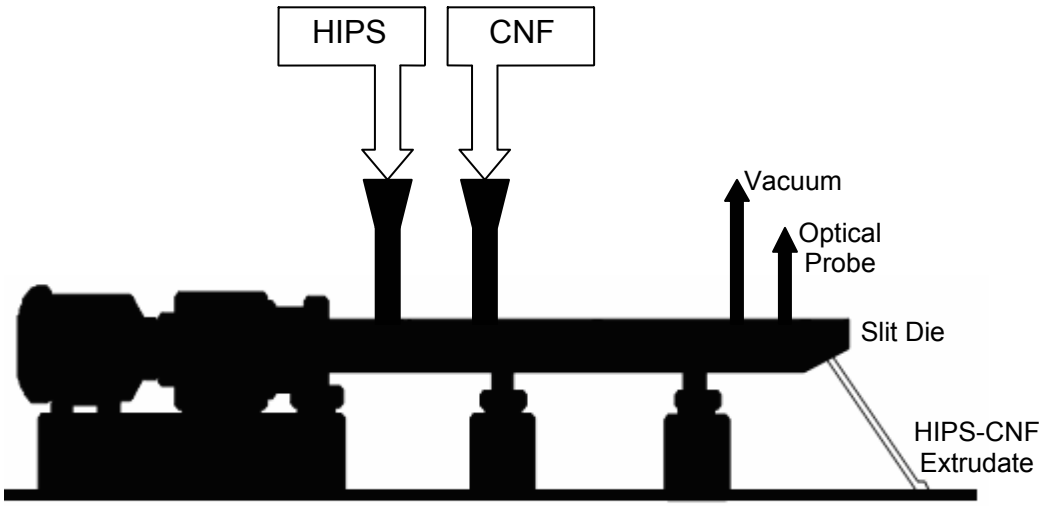

Figure 3.1. Schematic of the Twin Screw Extrusion system used for the combinatorial approach to produce HIPS-CNF composites for mechanical characterization.

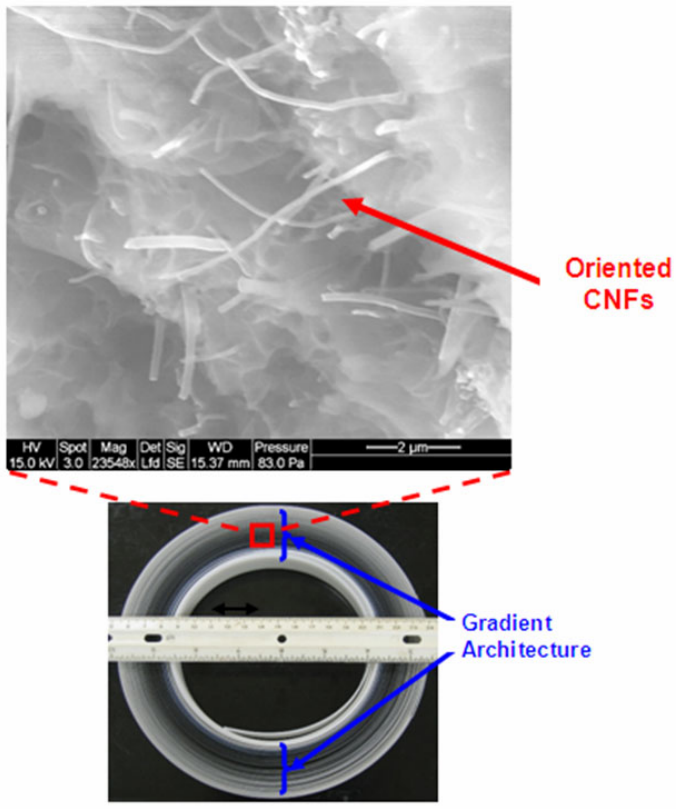

Figure 3.2. A roll of the extrudate obtained in response to an impulse input of Pyrograf CNFs to HIPS in the TSE and a SEM micrograph from a cross-section of the compositional gradient showing the alignment of CNFs due to the flow of the extrudate through a slit die.

3.1.2 Nano-enhanced epoxy resin: *Bottom-up*

3.1.2.1 Nano-enhanced West System® epoxy resin

West System® 105 epoxy resin with 206 hardener was chosen as the matrix material due to its availability and ease of use. In order to create the nano-enhanced composite materials for tensile and compressive testing, the epoxy resin was thoroughly mixed with PR-19 grade Carbon Nanofibers (CNFs), with diameter 100-200 nm, length 10-30 μm, and density 1.87 g/cm^3, which were obtained from Applied Sciences – the same CNFs that were used as a nanoscale filler in the HIPS extrudate. Once thoroughly mixed, the resin-CNF mixture was placed in a VWR Aquasonic model 75D ultrasonic bath for 1.5 hours, 3 hours or 6 hours to help break up agglomerations of CNFs. A fourth set of composites was made with no sonication. After sonication, the resin-CNF mixture was placed in an ice bath to cool the mixture down to room temperature, which prolongs the useful working time after the hardener is added.

Once the resin-CNF mixture is at room temperature, West System 206 hardener was added in the ratio of 5:1 epoxy to hardener. Immediately after adding the hardener, the mixture was homogenized using a dual propeller mixing impeller, seen in Figure 3.3. The mixing impeller was mounted on a drill press, and the epoxy, hardener and CNF mixture was mixed for 3 minutes. Mixtures containing CNFs were made with 1, 3, 5, 7 and 10 weight percent. After mixing, the nano-enhanced epoxy was degassed in a vacuum chamber at 560 mmHg for 5 minutes. The composite was sandwiched between two 0.020” thick sheets of Nylon 6/6, and sealed in a polyethylene bag fitted with a valve attached to a Gast ROC-R model ROA-P131-AA vacuum pump. A cotton mat was placed beneath

the valve to prevent blockages in air flow, as well as to prevent excess polymer from entering the vacuum lines. The polyethylene bag containing the curing composites was placed between the platens of a Carver hydraulic unit model #3912 press using minimal force to ensure an even thickness throughout the material. This setup can be seen in Figure 3.4. These composites were cured at 450 mmHg vacuum at room temperature for 48 hours, and then cured for an additional 48 hours at 80°C at atmospheric pressure. Table 3.1 shows all materials that were made with this process. It can clearly be seen from Figure 3.5 that higher sonication time affects a decrease in the size of agglomerations.

Figure 3.3. Mixing impeller - 1 3/8" propeller diameter.
Made of type 304 stainless steel.

Figure 3.4. Vacuum assisted curing of nano-enhanced West System epoxy.

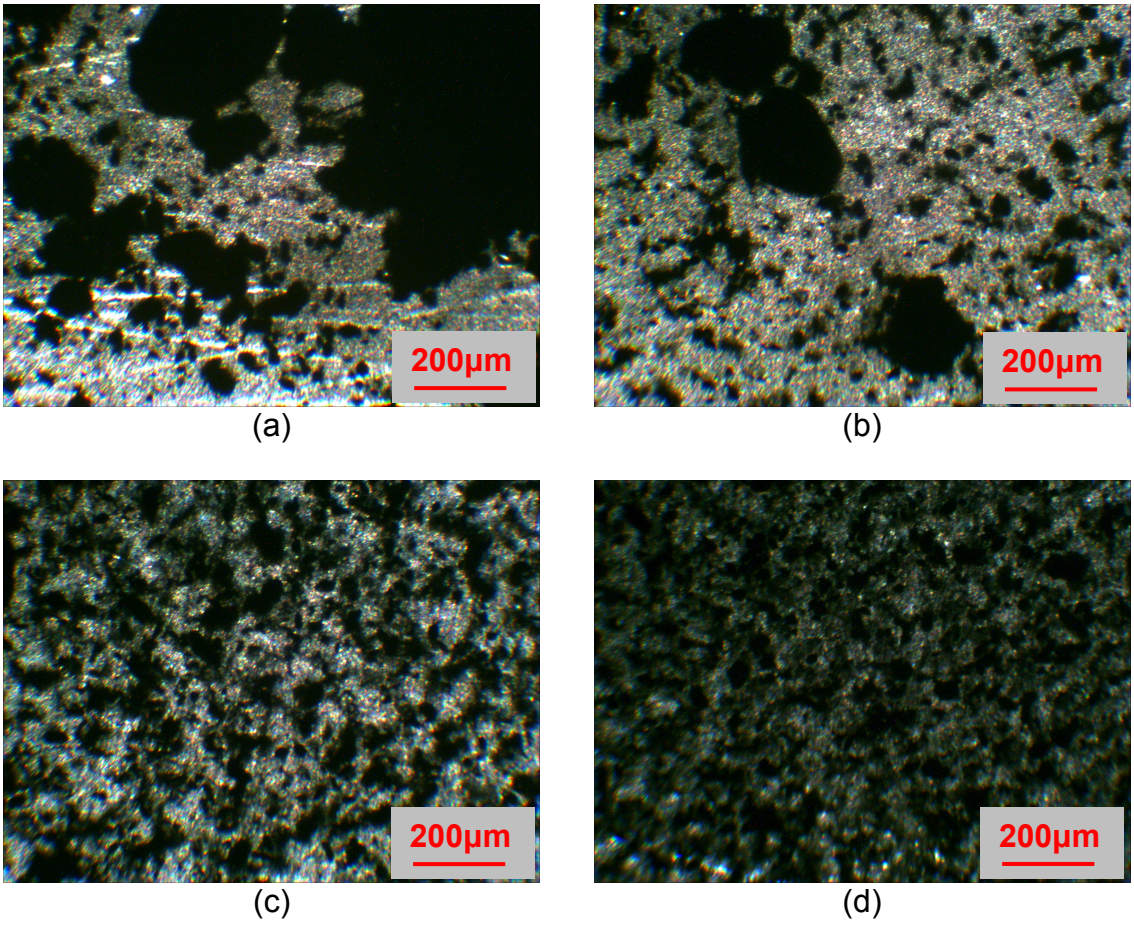

(a) (b)

(c) (d)

Figure 3.5. Effects of sonication on 3 wt. % CNF in West System epoxy.
(a) No sonication, (b) 90 minutes sonication,
(c) 3 hours sonication, (d) 6 hours sonication.
Images obtained using transmission light microscopy.

Neat Epoxy No Sonication	1 wt. % Epoxy No Sonication	3 wt. % Epoxy No Sonication	5 wt. % Epoxy No Sonication	7 wt. % Epoxy No Sonication	10 wt. % Epoxy No Sonication
Neat Epoxy 1.5 Hours Sonication	1 wt. % Epoxy 1.5 Hours Sonication	3 wt. % Epoxy 1.5 Hours Sonication	5 wt. % Epoxy 1.5 Hours Sonication	7 wt. % Epoxy 1.5 Hours Sonication	10 wt. % Epoxy 1.5 Hours Sonication
Neat Epoxy 3 Hours Sonication	1 wt. % Epoxy 3 Hours Sonication	3 wt. % Epoxy 3 Hours Sonication	5 wt. % Epoxy 3 Hours Sonication	7 wt. % Epoxy 3 Hours Sonication	10 wt. % Epoxy 3 Hours Sonication
Neat Epoxy 6 Hours Sonication	1 wt. % Epoxy 6 Hours Sonication	3 wt. % Epoxy 6 Hours Sonication	5 wt. % Epoxy 6 Hours Sonication	7 wt. % Epoxy 6 Hours Sonication	10 wt. % Epoxy 6 Hours Sonication

Table 3.1. Nano-enhanced West System epoxy samples

3.1.2.2 Nano-enhanced Hysol 9309.2 thermoset adhesives

Hysol 9309.2 was used as a filled epoxy adhesive that is qualified for space flight applications. It is a bisphenol A/epichlorohydrin epoxy resin with 10 wt. % of butadiene-acrylonitrile copolymer, 5 wt. % of 6 micron silica fibers, and 1 wt. % titanium dioxide. Single walled CNTs from Southwest NanoTechnologies Inc. were used to nano-enhance the thermoset adhesive. The CNTs which were used were CoMoCat SWeNT, purified single walled grade SG 65 with a mean tube diameter of 0.8 ± 0.1 nm and aspect ratio of 1,000:1, carbon content was 90% by weight, >50% of tubes were (6, 5) chirality and > 90% of tubes were semiconducting, as stated on their website [Sout09a].

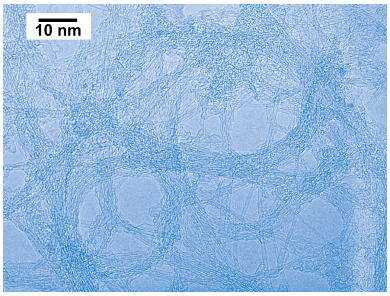

Figure 3.6. Typical TEM image for SWeNT SG 65 [Sout09b].

The nano-enhanced thermoset adhesives were fabricated using a high-powered sonication technique designed to distribute the carbon nanotubes evenly in the 9309.2 (Hysol) epoxy host material. CNTs were sonicated (using a Cole Parmer Ultra Sonicator, 23% amplitude) in the B-part for two hours. This CNT/B-part solution was then mixed with the A-part of the epoxy in a Thinky planetary centrifugal mixer at 2,000 rpm for three minutes, then a de-foaming step at 1,000 ramp for one minute to prevent porosity build-up in the epoxy. Samples were cast onto Teflon tape, and doctor-bladed to control thickness of the films. Samples were allowed to set for 24 hours at room temperatures followed by a cure step in air. The Hysol 9309.2 was prepared with 0, 0.2 and 0.5 wt. % CNT loading. Because of the lower density and smaller diameter of the single walled CNTs, a lower wt. % was needed to achieve effects like percolation and surface interaction with the polymer matrix than was required for MWCNTs or CNFs. Each of these loadings had samples cured at 1, 2, 3, 24, 48, and 96 hours at 80°C.

3.1.3 Hierarchically-structured nano-enhanced polymers: *Top-down*

3.1.3.1 Hierarchically-structured West System thermoset nano-enhanced polymers

The same method described in section 3.1.2.1 was used to make hierarchically-structured nano-enhanced polymers. All hierarchically-structured West System epoxy specimens used nano-enhanced West System that was sonicated for 6 hours. In the case of the hierarchically-structured nano-enhanced polymers, one or more pieces of 0.05mm thick carbon fiber veil from Fibre Glast

Developments Corporation (Figure 3.7) were impregnated with the nano-enhanced West System epoxy, sandwiched between two 0.020" thick sheets of Nylon 6/6, and sealed in a polyethylene bag fitted with a valve attached to the vacuum pump. These composites were also cured at 450 mmHg vacuum at room temperature for 48 hours in the Carver press using minimal force to ensure an even thickness throughout the material, and then cured for an additional 48 hours at 80°C at atmospheric pressure for consistency of processing conditions as compared to the nano-enhanced West System epoxy.

Due to the scale of the pressure gauge on the carver press (smallest increment is 250 lbs.), it is difficult to apply small amounts of force with a high level of consistency. Additionally, the samples' viscosity increases with increasing CNF loading. Due to these factors, the thickness of the specimens is not uniform among different CNF loadings and different sonication times. The carbon fiber veil is consistent in thickness and fiber dispersion. Because of the variability in thickness of the specimens, the wt. % of CMF loading varies in different sample sets. A summary of the CMF loading for the different sample sets can be seen in Table 3.2.

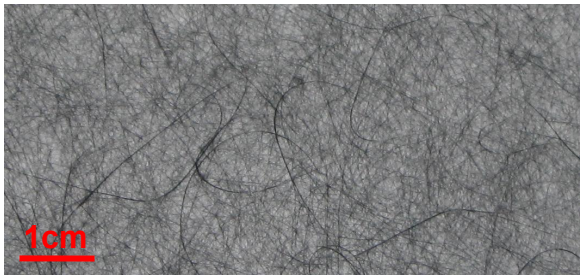

Figure 3.7. Carbon fiber veil from Fibre Glast Developments Corporation. Image taken with a digital camera.

Sonication (hours)	wt. % CMF					
	0 wt. % CNF	1 wt. % CNF	3 wt. % CNF	5 wt. % CNF	7 wt. % CNF	10 wt. % CNF
0	2.30	1.69	2.89	2.74	2.69	1.20
1.5	2.16	2.65	2.84	2.48	2.10	1.34
3	1.35	2.71	3.39	2.40	1.50	1.17
6	2.14	1.67	3.02	3.49	2.64	1.62

Table 3.2. Summary of CMF loading in hierarchically-structured nano-enhanced West System composites.

3.1.3.2 Hierarchically-structured nano-enhanced thermoplastics

Hierarchically-structured nano-enhanced polymers were made in a batch process using Polyethylene 722, supplied by Dow Plastics. This injection molding grade polymer is a Low Density Polyethylene (LDPE). The LDPE is processed using a solvent/non-solvent extraction method in order to create sample materials loaded with CNFs, CMFs, and combinations of CNFs and CMFs. Samples of pure LDPE have been created in this same manner. These sample materials are then hot pressed to obtain the proper sample geometry.

The solvent used in this process is Toluene, and the non-solvent used is Acetone. The LDPE is dissolved in Toluene at 60°C, while undergoing mixing with a magnetic stir-bar. If the sample is to be loaded, a dispersion of CNFs, CMFs or a combination is first created by placing the requisite amount of CNFs and/or CMFs in Toluene (at approximately 0.01 weight%) and sonication is commenced for a period of 24 hours; see Figure 3.8. Once the CMFs and/or CNFs are dispersed, the fiber – Toluene dispersion is heated to 60°C while undergoing mixing with a magnetic stir-bar. At this point the LDPE is introduced

and allowed to dissolve under heat and stirring. The solution (with or without CMFs and/or CNFs) is then slowly poured into the room temperature Acetone non-solvent, which is also undergoing mixing with a magnetic stir-bar. As can be seen in Figure 3.9, the fibers remain well dispersed. At this point, the Acetone – Toluene solution is separated from the LDPE (with or without CMFs and/or CNFs) with a Büchner funnel, Whatman® ashless filter paper and a Büchner flask under vacuum; see Figure 3.10. The loaded or unloaded LDPE is then dried in a vacuum oven at 80°C, 750 mmHg vacuum, and ready to be hot pressed.

Figure 3.8. CMFs dispersed in Toluene after sonication. Image obtained with a digital camera.

Figure 3.9. CMFs dispersed in LDPE after non-solvent extraction.

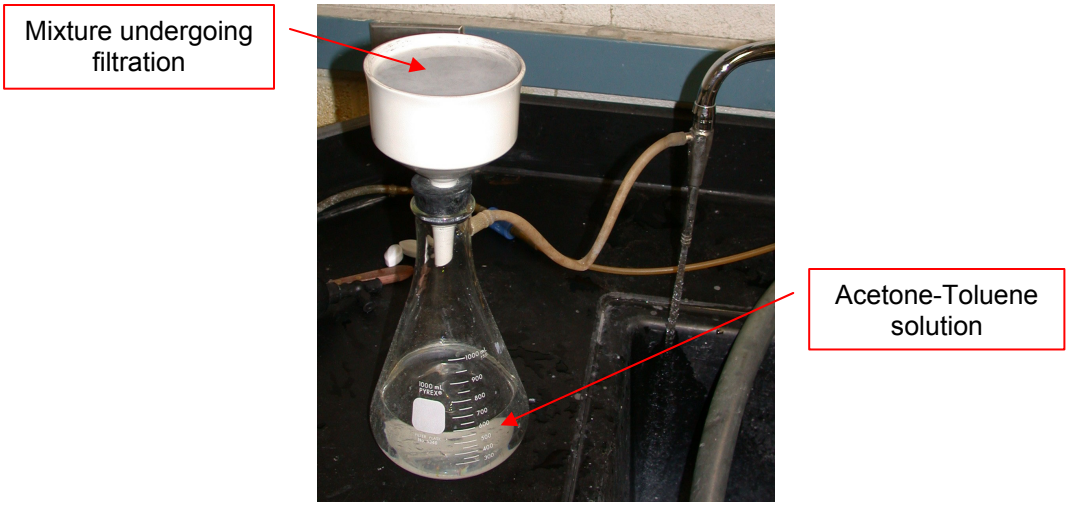

Figure 3.10. Acetone-Toluene solution is filtered out of the mixture.

The material to be hot pressed is placed in a mold with 6mm × 6mm cylindrical cavities. The mold is then placed between sheets of Kapton to prevent the material from adhering to the platens of the hot press. The hot press platens are preheated to 170°C, and the mold with material and Kapton is placed on the bottom platen of the hot press. 5000 lbs. of pressure is applied to the platens of the hot press, and that pressure is maintained for 5 minutes. The mold is then removed with the Kapton, and allowed to cool before removing the specimens from the mold cavities.

3.2 Experimental methods

3.2.1 Nanomechanical characterization

The Hysitron TriboIndenter® (see Figure 3.12) is a test system that is designed to measure material properties at the nano scale. The TriboIndenter is

capable of nanoindentation (both quasi-static and dynamic), scratch testing, and nanoscale dynamic mechanical analysis (nanoDMA).

In addition to characterization, the TriboIndenter is capable of imaging by rastering its ~150μm radius indenter tip across a surface to acquire height data at each of the 256×256 points in a region of interest of up to 60μm square. This height data can be visualized as if it were a topographical map of the surface. The region of interest is limited by the nanoindenter tip radius. In this research, a Berkovich tip was used, with a radius of approximately 150nm, as can be seen in Figure 3.11. The Berkovich tip is pyramidal, with a total angle of 142.3°. Larger and smaller radius tips are available.

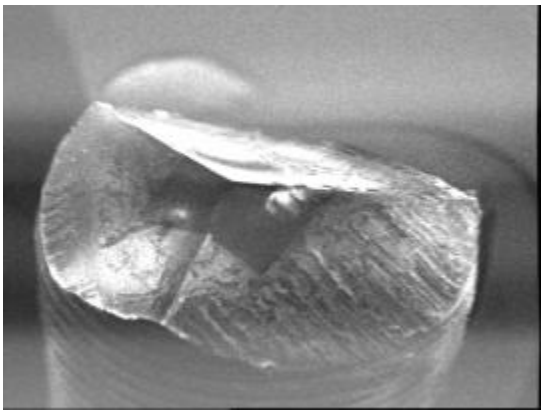

Figure 3.11. SEM image of typical berkovich tip [Hysi_a]

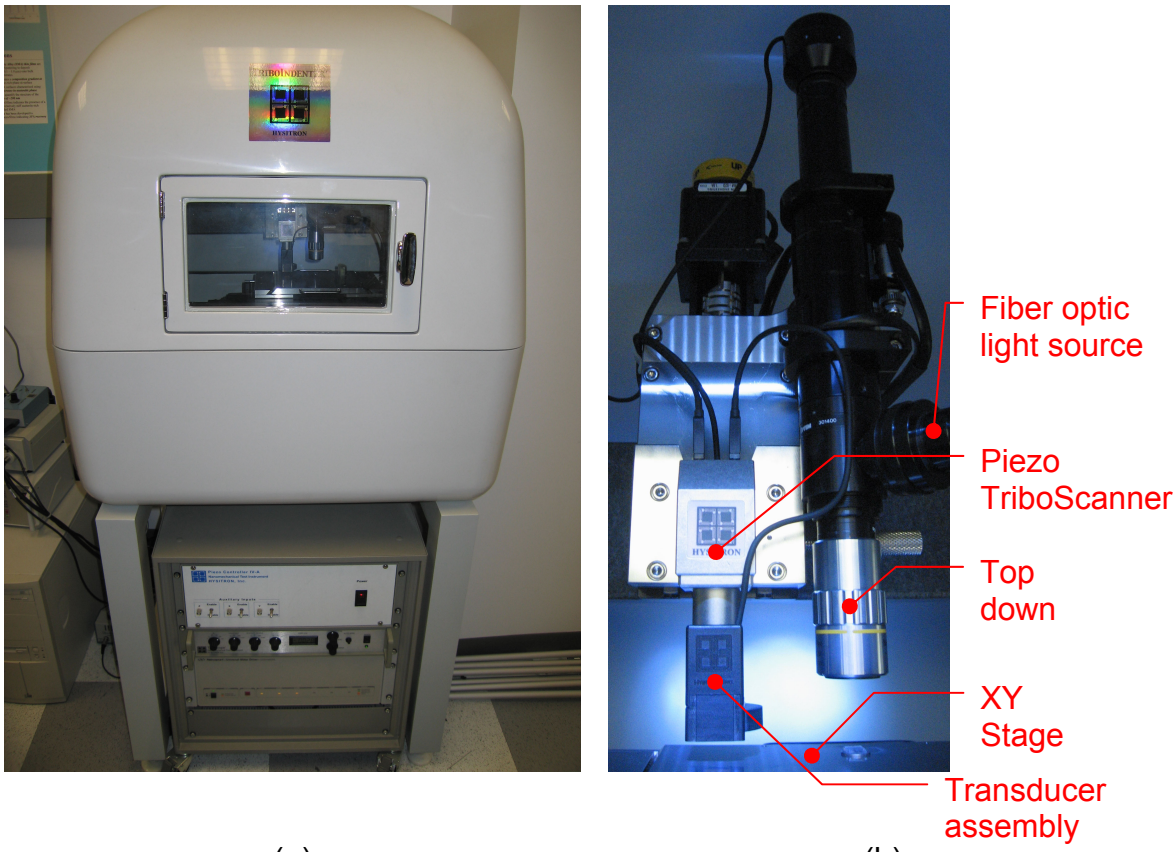

Figure 3.12. Hysitron TriboIndenter® (a) External view of acoustic enclosure and controlling electronics. (b) Optics and electromechanical actuators. The nanoindenter tip is mounted on the transducer assembly.

In quasi-static mode, the Triboindenter is capable of making indents at the nano scale. These nanoindents can be a single loading and unloading event, or can be a series of loading, partial unloading and reloading events. Figure 3.13 shows model load profiles. By analyzing these indents, we are able to determine the hardness and reduced modulus of materials at the nanoscale.

The reduced modulus is determined by Equation 3.1:

$$\frac{1}{E_r} = \left(\frac{1-\nu^2}{E}\right)_{specimen} + \left(\frac{1-\nu^2}{E}\right)_{indenter} \qquad \textbf{3.1}$$

where E_r is the reduced modulus and E and ν are the Young's modulus and Poisson's ratio of the specimen and the indenter respectively. The Elastic

modulus of the indenter ($E_{indenter}$) is 1140GPa, and Poisson's ratio ($\nu_{indenter}$) is 0.07 [Hysi_a].

The hardness is determined by Equation 3.2:

$$H = \frac{P_{max}}{A} \qquad \textbf{3.2}$$

where P_{max} is the maximum indentation force and A is the resultant projected contact area at that load, determined by a tip area function calibrated to each unique nanoindenter tip.

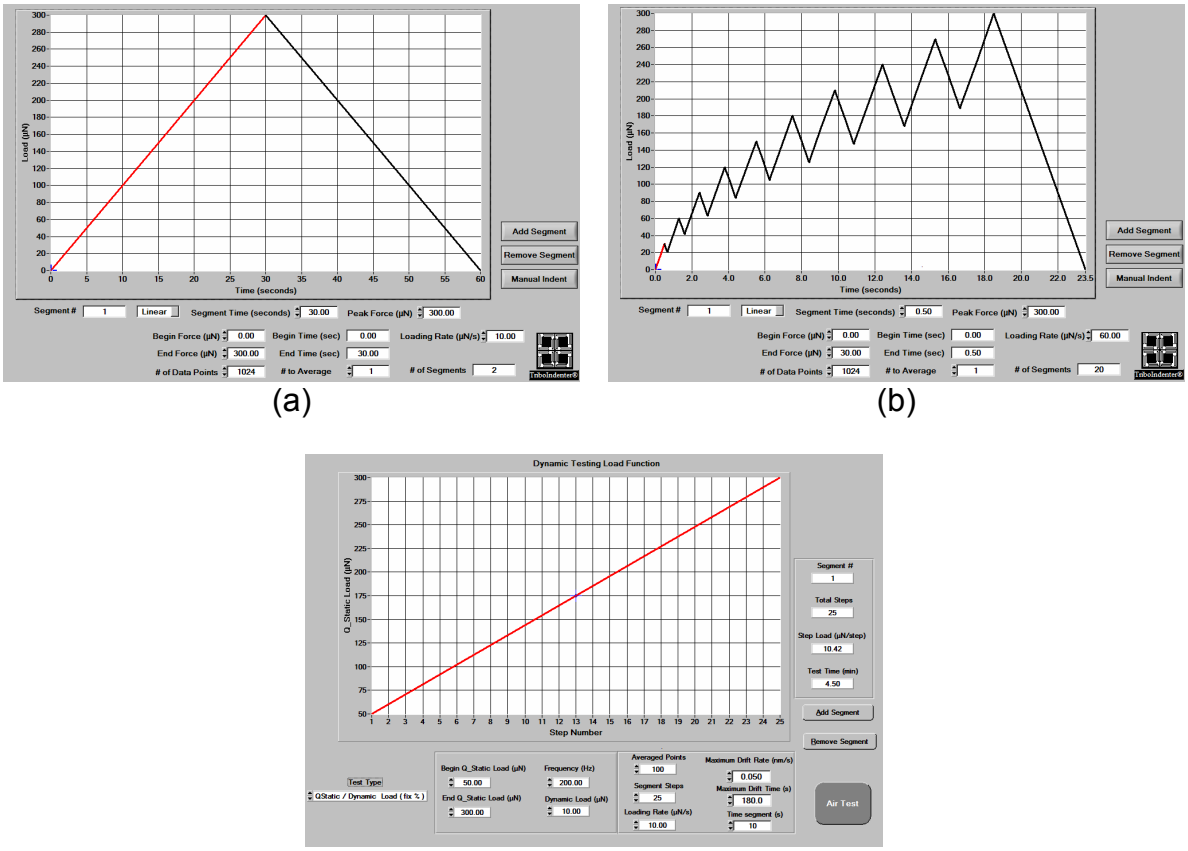

Figure 3.13. Model load profiles for nanoindentation. (a) Single indent with maximum load of 300 μN. (b) Partial unload indent with maximum load of 300 μN and 10 unloading – reloading segments. (c) nanoDMA indent at 200Hz with a quasi-static load sweep from 50 μN to 300 μN, maintaining a fixed (10%) dynamic load.

In nanoDMA mode, the Triboindenter is able to make indents while oscillating the tip in a controlled manner. This is similar to partial unload quasi-static indents, but more control is available over tip loading and oscillation. Also in nanoDMA mode, it is possible to measure the complex modulus at each of the 256×256 points in a region of interest of up to 60μm square, referred to as modulus mapping. Modulus mapping is very similar to imaging, however the indenter tip is oscillating as it rasters [Hysi_b, Hysi_c].

While modulus mapping is able to garner the material properties over an entire area of interest, the data is not as stable as quasi-static indentation or nanoDMA indentation. The tip oscillation in modulus mapping is very slight, and very low forces are applied, typically less than 5 μN. Because of this, the modulus maps are only able to get material properties very close to the surface. In addition, the topography can easily affect a change in the reported material properties from modulus mapping.

That being said, modulus mapping is a great way to see how material properties change throughout an area of interest in a relatively short period of time. In order to make a series of 100 nanoindents, approximately 10 hours is required. If these 100 nanoindents are arranged in a grid, we can get a decent idea of how the properties change throughout the area. Modulus mapping, on the other hand, generates 65,536 data points in approximately 30 minutes.

3.2.1.1 Nanoindentation

A series of quasi-static nanoindents was made in the nano-enhanced PS samples, as well as the nano-enhanced Hysol 9309.2 adhesives. For the nano-enhanced Hysol 9309.2 adhesive samples, each quasi-static nanoindent reached a maximum load of 300 μN over the course of 30 seconds of loading, and then unloaded in 30 seconds as well. These quasi-static indents were used to determine local material properties at specific locations, as well as to create extrapolated maps of the local material properties through the use of a regularly spaced grid of indents.

Nanoindentation was also used in the determination of localized material properties of microfibers from the core of a palmetto tree. For these microfibers, each quasi-static nanoindent reached a maximum load of 400 μN over the course of 10 seconds of loading, and then unloaded in 10 seconds as well.

3.2.1.2 NanoDMA and modulus mapping

A series of dynamic nanoindents was made in the nano-enhanced PS samples, as well as the nano-enhanced Hysol 9309.2 adhesives. In addition, modulus mapping of these materials as well as palmetto wood was completed. The modulus maps were compared (in certain instances) to extrapolated maps of material properties created via quasi-static nanoindentation.

3.2.2 Microtensile testing

The microtensile tester was designed to execute tensile testing of specimens with microscale features. This system employs custom linear air bearings from Nelson Air Corporation to minimize friction, and New Focus model 8302 picomotors for actuation. A Point Grey Flea2 (FL2-14S3C) digital camera mated to a stereo microscope from Edmund Industrial Optics was used as a video extensometer for data acquisition of the strain in the gage section of the specimen. The sample was illuminated with an Edmund Industrial Optics model MI-150 high intensity fiber optic illuminator. The video extensometer uses Correlated Solutions (Columbia, SC) Vic-Gauge 2006 software to acquire strain data through real-time Digital Image Correlation (DIC) analysis. Vic-Gauge 2006 also allows the acquisition of load data, which is acquired after processing via a National Instruments PXI-1042. The picomotor control software was written in National Instruments LabView by Huiqing Jin [Jin04].

Using DIC on both sides of the specimen, it has been verified that bending deformations were negligible. This may be due in part to the air bearings, which are capable of very small rotational adjustments and could therefore minimize bending effects similar in principle to universal joints.

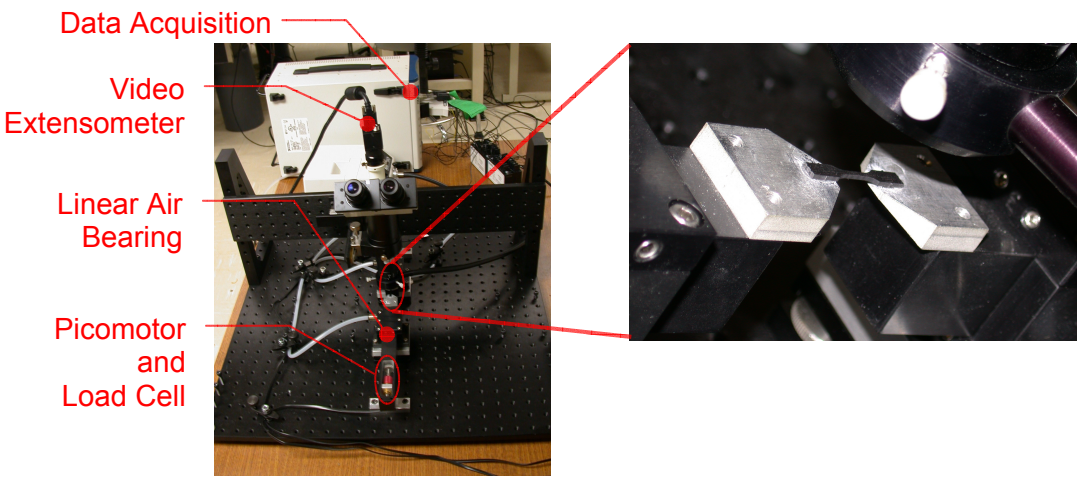

Figure 3.14. Microtensile tester

3.2.3 Macroscale characterization

To characterize the macroscale behavior of hierarchically-structured polymer composites, we used the following methods: (a) quasi-static compression, (b) quasi-static three-point bend, (c) dynamic Izod testing, (d) dynamic compression via Split Hopkinson Pressure Bar (SHPB) and (e) Dynamic Mechanical Analysis (DMA).

3.2.3.1 Quasi-static compression testing

An Imada model MX 500 load frame with a Z2H-440 2 kN load cell was prepared to carry out quasi-static compression testing. This load frame has an analog speed control, which was set to provide the lowest strain rate possible. Load and displacement data was acquired with Vic-Gauge 2006. The load was acquired after processing via a National Instruments PXI-1042. The use of DIC allows the direct measurement of strain, which makes the inevitable presence of

machine compliance irrelevant to the data collected. Specimens were tested at a strain rate of 10^{-4}/sec.

3.2.3.2 Quasi-static three point bend testing

An Imada model MX 500 load frame with a Z2H-440 2 kN load cell was prepared to carry out three point bend testing. This load frame has an analog speed control, which was set to provide the lowest strain rate possible. Load and displacement data was acquired directly into Microsoft Excel through a proprietary data acquisition system provided with the load frame by Imada.

(a) (b)

Figure 3.15. Imada load frame set up for 3-point bend testing.

3.2.3.3 Dynamic Izod impact testing

Izod impact testing was completed on a Tinius Olsen Model Impact 104, seen in Figure 3.16. Energy is transferred by a weighted pendulum to a notched

or un-notched sample in a cantilever configuration, as in Figure 3.17. The energy required to break the sample is lost by the pendulum, which continues on its path. By measuring the reduction in the height of the up-swing, the energy lost by the pendulum can be calculated.

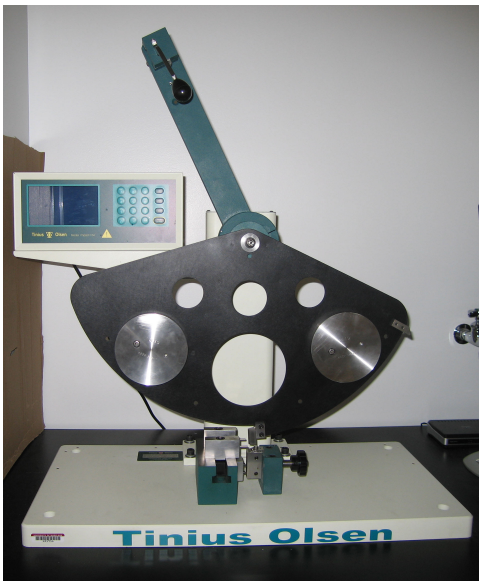

Figure 3.16. Tinius Olsen Model Impact 104 used for Izod impact and Charpy impact testing.

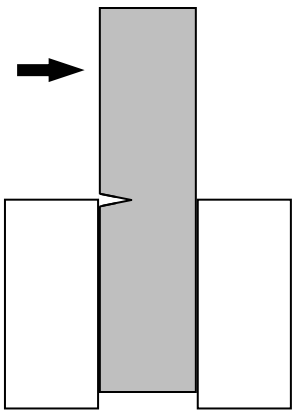

Figure 3.17. Schematic of cantilevered notched Izod impact specimen. Pendulum swings in direction of arrow.

3.2.3.4 Dynamic Charpy impact testing

Dynamic Charpy impact testing was also completed using a Tinius Olsen Model Impact 104. Energy is transferred by a weighted pendulum to a notched or un-notched sample in a configuration similar to a 3-point bend test, as in Figure 3.18. The energy required to break the sample is lost by the pendulum, which continues on its path. By measuring the reduction in the height of the up-swing, the energy lost by the pendulum can be calculated.

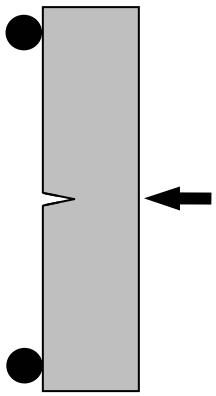

Figure 3.18. Schematic of notched Charpy impact specimen. Pendulum swings in direction of arrow.

3.2.3.5 Dynamic compression with Split Hopkinson Pressure Bar (SHPB)

The SHPB is a common method of testing samples in dynamic compression for the stress-strain response of materials. In this test, a sample is placed between two identical bars axially aligned with an air gun. A shockwave is transmitted to the incident (first) bar by an impact generated by a striker shot from the air gun. This shockwave propagates through the incident bar into the sample, and subsequently into the transmitted (second) bar. Strain gages are mounted on both incident and transmitted bars, and connected to an oscilloscope

through bridge amplifiers (BAMs) for digital data acquisition. Through comparison of the incident and transmitted shockwaves, dynamic material properties can be determined. A schematic of the SHPB can be seen in Figure 3.19.

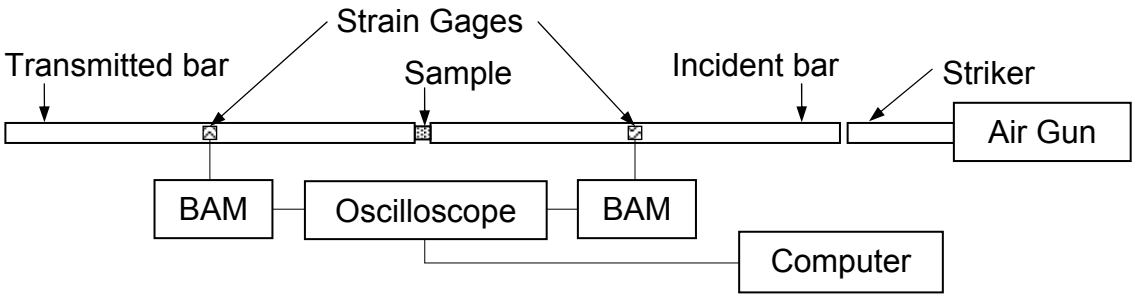

Figure 3.19. Schematic of Split Hopkinson Pressure Bar. Two strain gages are mounted on opposing sides of each bar.

3.2.3.6 Dynamic Mechanical Analysis (DMA)

A dynamic mechanical analyzer measures the stored and dissipated energies of a viscoelastic sample put under oscillation at varying temperatures. The stored energy depends on the polymer type, temperature, and frequency of oscillation and is represented by the modulus. The dissipated energy is represented by the loss modulus and is due to molecular friction occurring in viscous flow. The peak of the loss modulus was chosen as the glass-transition temperature. A Thermal Analysis (TA) Instruments 2980 DMA in a single-cantilever mode was used for testing (Figure 3.20). The specimens (4 mm wide x 8 mm long x 1.5 mm thick) were ramped at 5°C/min from room temperature to 120°C. All samples were tested in air.

Figure 3.20. Thermal Analysis (TA) Instruments 2980 DMA

3.2.3.7 Gas pycnometry

A gas pycnometer determines volume by measuring displaced gas. The pycnometer pumps a gas into a sample chamber and determines the pressure with a transducer. Then the gas is discharged into a second, empty chamber in order to determine the volume of material placed within the sample chamber. By taking a measurement of the mass of the material that is placed in the pycnometer, a measurement of volume can be easily obtained. Gas pycnometry was completed using a MicroMetrics AccuPyc 1330 pycnometer with Helium gas.

Figure 3.21. MicroMetrics AccuPyc 1330 pycnometer with Helium gas.

Chapter 4 Combinatorial processing of hierarchically-structured nano-enhanced thermoplastics

4.1 Characterization of the compositional gradient using pycnometry versus thermogravimetric analysis

While the composition of the steady-state nano-enhanced polymers could be determined from the relative feed rates of the polymer and nanoscale filler, the compositional gradient of the composites processed in the combinatorial approach had to be directly characterized or predicted. The compositional gradient was predicted *a priori,* as was described in [Kota08b], and characterized *a posteriori* using TGA and pycnometry measurements. The procedure used to determine the composition using TGA is described in detail elsewhere [Kota08b]. In order to determine the composition using pycnometry, the following relationship based on a simple rule of mixtures was used:

$$w_{\mathrm{CNF}} = \frac{1/\rho_{\mathrm{c}} - 1/\rho_{\mathrm{PS}}}{1/\rho_{\mathrm{CNF}} - 1/\rho_{\mathrm{PS}}} \qquad 4.1$$

where w_{CNF} is the weight fraction of CNFs, ρ_c is the density of the composite measured using a MicroMetrics AccuPyc 1330 pycnometer, ρ_{CNF} is the density of the CNFs, and ρ_{PS} is the density of the polystyrene.

Comparisons between the TGA and pycnometry results can be seen in Figure 4.1. Relative to TGA, pycnometry provides a much faster analysis and is easier to perform while producing similar results. Although it requires more mass (typically 1 g compared to 100 mg), a typical test involving 10 volumetric

measurements for statistical purposes can be conducted in approximately 20 minutes. To measure the wt. % for a single specimen using the previously established TGA technique required a test time of at least 3 hours at faster heating rates of 5°C/min. Thus, pycnometry can be a more desirable technique than TGA when it is important to verify the weight fraction of reinforcement for a large number of samples, and can also be easily used in conjunction with TGA to provide additional verification of the compositional gradient *a posteriori*. Furthermore, some constituents in nano-enhanced polymers may not provide clean separation of the thermal decomposition peaks, which makes pycnometry a very desirable technique for composition characterization.

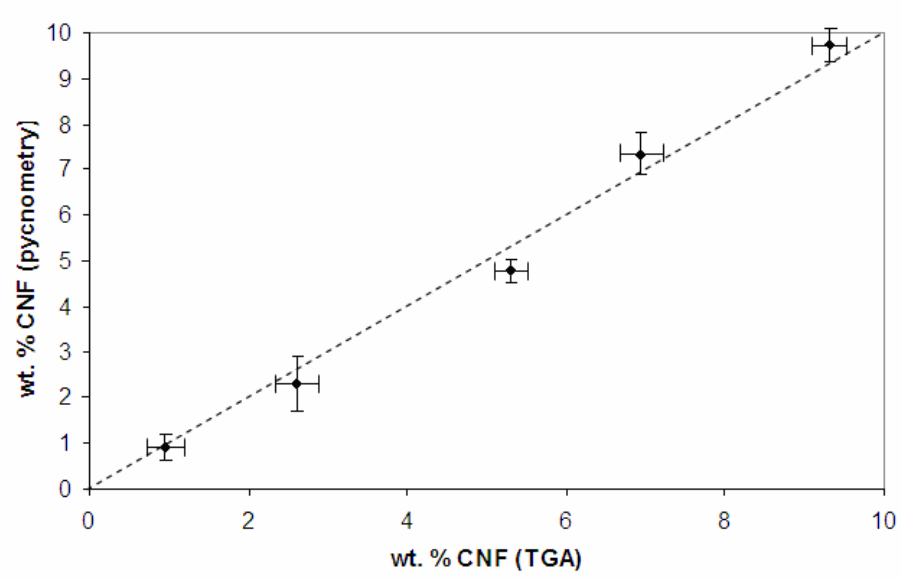

Figure 4.1. Comparison of weight percentage of CNF reinforcement in a nano-enhanced polymer obtained with TGA and with pycnometry indicating nearly identical results (dashed line).

The main advantage of a single combinatorial experiment over several steady-state experiments to produce composites over a compositional range is the minimal usage of expensive nanoscale fillers. In this work, composites

ranging from 0 to 10 wt. % of CNFs were produced using a total of 8.4 g of CNFs in the combinatorial approach. On the other hand, the steady-state composites required 2.4, 7.3, 12.6, 18.1, and 26.6 g of CNFs for the 1, 3, 5, 7, and 10 wt. % of CNFs respectively. Thus, the combinatorial approach requires about 87% less total CNFs.

In addition to rapid production of the composites via the combinatorial approach, it is important to rapidly and non-destructively characterize their composition. Figure 4.2 shows the compositional gradient of the composites processed in the combinatorial approach that was predicted a priori by the convolution model and verified a posteriori by pycnometry. The results from the convolution model and pycnometry correlate well with those from TGA. This establishes the validity of two rapid and high-throughput techniques to determine the compositional gradients instead of the time consuming and destructive TGA.

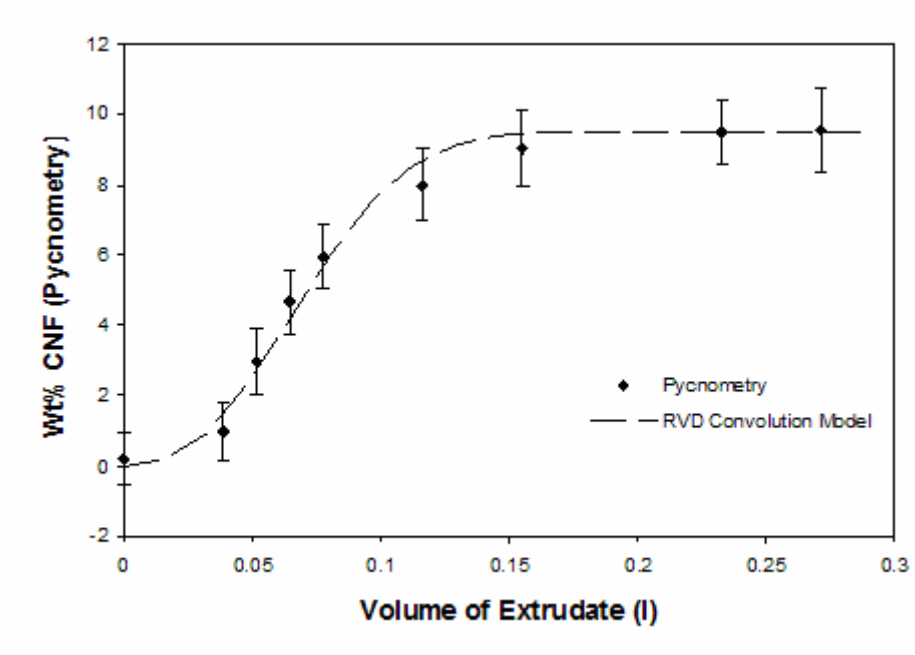

Figure 4.2. The compositional gradient determined by pycnometry resulting from a 10 wt. % step input of the filler and prediction from the RVD Convolution model.

In order to comprehensively validate the applicability of the combinatorial approach it is important to compare the quasi-static mechanical properties of the composites processed in the combinatorial approach with composites processed in steady-state. Representative stress-strain curves for the specimens at 0, 5, and 10 wt. % CNF loading are seen in Figure 4.4. In this work, tensile modulus, tensile strength, and strain to failure were chosen as the properties for comparison. Figure 4.5 compares the quasi-static tensile properties of sub-scale steady-state sub-scale combinatorial, and ASTM type I steady-state specimens in the composition range of 0 to 10 wt. % CNFs. It is evident that the results are nearly identical for the sub-scale specimens obtained from the combinatorial approach and the steady-state processing with the tensile modulus increasing linearly from 1.9 to 3.2 GPa, the tensile strength increases from 16 to 24 MPa and the strain to failure decreasing from 30% to 5% as the composition increases from 0 to 10 wt. % CNFs. Therefore, the use of a single combinatorial experiment instead of several steady-state experiments for determining the processing-structure-property relationships for nano-enhanced polymers is validated.

Provided sufficiently small samples are used, the combinatorial approach allows characterization of the material properties over a continuous range of composition without batch-to-batch variation in making the composites.

4.2 Characterization of mechanical property variation with CNF loading in thermoplastics

To characterize the quasi-static mechanical properties of the nano-enhanced polymers processed in the combinatorial approach, the sub-scale specimens were tested in a custom-built microtensile tester (Figure 3.14). This system was designed to accurately test sub-scale ASTM type I specimens using loads of less than 25 N, allowing for specimens with gage lengths 10 mm or less, widths 1.25 mm or less, and thicknesses of 1 mm or less to be easy obtained with nearly homogeneous compositions from within the gradient.

The polymer composites produced from known compositions from the steady-state experiments were characterized for their quasi-static mechanical properties and compared with those produced from the combinatorial approach. Two different sizes of specimens were prepared and tested at strain rates of 10^{-4}/sec: (a) ASTM type I specimens and (b) sub-scale ASTM type I specimens (Figure 4.3). The ASTM type I specimens were prepared in accordance with ASTM D638-03 Type I, and the sub-scale specimens were prepared such that they were proportional in size to ASTM type I specimens, but with a gage section that is a factor of 10 smaller. This geometry is closer to the ASTM Type V, but the width is approximately one third the size and the gage length is about one sixth smaller. The sub-scale specimens were CNC machined on a Boxford A3HSRmi^2 with a 1/64" end mill because larger end mills tended to overheat and melt the material fairly quickly. The ASTM type I specimen seen in Figure 4.3a has a total length of 167.5 mm, a gage length of 50 mm, a gage width of 12.7

mm, an overall width of 19.1 mm, and a thickness of approximately 1 mm. In contrast, the sub-scale specimen in Figure 4.3a and Figure 4.3b has a total length of 25.4 mm, a gage length of 5 mm, a gage width of 1.25 mm, an overall width of 3.7 mm, and approximate thickness ranges between 0.1 and 1 mm.

The sub-scale specimens were mounted to one axis of the microtensile tester with cyanoacrylate. Each sample was mounted as close to parallel as possible to the axis of the microtensile tester in order to minimize shear stress. After the cyanoacrylate had cured, the air supply for the air bearings was turned on to approximately 20 psi. At this point, the data acquisition software was initiated and the picomotors were actuated.

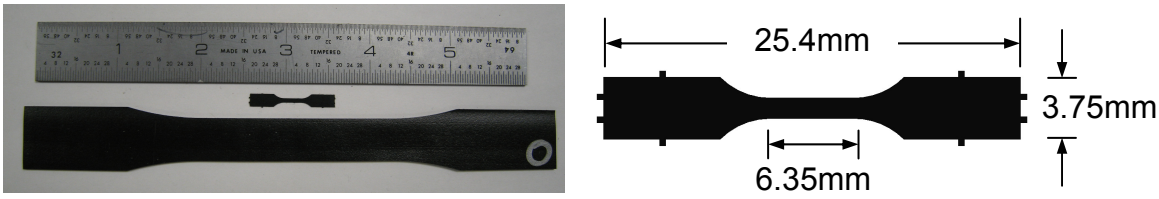

Figure 4.3. (a) sub-scale ASTM type I specimen with a gage length of 6.35 mm, along with a full-scale ASTM type I specimens which is seen beneath it for comparison, (b) dimensions of sub-scale ASTM type I specimen.

Steady-state composites were prepared in both the ASTM type I full-scale and sub-scale sizes, but the composites processed in the combinatorial approach were prepared only at sub-scale. The reason for this is the standard size specimens would have 50 mm of the composition gradient in the gage section, while the sub-scale specimens could be prepared with only 5 mm of the composition gradient is in the gage section, a 10X reduction in gradient effects.

Thus, the sub-scale specimens not only minimized the material needed for characterization, but also the compositional variation in the composites processed in the combinatorial approach to obtain more homogeneous specimens. With the sub-scale specimens, it is also possible to investigate the anisotropic effects of the extrusion process by obtaining specimens transverse to the direction of the compositional gradient with only 1 mm of the compositional gradient in the gage section, provided the width of the compositionally-graded extrudate were greater than the length of the specimen, which is 25.4 mm.

The ASTM type I specimens were tested using a Tinius Olsen tensile tester with a 25 kN load cell. The strain was calculated from the crosshead displacement using compliance correction, which has been verified in the gage section using DIC.

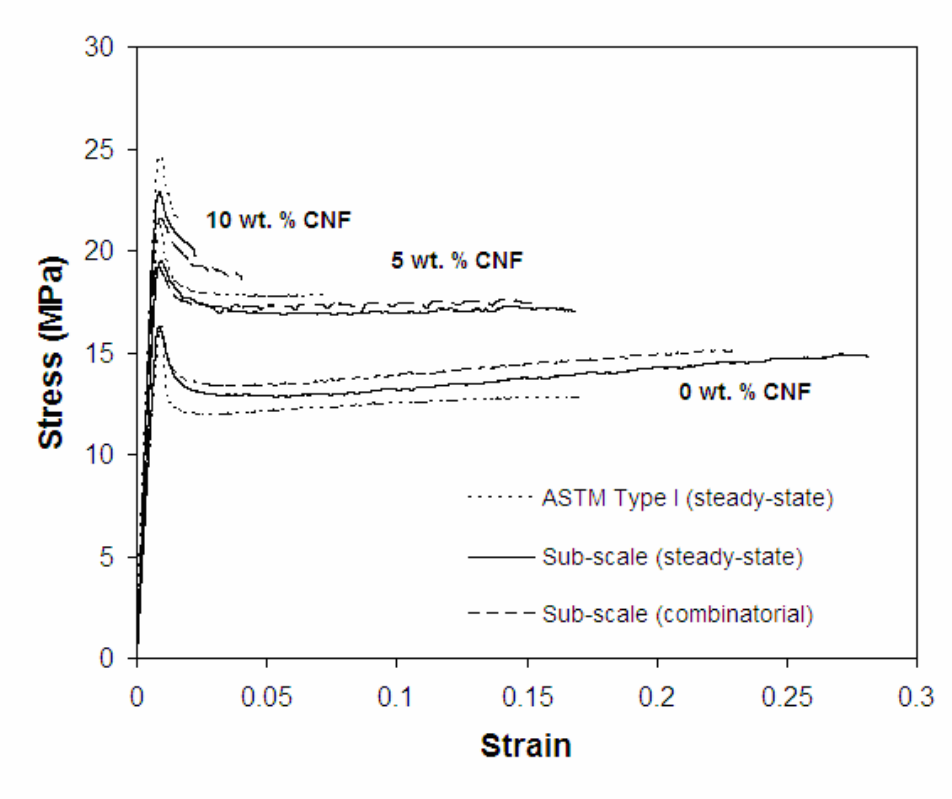

Figure 4.4. Representative stress-strain curves at 0, 5 and 10 wt. % for specimens processed at steady-state, tested in sub-scale and ASTM Type I geometries as compared to specimens processed combinatorially and tested in sub-scale geometries.

It is evident from Figure 4.5 that tensile modulus and tensile strength results for sub-scale and full-scale ASTM type I steady-state specimens are identical, but strain to failure of the latter is approximately 50% lower. This reduction in ductility may be due to the possibility that there is an increase in the number of processing-related defects, such as microporosity, as the specimen size increases. Thus, it has been demonstrated that the sub-scale testing technique and geometry can be used to obtain valid quasi-static mechanical properties for nano-enhanced polymers.

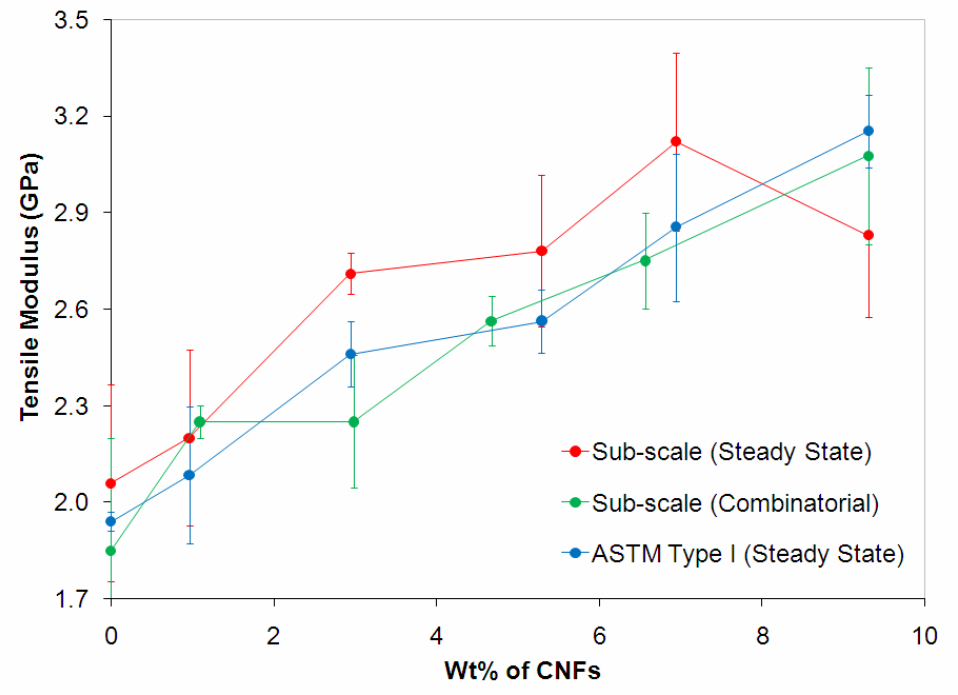
Tensile Modulus (GPa)
3.5
3.2
2.9
2.6
2.3
2.0
1.7
0
2
4
6
8
10
Wt% of CNFs
Sub-scale (Steady State)
Sub-scale (Combinatorial)
ASTM Type I (Steady State)

(a)

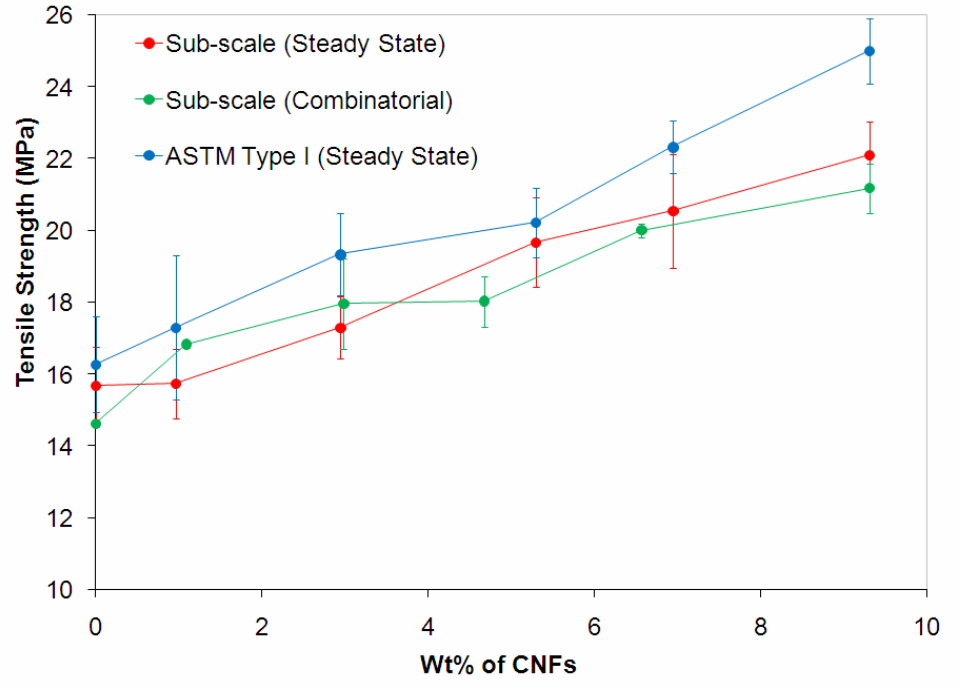
Tensile Strength (MPa)
26
24
22
20
18
16
14
12
10
0
2
4
6
8
10
Wt% of CNFs
Sub-scale (Steady State)
Sub-scale (Combinatorial)
ASTM Type I (Steady State)

(b)

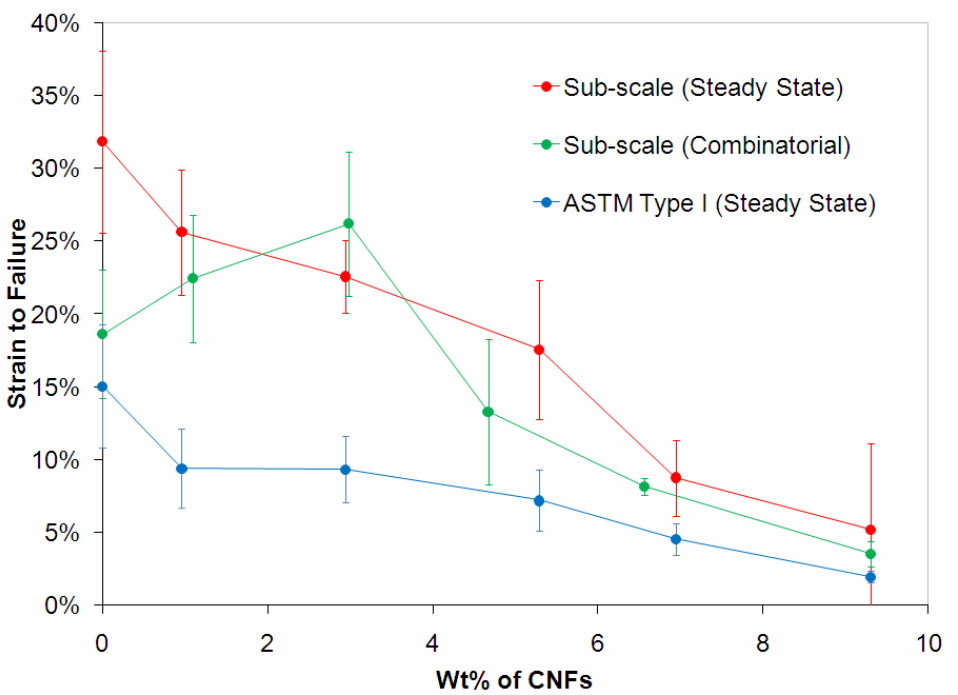

(c)

Figure 4.5. Comparison of quasi-static mechanical properties obtained with sub-scale specimens obtained from processing in steady-state and in the combinatorial approach, as well as ASTM type I specimens obtained from processing in steady-state. (a) Tensile Modulus, (b) Tensile Strength, and (c) Strain to Failure.

4.3 Summary

Using this combinatorial approach to materials processing allowed a fast characterization of many different loading levels of CNF using PS as a model thermoplastic. The ability to quickly determine the wt. % of CNF at any point along the compositional gradient allowed for rapid transition from a gradient material to tensile specimens with known wt. % of CNF. The insights that were garnered through the characterization and modeling of these model polymers provide a basis for developing a multi-scale mechanical characterization approach to the understanding of processing-structure-property relationships in hierarchically-structured nano-enhanced thermoplastics that then can be

extended to thermosets using West system as a model epoxy. Furthermore, the relative benefit of using microscale ingredients in addition to the nanoscale to control the hierarchical structure can be understood adding chopped CMFs to LDPE, which is a thermoplastic more amenable to processing into compression specimens that can be easily used to simultaneously characterize and model strain rate effects. For the thermosets, Carbon fiber veils that are often used as EMF shielding were studied since they would enhance multifunctional properties as well.

Chapter 5 Multi-scale mechanical characterization and modeling of hierarchically-structured nano-enhanced thermoplastics and epoxies

5.1 Nano-mechanical testing and multi-scale modeling of nano-enhanced thermoplastics

In order to obtain further insight into the structure of the nano-enhanced polymers and the effects on the static mechanical properties at the nanoscale, a Hysitron Triboindenter was used to test the elastic modulus. Optical micrographs from a 5 wt. % CNF in PS specimen clearly indicated the presence of agglomerates of CNFs in the nano-enhanced polymers (Figure 5.1a). Additional details of the structure of the agglomerates and the dispersion of the CNFs can be seen in Figure 5.2 from a backscattered SEM image of the 5 wt. % CNF in PS specimen. This gives rise to the model of the hierarchical structure formed by the interaction between the agglomerates and dispersed CNFs seen in Figure 5.1b.

Using the nanoindenter, it was possible to isolate the modulus of the microscale structures represented by the agglomeration of CNFs from that of the matrix material reinforced by dispersed CNFs. By isolating the moduli of the microscale structures from the matrix, it is possible to develop a multi-scale model of the effects of these structures on the hierarchically-structured polymer composite in a manner that is similar to the multi-scale model previously developed by the Bruck research group for describing the effects of MWCNT

percolation on rheological properties of the composite in the melt state [Kota07c]. Thus, the average modulus of an individual agglomerate was determined to be 4.2 GPa, while the matrix surrounding it was 2.7 GPa.

To develop a multi-scale model of the effects of the CNFs in the matrix and agglomerates, the hierarchically-structured polymer composite was modeled as being reinforced by dispersed nanofibers and microscale agglomerates of nanofibers that were fully infiltrated by polymer creating highly filled regions rather than the interpenetrating-phase structure used in the multi-scale model of rheological properties. To determine the concentration of fibers in the, the volume fraction of the agglomerates, $v_{agglomerate}$, were directly determined from the optical micrograph, and then used with the volume fraction of CNFs, v_{CNF}.to determine the elastic modulus of the bulk composite, $E_{composite}$, from the modulus of the polymer matrix, E_{matrix}, and the modulus of the nanofibers, E_{CNF}, using a linear Rule-of-Mixtures (ROM) formulation as follows:

$$E_{composite} = E_{CNF}\left(v_{CNF} - \frac{v_{agglomerate}E_{agglomerate}}{E_{CNF}}\right) + E_{agglomerate}v_{agglomerate} + \\ + E_{matrix}\left(1 - v_{agglomerate} - v_{CNF} + \frac{v_{agglomerate}E_{agglomerate}}{E_{CNF}}\right) \quad \textbf{5.1}$$

for a 5 wt. % CNF nano-enhanced polymer, the volume fraction of agglomerates was determined to be 10%. In this model, it is assumed that the volume fraction of the dispersed CNFs is high enough that the nanofibers “percolate” and create an interpenetrating phase composite with the polymer matrix that has a modulus well-predicted by a linear ROM formulation, similar to the model proposed for rheological properties.

Since the nanoscale contribution to the modulus from the nanofiber was not known, it was determined indirectly by extrapolating the small-scale tensile data to 100 wt. % CNF, which resulted in a modulus of 15 GPa. Using this value, the bulk modulus of the composite was predicted to be 2.6 GPa, which was nearly identical to the measured value. In addition, Equation 5.1 can be used to determine the maximum value that would be expected for no agglomerates. The result is 2.8 GPa, which is only about 8% greater than what was obtained. Thus, it may be concluded that although the CNFs are not "perfectly" dispersed in the polymer matrix, the hierarchically-structured polymer composite actually has a similar modulus. Furthermore, the applicability of a linear ROM formulation provides evidence that the percolated nanoscale CNFs provide a "load transfer" mechanism between the microscale agglomerates rather than just isolating the load bearing capacity of the agglomerates from each other, which would produce a "softer" response better predicted by an inverse ROM formulation.

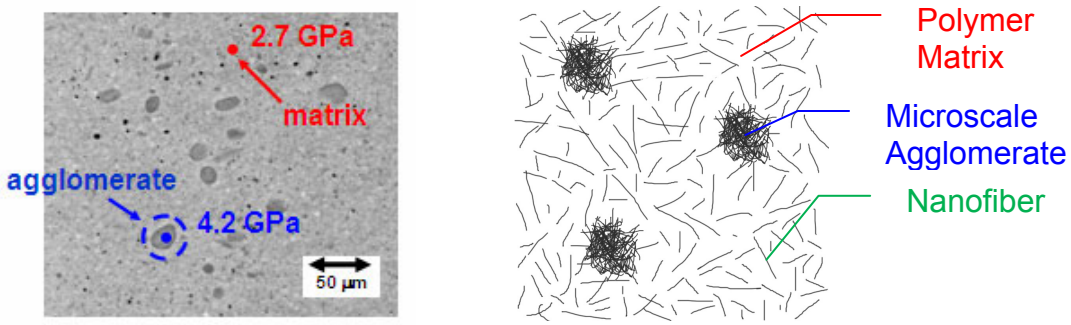

Figure 5.1. Nanomechanical characterization of agglomerates in 5 wt. % CNF polymer composite and model of CNF filler in matrix and agglomerates used to predict bulk elastic modulus.

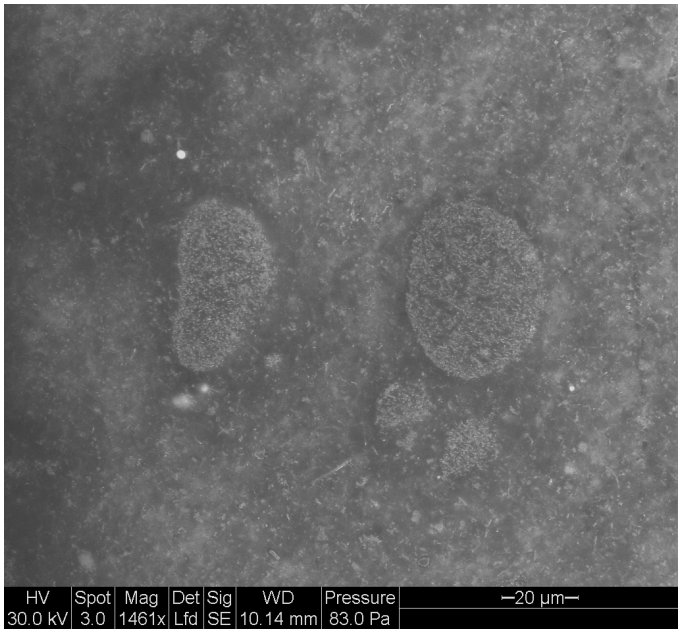

Figure 5.2. Back-scattered SEM image of agglomerates and surrounding dispersed CNFs from a 10 wt. % CNF in PS sample.

5.2 Characterization of mechanical property variation with CNF loading and processing conditions in West System epoxy

5.2.1 Optical characterization

In order to optically determine the effects of sonication, optical micrographs were obtained with an OptixCam Summit 5.0 digital camera mated to a Versamet-2 Unitron 7103 inverted microscope with a 5x objective lens using transmitted light, as can be seen in Figure 5.3 for the 7 wt. % CNF composite which was the highest loading whose microstructure could be easily distinguished using the transmitted light mode. It can clearly be seen that the length of sonication time has a direct effect upon the agglomeration size and the subsequent hierarchical structure that develops. Furthermore, as the CNFs become more dispersed, the transmissivity of the composite decreases and the images become darker. It does appear, however, that the amount of energy

delivered to the agglomerations during sonication is not sufficient to completely disperse the CNTs. Thus, the optical micrographs provide direct evidence of the break-up of agglomerates and increase in dispersion with sonication time.

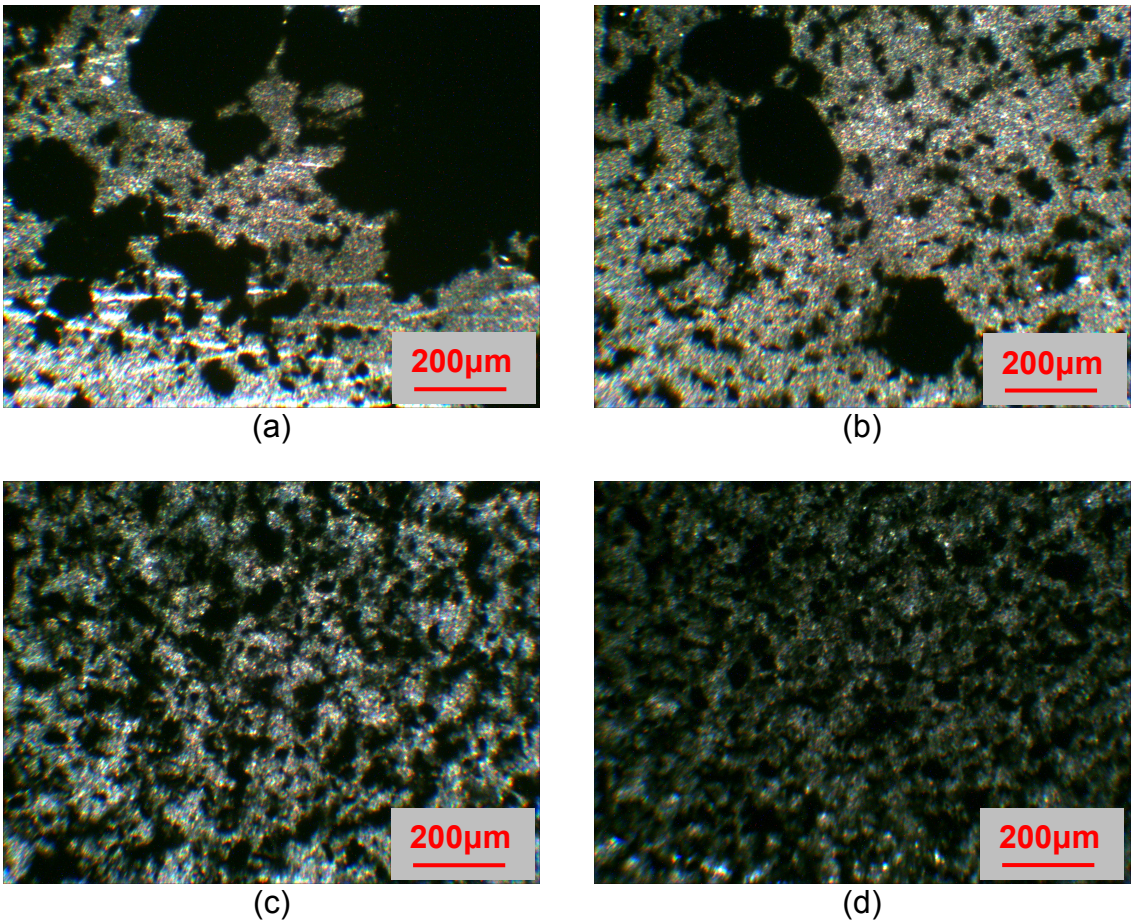

Figure 5.3. Effects of sonication on 7 wt. % CNF in West System epoxy.
(a) No sonication, (b) 90 minutes sonication,
(c) 3 hours sonication, (d) 6 hours sonication.
Images obtained using transmission light microscopy.

5.2.2 Microtensile characterization

The effects of sonication time on tensile mechanical properties were also obtained using microtensile testing. The results can be seen for 1, 3, 5, 7, and 10 wt. % CNF in Figure 5.4 for tensile modulus, tensile strength, and % elongation to break as a function of the wt. % CNF loading. In Figure 5.5, the data is presented as a function of the sonication time. In both figures, it can easily be seen that the material properties are affected by sonication time. However, it appears that increasing the wt. % of CNFs does not necessarily result in a continuous increase in the mechanical properties with sonication time. Thus, it would appear that the evidence of the limit of dispersion seen in the optical micrographs is also evident in the tensile mechanical properties.

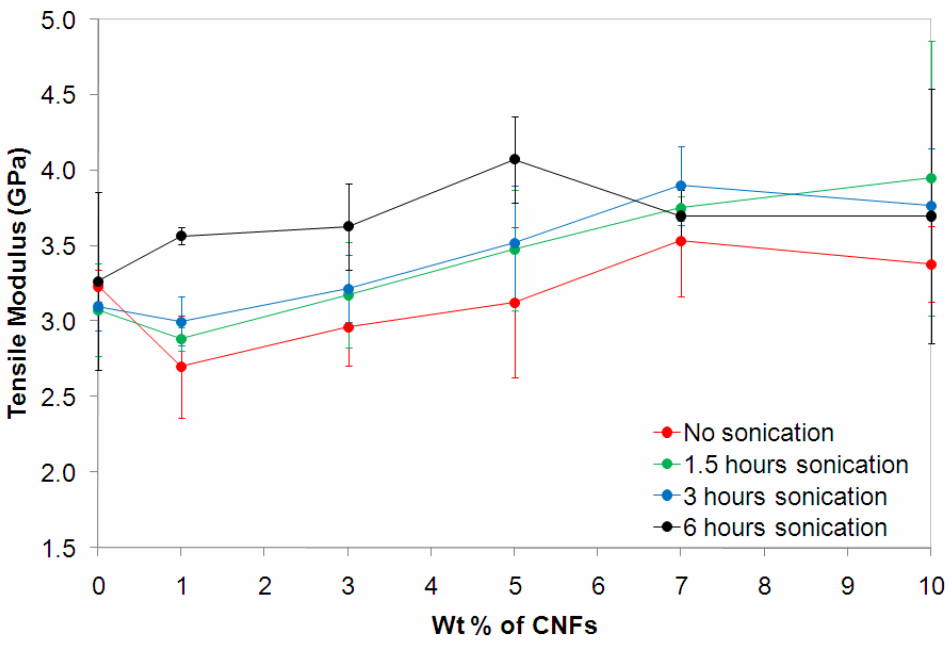

(a)

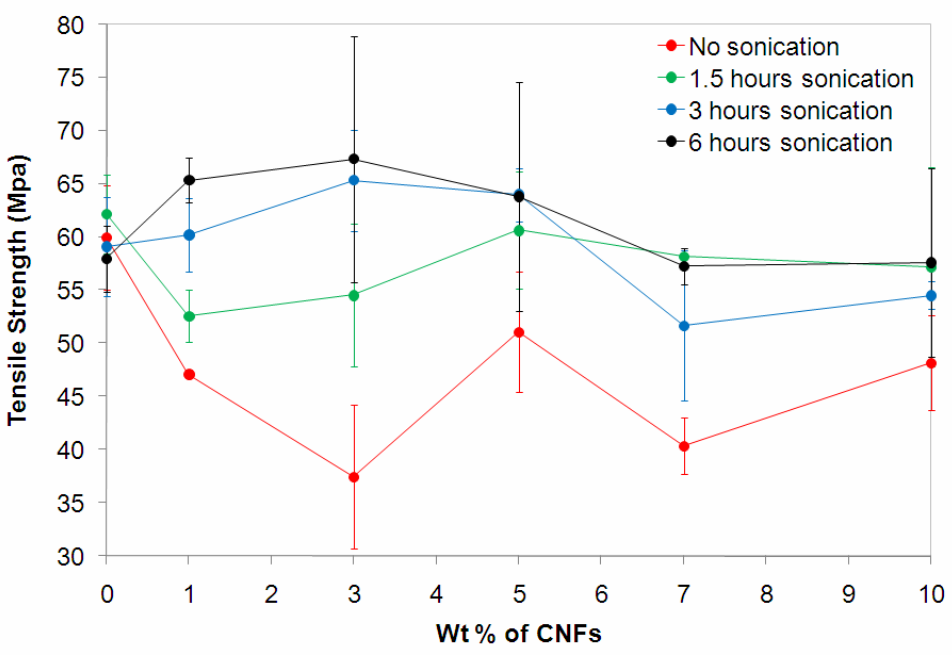

(b)

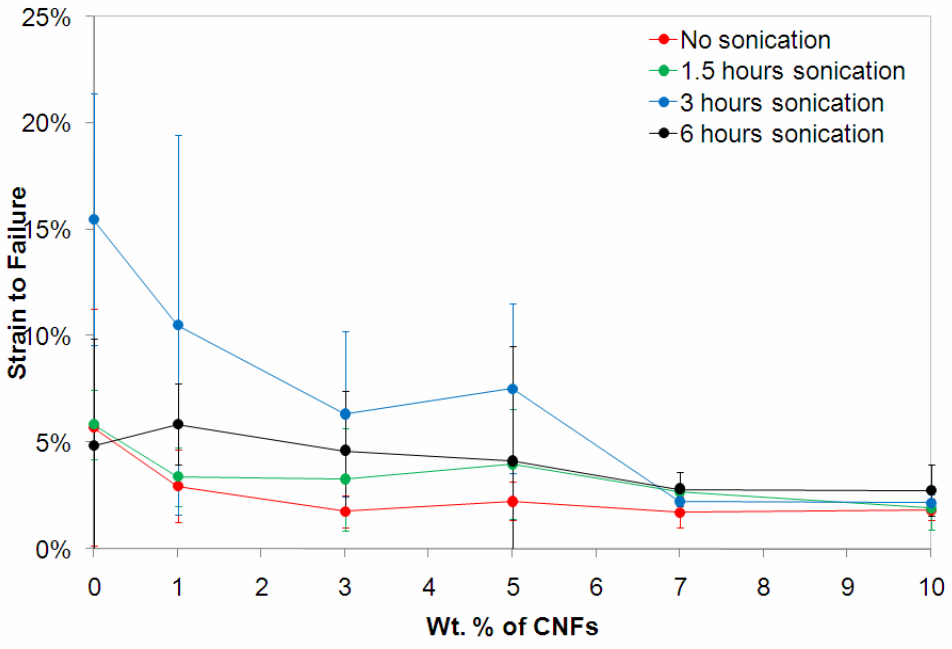

(c)

Figure 5.4. Properties as a function of CNF loading in nano-enhanced West System epoxy. (a) Tensile modulus, (b) tensile strength and (c) strain to failure.

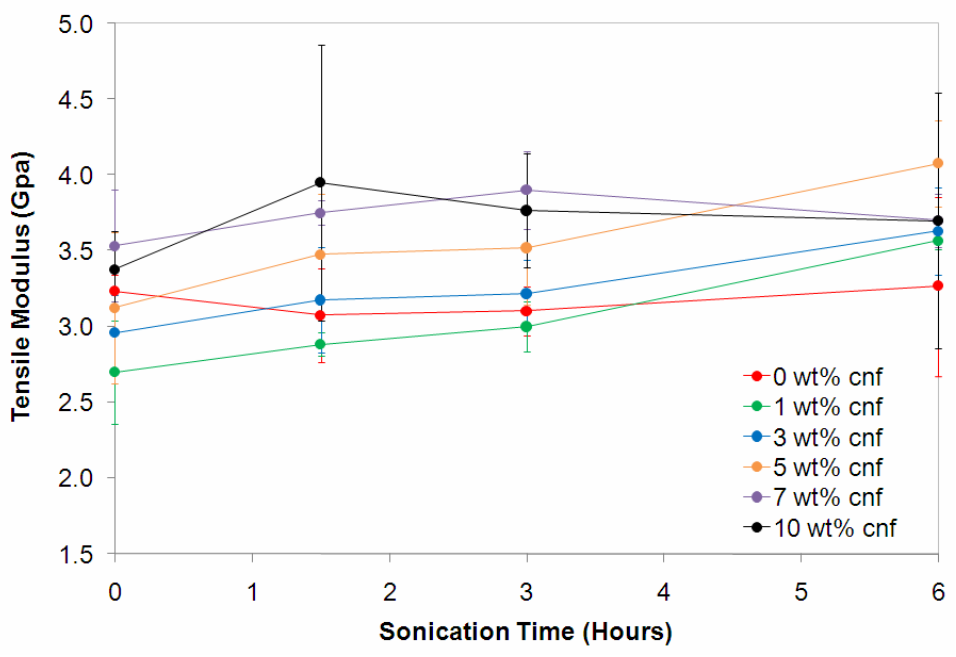
Tensile Modulus (Gpa)
5.0
4.5
4.0
3.5
3.0
2.5
2.0
1.5
0
1
2
3
4
5
6
Sonication Time (Hours)
0 wt% cnf
1 wt% cnf
3 wt% cnf
5 wt% cnf
7 wt% cnf
10 wt% cnf

(a)

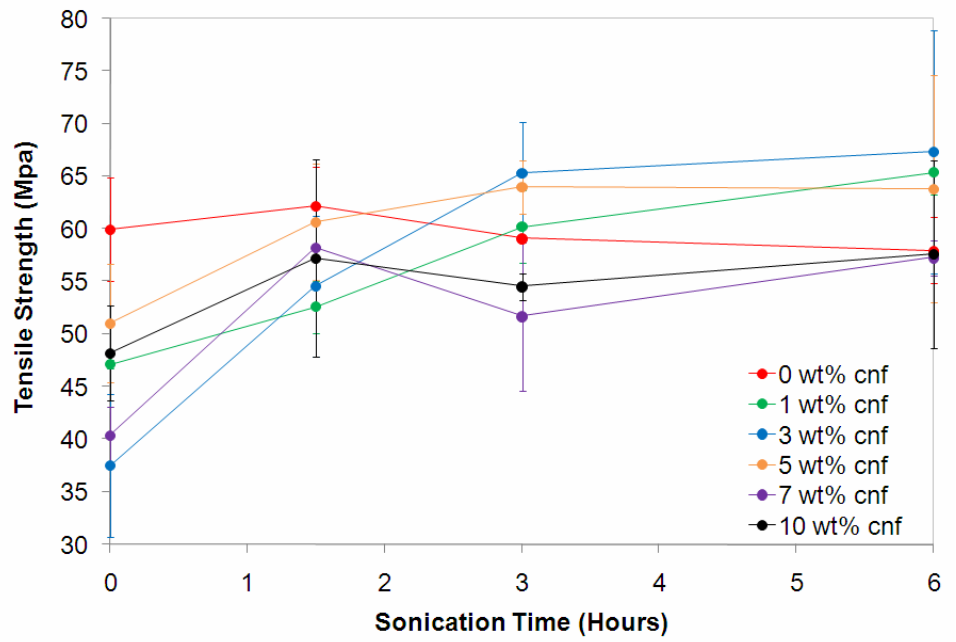
Tensile Strength (Mpa)
80
75
70
65
60
55
50
45
40
35
30
0
1
2
3
4
5
6
Sonication Time (Hours)
0 wt% cnf
1 wt% cnf
3 wt% cnf
5 wt% cnf
7 wt% cnf
10 wt% cnf

(b)

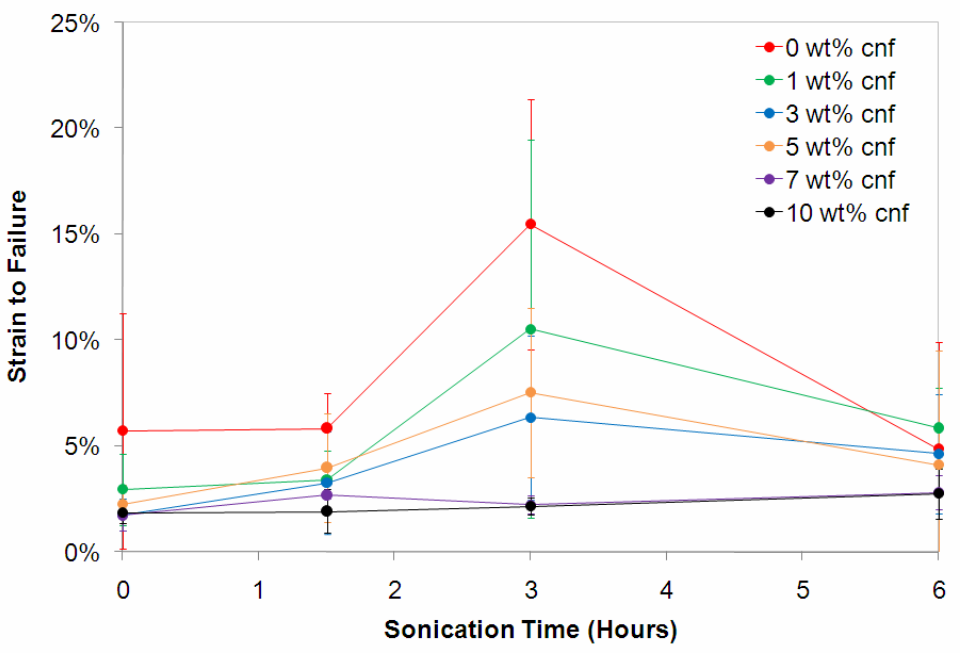

(c)

Figure 5.5. Properties as a function of sonication time of nano-enhanced West System epoxy. (a) tensile modulus, (b) strength and (c) strain to failure.

In order to gain greater insight into the dispersion of the CNFs due to sonication in solvent-processed thermoset polymers, the previously developed multi-scale model used for the melt-processed thermoplastic polymers was applied to predicting the tensile mechanical properties as a function of sonication time. It was assumed that the addition of CNFs would be in agglomerate form and would be fully infiltrated consistent with the previous model reflected in Equation 5.1. However, as the material is sonicated the amount of agglomerates infiltrated decrease and a percentage of the nanofibers disperse. Based on the previous data from section 5.1, the values predicted for the Tensile Modulus can be seen in Table 5.1 along with the measurements of the volume fraction of agglomerate, the modulus of the agglomerate, and the volume fractions of dispersed CNFs. A plot of the resulting moduli for the composites as a function

of the sonication time can be seen in Figure 5.6. These predictions are very similar to the experimental results in Figure 5.5a.

The values for the model indicate that there is a volume fraction of agglomerates that is significantly greater than that expected for the wt. % CNFs since the agglomerates are dispersed over larger volumes. Furthermore, they are much harder than the matrix material, consistent with the effects seen in the melt-processed thermoplastic polymers. As sonication time increases, these agglomerates are broken up, but there appears to be a dispersion limit to the amount of dispersed CNFs that can be absorbed into the matrix. This value would tend to be 3 to 3.5 vol. % from the measurements of agglomerate volume fraction and the properties of the agglomerates, and indicates a dispersion limit for the CNFs in the adhesive that limits the development of the hierarchical structure as was evidenced in the optical micrographs. This dispersion limit is most probably a function of the temperature and the ultrasonic energy. Increases in both will most likely increase the dispersion limit to higher values due to the disruption of the adhesive combined with lower viscosity. Because of this dispersion limit, it would appear that the benefits of sonication are limited to smaller wt. %, in this case below 7 wt. %. At higher wt. % the agglomerates in the mixture with no sonication are sufficiently infiltrated during mixing that they experience very little improvement as the dispersed CNFs saturate the adhesive.

Wt. % CNF	Sonication Time (hr)	V_{CNF}	$V_{agglomerate}$	$E_{agglomerate}$ (GPa)	$E_{composite}$ (GPa)
1	0	0.0014	0.02	4.2	3.23652
1	1.5	0.004067	0.01	4.4	3.0388
1	3	0.004133	0.01	4.3	3.0386
1	6	0.007	0	n/a	3.259
3	0	0.004	0.06	4	3.2362
3	1.5	0.008	0.04	4.5	3.096
3	3	0.013867	0.02	4.6	3.1384
3	6	0.017133	0.01	4.3	3.354173
5	0	0.004667	0.1	4.4	3.268867
5	1.5	0.0176	0.06	4.1	3.1692
5	3	0.0276	0.02	4.8	3.2592
5	6	0.030867	0.01	4.7	3.473027
7	0	0.0004	0.14	5.1	3.31732
7	1.5	0.016	0.1	4.8	3.216
7	3	0.0292	0.06	4.7	3.2964
7	6	0.034933	0.04	4.9	3.526813
10	0	0.0066	0.18	5.2	3.41368
10	1.5	0.015667	0.16	5	3.28
10	3	0.023267	0.14	4.9	3.3172
10	6	0.0314	0.12	4.7	3.52632

Table 5.1. Constants obtained from the multi-scale ROM model that quantifies effects of sonication time on tensile modulus of the composite due to the formation of the hierarchical structure due to dispersion of the CNFs.

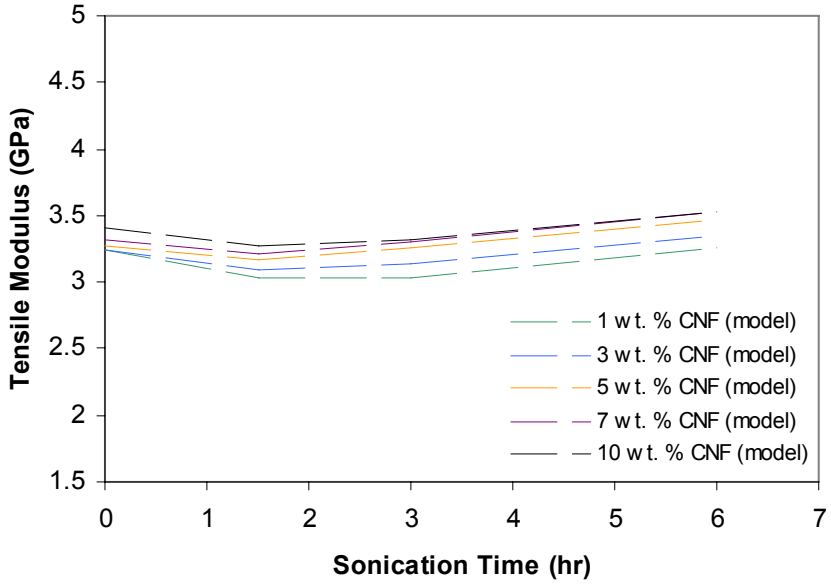

Figure 5.6. The predicted variation in the tensile moduli with sonication time.

From the data in Table 5.1, it is now possible to define the "degree of dispersion", *D*, as a function of sonication time, *t*, where the degree of dispersion is relative to the maximum amount of solubility of the CNFs in the epoxy. The dispersion process itself can be modeled using the following conventional Avrami equation below (Equation 5.2):

$$D = 1 - \exp\left(\frac{t}{\tau}\right)^{p} \qquad \textbf{5.2}$$

where τ is the time constant for the dispersion process and *p* is the Avrami exponent. Thus, the Avrami equation can be used to extract the time constant for the dispersion process associated with sonication. The degree of dispersion from the data in Table 5.1 and the resulting fit of the Avrami equation can be seen in Figure 5.7. The resulting time constant for the diffusion process was determined to be 2 hours, while the exponent was determined to be 1. Thus, the

physics of the dispersion process for sonication is such that 2 hours would be the time required to achieve reasonable dispersion.

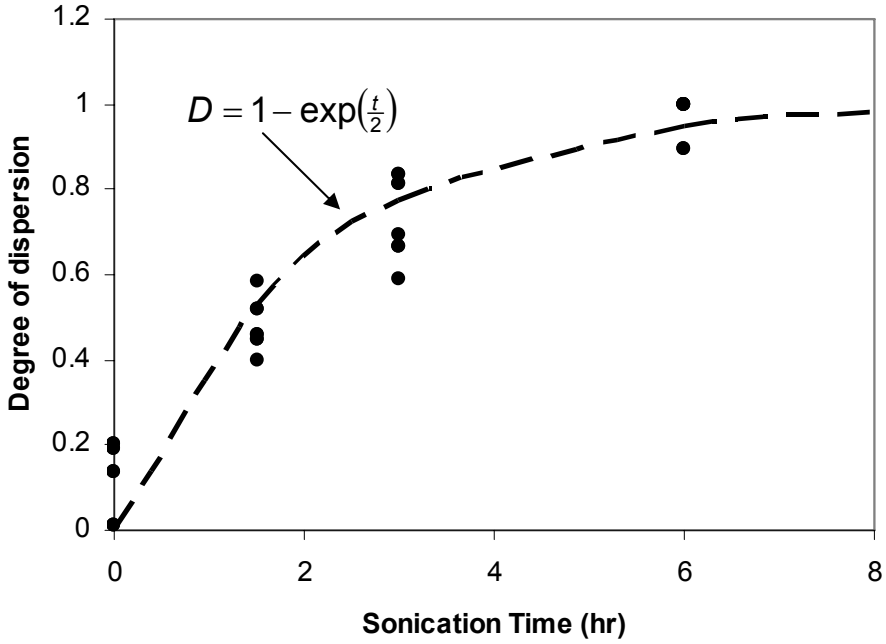

Figure 5.7. The degree of dispersion versus sonication time with the Avrami fit to determine the time constant.

5.2.3 Nanomechanical characterization using modulus mapping

Modulus maps were made of the four different sonication times were also made for the nano-enhanced West System epoxy to determine the effects of dispersion on the mechanical property variations at the nanoscale. An example of the maps for the complex modulus of 3 wt. % CNF specimens at different sonication times can be seen Figure 5.8. The topographical representations of the surface of these specimens can also be seen in Figure 5.9 for comparison. Note that the surface geometry has an effect on the perceived complex moduli of

the materials and therefore quantitatively affects the accuracy of these measurements and the ability to compare directly with the microtensile characterization results, unlike the quasi-static nanomechanical measurements. However, it can still be used to compare with the optical micrographs to determine the effects of dispersion on the localized property distributions.

From these modulus maps, it can be directly seen that the dispersion of the CNFs as a function of sonication time can be seen through the homogenization of the property fields on the nanoscale. For no sonication, large agglomerates cause significant variation across the property fields. As the sonication time increases, this variation is reduced until after 6 hours of sonication there are few areas of property variation that can be easily distinguished and the only variation that remains is associated with the surface roughness of the specimen due to polishing.

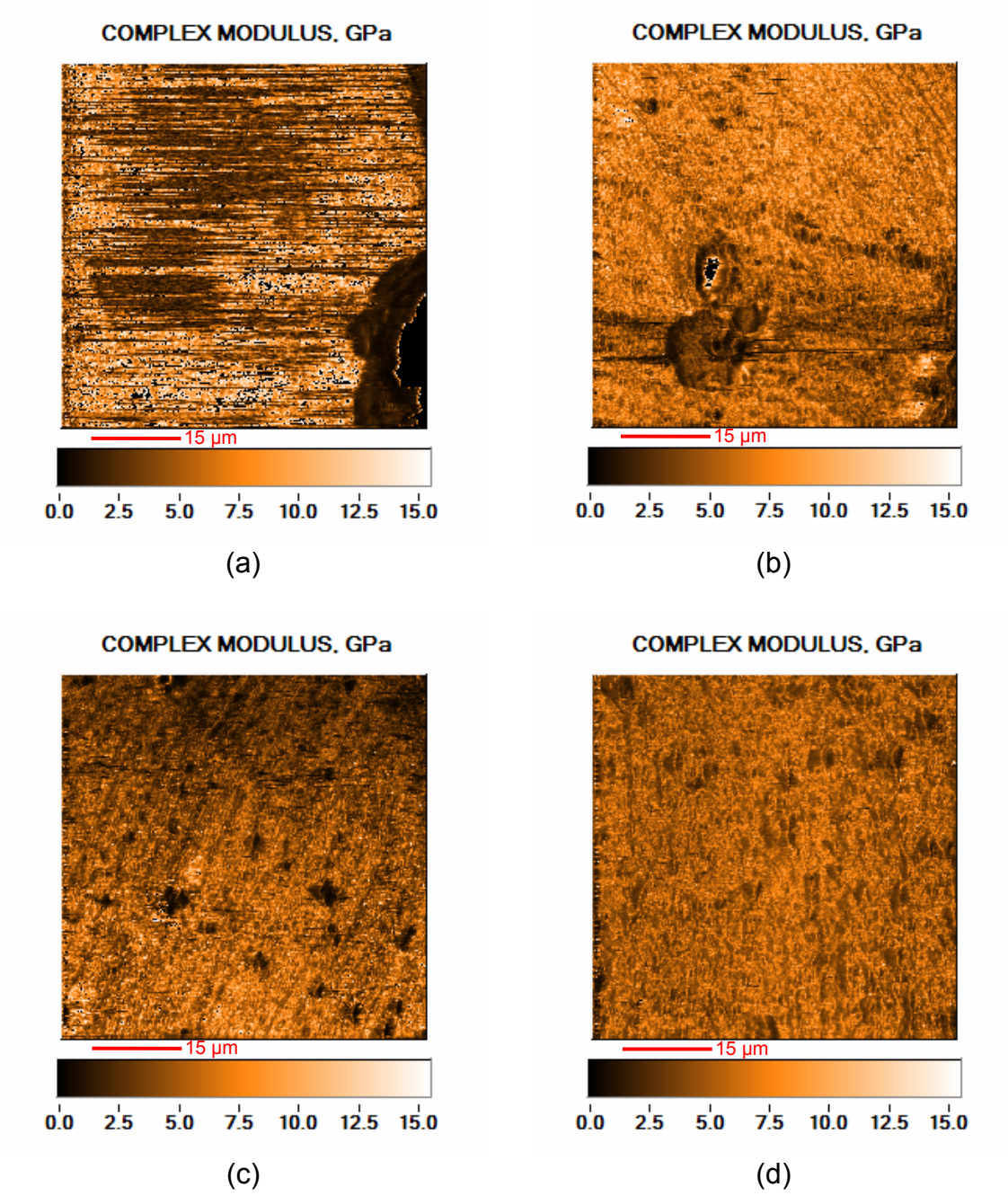

Figure 5.8. 60 µm modulus maps of 3 wt. % CNF in West System with (a) no sonication, (b) 1.5 hours of sonication, (c) 3 hours of sonication and (d) 6 hours of sonication during processing.

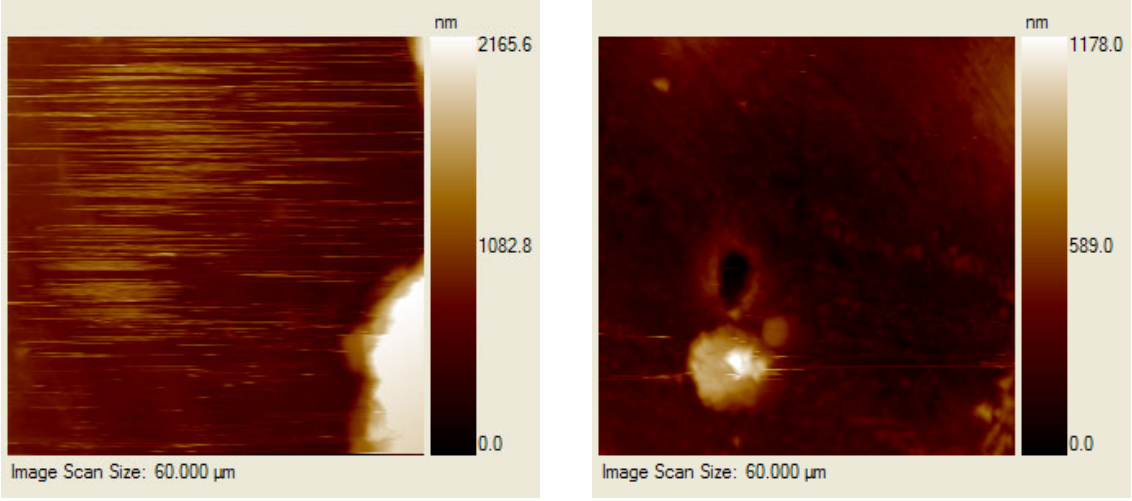

(a) (b)

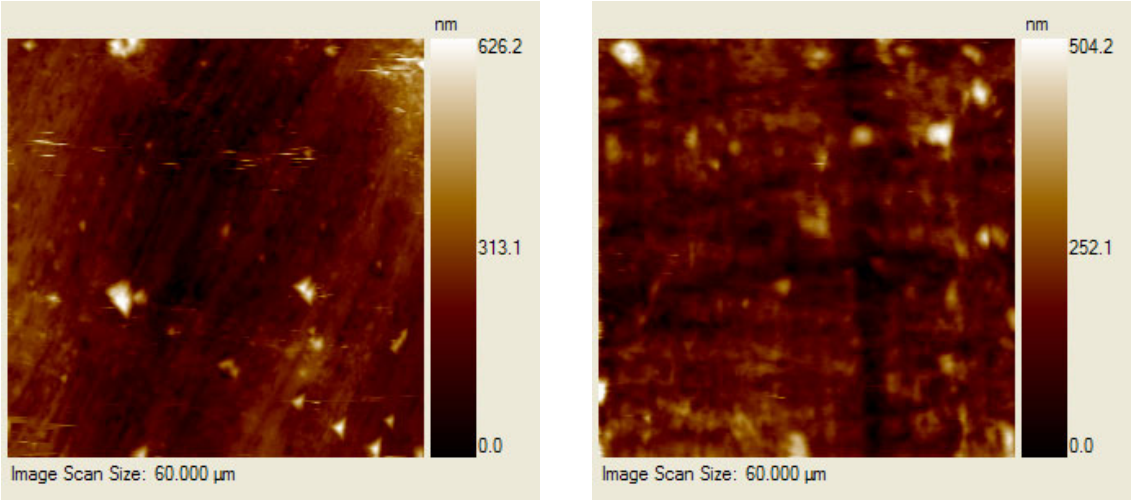

(c) (d)

Figure 5.9. Topographical representations of 3 wt. % CNF in West System with (a) no sonication, (b) 1.5 hours of sonication, (c) 3 hours of sonication and (d) 6 hours of sonication during processing.

5.3 Quasi-static and dynamic compression characterization and modeling of nano-enhanced thermoplastics with CMF reinforcement

In order to understand the effects of adding CNFs to polymer composites with CMFs, cylindrical specimens were prepared that were 6 mm in diameter and 6 mm in length with 0 wt. % CNF/CMF, 10 wt. % CNF, 10 wt. % CMF, and 5 wt. % CNF/5 wt. % CMF in order to understand the enhancement of the polymer matrix performance by the addition of CNFs and CMFs, as well as the relative performance of equal amounts of CNFs, CMFs or a combination of the two.

Quasi-static compression tests were conducted in the Imada screw-driven load frame, while dynamic compression tests were conducted in a Split Hopkinson Pressure Bar using 16 mm diameter aluminum bars that were 1 meter in length. All tests were conducted at strain rates of 2500/sec. The results can be seen in Figure 5.10. From these results, it can be seen that the CNF increases the strength of the polymer by 5 MPa, while there is nearly a 35 MPa increase when CMFs are added, about 7 times greater. Also, the CNFs have a rule-of-mixtures (ROM) filler effect on the CMF-reinforced polymer composite, similar to the multi-scale model for the tensile properties, that is described by the following stress-strain formulation:

$$\sigma_c = E_{LDPE}V_{LDPE}\varepsilon_c + E_{CMF}V_{CMF}\varepsilon_c + E_{CNF}V_{CNF}\varepsilon_c + E^t_{LDPE}V_{LDPE}\varepsilon_c + E^t_{CMF}V_{CMF}\varepsilon_c \qquad \textbf{5.3}$$

where the E and E^t are the effective modulus and tangent modulus of the polymer and CMF/CNFs can be seen in Table 5.2.

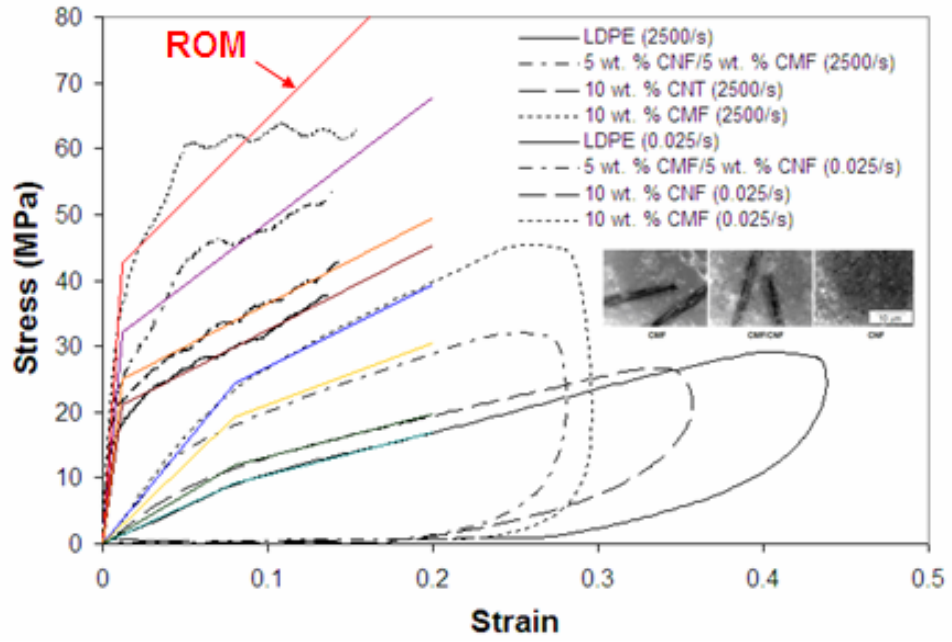

Figure 5.10. Dynamic compressive behavior of hierarchically-structured polymer composites with CMF and CNF filler at strain rates of 2500/sec indicating a slight increase in performance with CNF addition, and rule-of-mixture effect when added to a CMF composite.

Material	Property	Static Value	Dynamic Value
LDPE	Elastic Modulus	120 MPa	1800 MPa
	Tangent Modulus	65 MPa	130 MPa
	Elastic Strain Limit	0.08	0.012
CMF	Elastic Modulus	1850 MPa	18500 MPa
	Tangent Modulus	600 MPa	600 MPa
CNF	Elastic Modulus	600 MPa	7200 MPa

Table 5.2. Material Properties obtained from the ROM model in Equation 6.2 for the dynamic compressive behavior of the hierarchically-structured CMF-CNF composites.

The results in Table 5.2 indicate that the elastic behavior of the CMF reinforcement effectively increases by a factor 10 under dynamic compression. However, there appears to be no change in the tangent modulus due to the

increase in strain rate. Furthermore, the CNF appears to increase its elastic behavior by a factor of 12, with no effect on the tangent modulus of the composite at either low or high strain rates. Comparatively, the CNF reinforcement is about 33% of the stiffness of CMF reinforcement at low strain rates and nearly 40% of the stiffness at high strain rates.

The reduction in mechanical reinforcement of CNF relative to CMF is not surprising given the low value of inherent stiffness associated with CNF from the microtensile characterization due to the “spring-like” effect from the geometry of the CNF. The CMFs tend to be much straighter, and therefore have a much greater effective modulus. Furthermore the reinforcing effects tend to indicate that the fibers are not aligned in the direction of compressive loading and are closer to the transverse direction. Thus, it can be concluded that the CMF is a superior reinforcement to the CNF at both low and high strain rates for the thermoplastic polymer, and that the solvent-processed hierarchical composite does not exhibit any improvement in mechanical properties beyond that predicted from a Rule-of-Mixtures combination of CMF and CNF.

5.4 Characterization of mechanical property variation with CNF loading and processing conditions in West System epoxy – CMF hierarchically-structured composites

5.4.1 Microtensile characterization

After establishing the processing-structure-property relationship for hierarchically-structured polymer composites at multiple length scales using both thermoplastic and thermoset polymer matrices, it was decided to focus on developing hierarchically-structured polymer composites using a "top-down" approach based on the reinforcing of an epoxy matrix using a carbon-microfiber mat. The mat itself inherently has negligible structural properties, therefore it is not expected to provide substantial enhancement of the epoxy properties upon infiltration. Tests were then conducted using the CNF nano-enhanced polymers at different sonication times and the 1, 3, 5, 7, and 10 wt. % loadings that were previously investigated.

The hierarchically-structured nano-enhanced West System contains an embedded sheet of microscale carbon fiber 0.05 mm thick. This material does not appear to be sensitive to sonication time in the production of the nano-enhanced West System epoxy. As the uncured nano-enhanced West System flows around the carbon fibers during processing, CNFs tend to agglomerate around areas where micro fibers meet and along microfibers, counteracting the dispersive effects of sonication. Images of these agglomerations were taken with an OptixCam Summit 5.0 digital camera mated to a Versamet-2 Unitron 7103 inverted microscope with a 5x objective lens using transmitted light, as can be

seen in Figure 5.11. Once again, the enhanced dispersion of the CNFs due to sonication time is directly evident by the darker matrix in the optical micrographs.

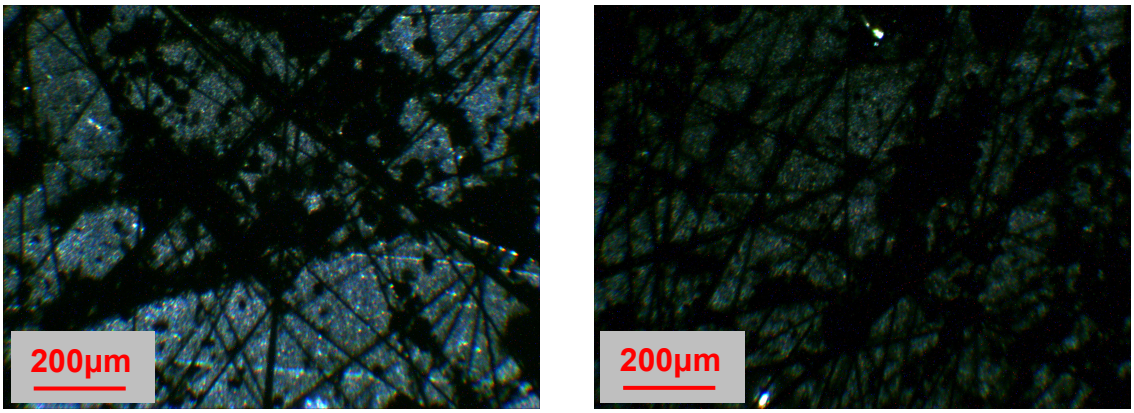

(a) (b)

Figure 5.11. Agglomeration of CNFs at microfiber junctions in 5 wt. % hierarchically-structured nano-enhanced West System (a) 90 min sonication and (b) 6 hr sonication. Images obtained using transmission light microscopy.

Microtensile results for these top-down hierarchically-structured polymer composites can be seen in Figure 5.12 as a function of wt, % CNF for the tensile modulus, tensile strength, and the strain to failure and as a function of sonication time in Figure 5.13. Clearly, the behavior is substantially different than the similar bottom-up hierarchically-structured polymer composites. To begin with, the microfiber mat does not appear to change the tensile modulus or strength of the epoxy; however, it does appear to reduce the strain to failure making the epoxy more brittle. It is likely that the microfiber mat adds defects to the epoxy matrix. Thus, it can be concluded that the microfiber mat may be used to enhance electrical properties for EMF shielding, but it has no inherent benefit on the mechanical properties of the epoxy.

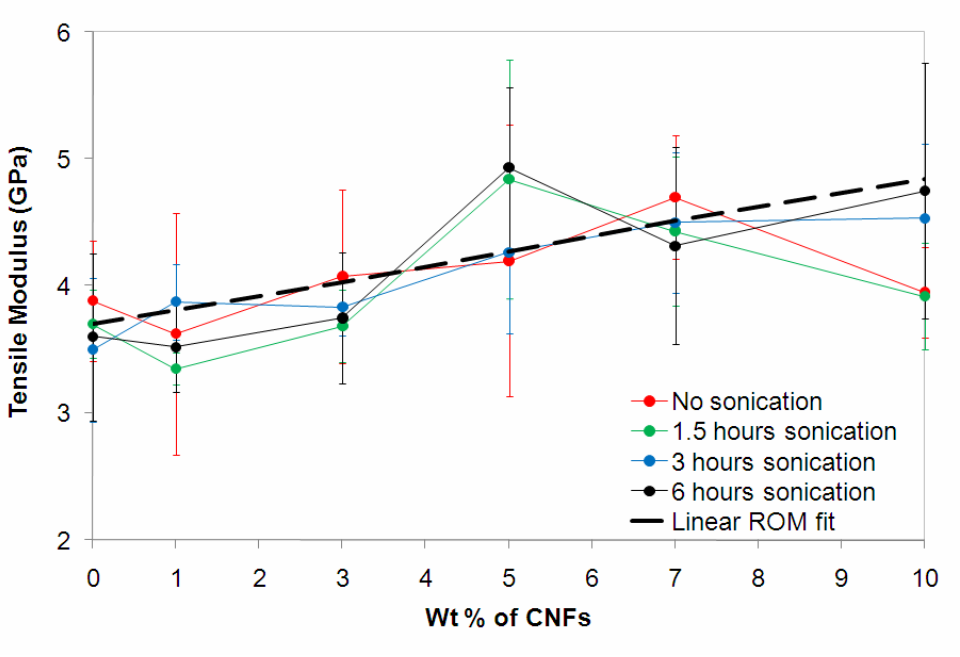
Tensile Modulus (GPa)
6
5
4
3
2
0
1
2
3
4
5
6
7
8
9
10
Wt % of CNFs
No sonication
1.5 hours sonication
3 hours sonication
6 hours sonication
Linear ROM fit

(a)

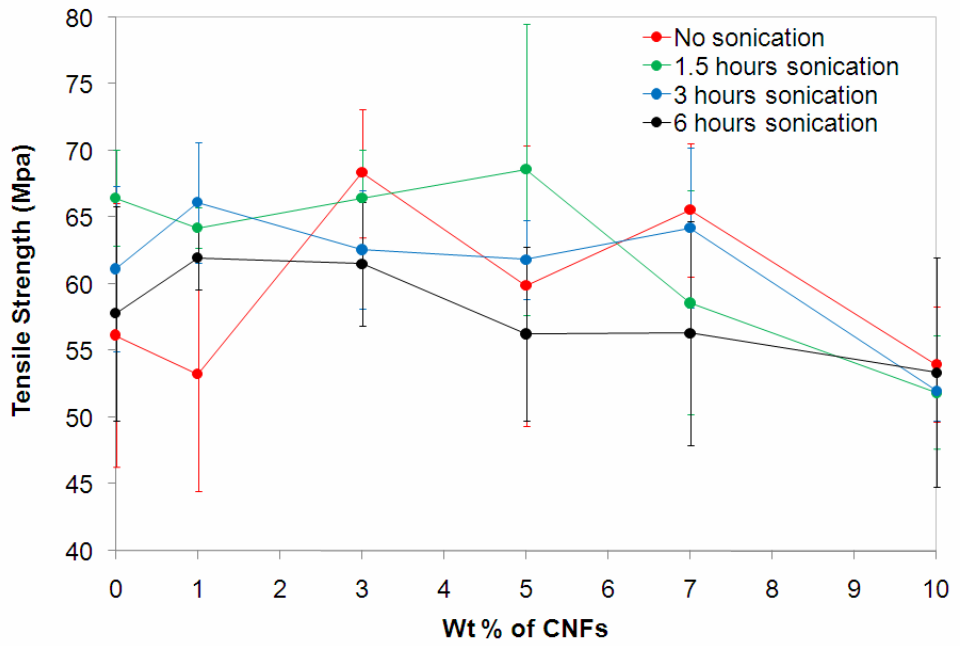
Tensile Strength (Mpa)
80
75
70
65
60
55
50
45
40
0
1
2
3
4
5
6
7
8
9
10
Wt % of CNFs
No sonication
1.5 hours sonication
3 hours sonication
6 hours sonication

(b)

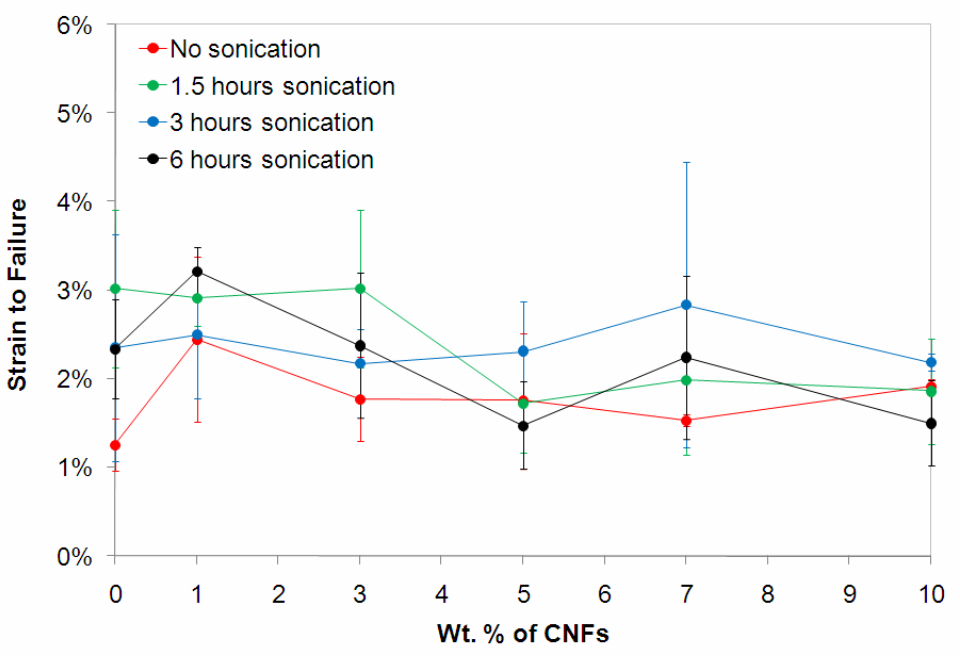

(c)

Figure 5.12. Comparison of sonication times as a function of wt. % CNF in West System epoxy. (a) tensile modulus, (b) tensile strength and (c) strain to failure.

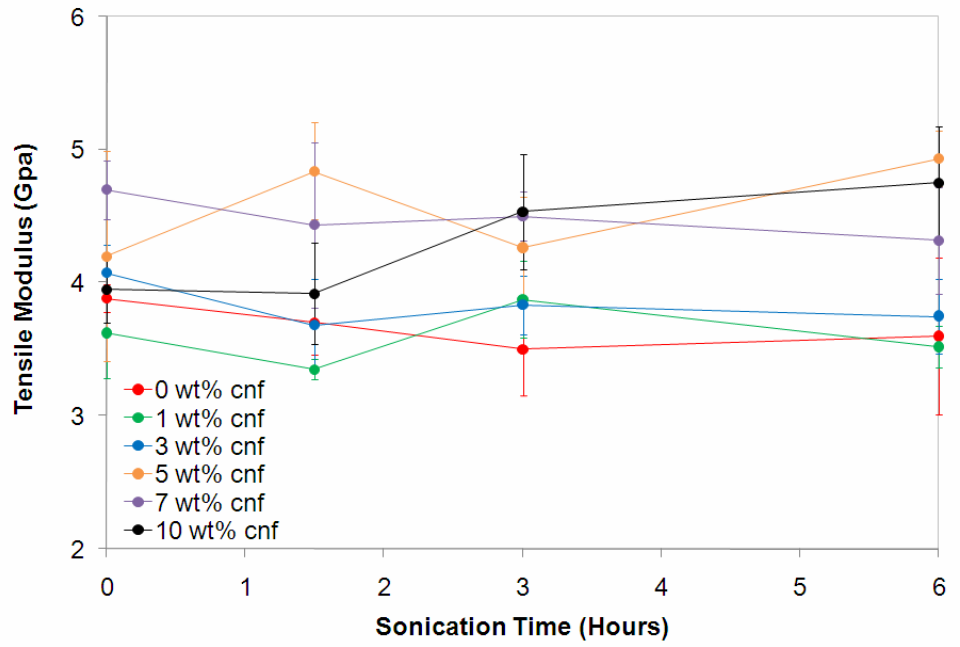

(a)

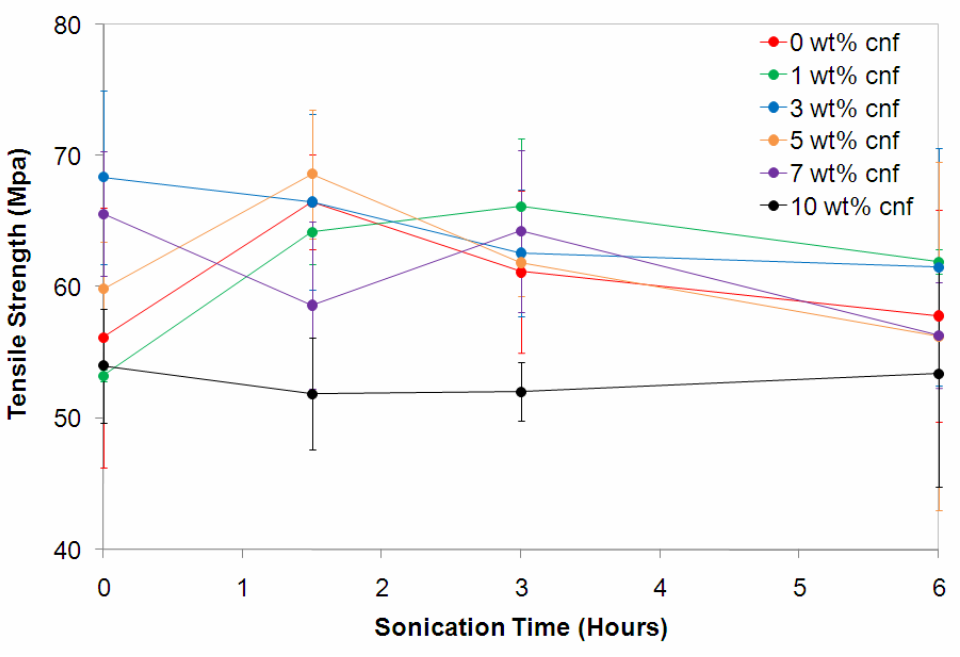

(b)

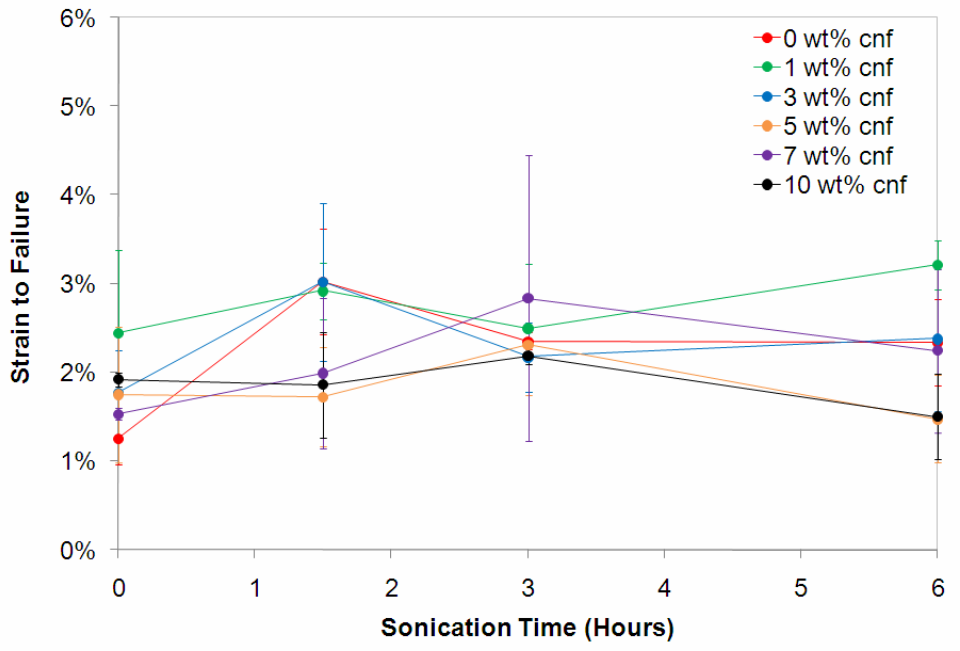

(c)

Figure 5.13. Comparison of wt. % CNF in West System epoxy as a function of sonication time. (a) tensile modulus, (b) tensile strength and (c) strain to failure.

However, addition of the CNF does change the mechanical properties substantially. Upon addition of over 5 wt. % CNF, the modulus of the epoxy can increase by more than 50% to between 4.5 and 5 GPa. However, the strength does not change appreciably until the 10 wt. % CNF loading. Furthermore, it is even greater than observed for bottom-up hierarchical composites. Thus, it would appear that the CNFs are interacting with the carbon-microfibers in such a way that they are enhancing load transfer and therefore enabling the microfibers to constrain the epoxy when they would not be able to otherwise. In fact, the modulus data follows the same linear ROM fit as the melt processed nano-enhanced polymers, except the effective modulus for the CNF used is slightly higher at 20 GPa. Thus, it would appear that employing the CMFs leads to the same type of benefits from hierarchical structure using solvent processing of epoxies as was achieved through melt processing of thermoplastics, but without the orientation effects of the CNFs. However, the interfacial CMF-epoxy matrix strength characteristics that could lead to enhanced strength of the composites does not seem to benefit from this interaction as the changes in strength are very similar to what would be achieved without the CMFs.

What is most surprising about these results is the apparent insensitivity of the mechanical properties to sonication. In the presence of the microfiber mat, the CNFs do not appear to be creating the same kind of bottom-up hierarchical microstructure that affected the evolution of the mechanical properties with sonication. Instead, it appears that the microfiber mat is acting more like a “filter” that appears to be limiting the introduction of dispersed fibers into the epoxy

matrix. This effect is also clearly evident in the optical micrographs. As a result, it is acting to "homogenize" the CNF-filled epoxy microstructure independent of sonication time. Thus, there is much greater consistency in the properties of the top-down hierarchically-structured polymer composites than the bottom-up.

About the only effect of sonication is on the strain to failure. As the sonication time increases, the strain to failure appears to increase about 1 to 2%. Since it has already been established that the degree of dispersion increases with sonication time, it is possible that there are a greater concentration of dispersed CNFs that may not affect the stiffness or strength appreciably, but may make it more difficult for cracks to develop and grow acting as micro-crack diffusers that enable the composites to sustain larger deformations before nucleating cracks of critical sizes to induce failure. Thus, it would appear that sonication would be a secondary benefit in the top-down fabrication process for these composites simply increasing ductility by doubling the strain to failure.

5.4.2 Nanomechanical characterization

5.4.2.1 Modulus mapping

In order to better understand the effects of the hierarchical structure of these materials at the nanoscale, modulus mapping was completed for a representative sample at two processing conditions. The complex modulus maps can be seen in Figure 5.14, the corresponding tan(δ) maps can be seen in Figure 5.15 and the topographical representations are shown in Figure 5.16. A summary of the reduced data is in Table 5.3.

In view of the fact that the microfibers are generally beneath the surface of these hierarchically-structured materials, in order to see any effects due to microfibers in modulus mapping, a relatively high dynamic force of 10μN was used. This greater force allows the indenter tip to probe further into the material, garnering information from more of the surrounding volume. Generally, a value of 1-3μN is used in this type of testing as a higher dynamic force makes the process less stable and more prone to noise.

The presence of the sub-surface microfibers can be seen in Figure 5.14, Figure 5.15 and Figure 5.16. Of greater interest are the regions of higher complex modulus in Figure 5.14a, indicating that CNF agglomerates are accumulating around the fibers. This is much less prevalent in Figure 5.14b, where 6 hours of sonication provides a more homogeneous dispersion throughout the matrix.

This high dynamic load modulus mapping technique greatly aides in distinguishing the local effects of different constituents in this hierarchically-structured material.

CNT wt. %	**Sonication time (hrs)**	**Complex Modulus (GPa)**		**Tan(δ)**	
		Average	Standard Deviation	Average	Standard Deviation
5	1.5	2.27	0.63	0.23	0.03
5	6	1.96	0.17	0.18	0.03

Table 5.3. Comparison of complex moduli and tan(δ) in hierarchically-structured nano-enhanced West System with 5 wt. % CNF and embedded CMF after 90 minutes and 6 hours of sonication.

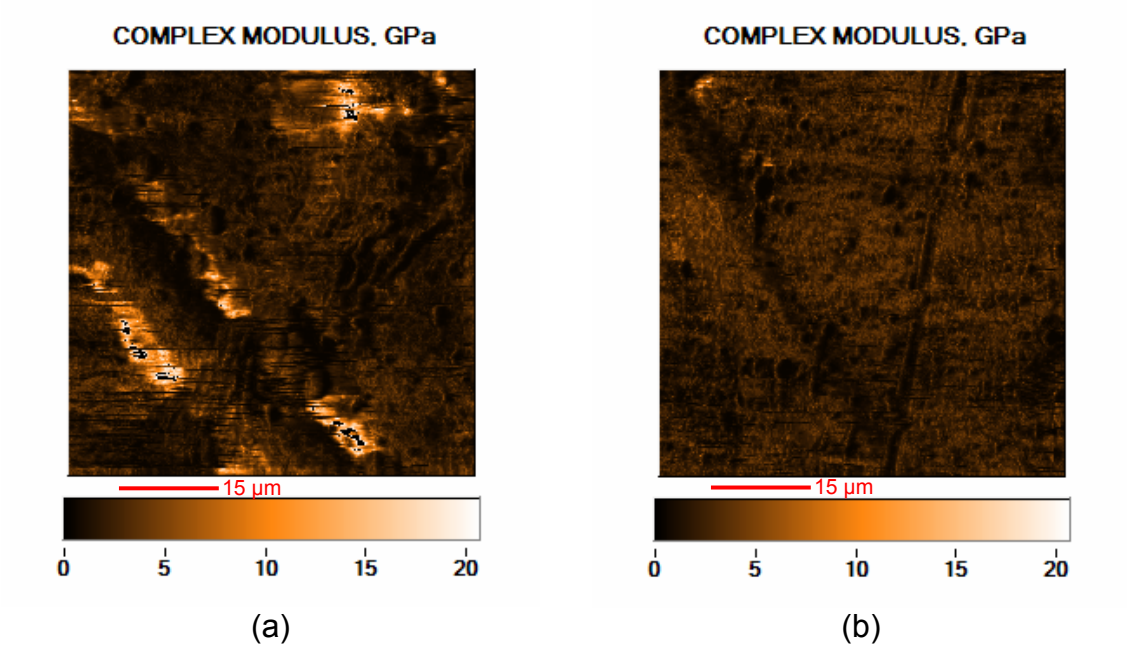

Figure 5.14. Complex moduli from hierarchically-structured nano-enhanced West System with 5 wt. % CNF and embedded CMF after (a) 90 minutes sonication and (b) 6 hours sonication.

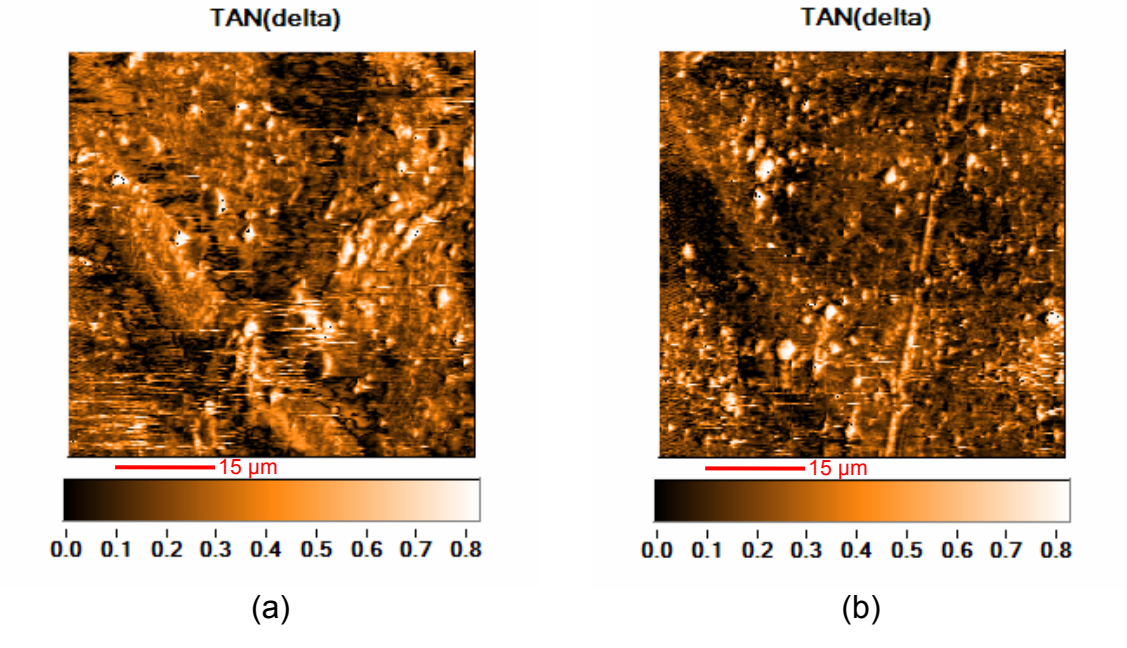

Figure 5.15. Tan(δ) from hierarchically-structured nano-enhanced West System with 5 wt. % CNF and embedded CMF after (a) 90 minutes sonication and (b) 6 hours sonication.

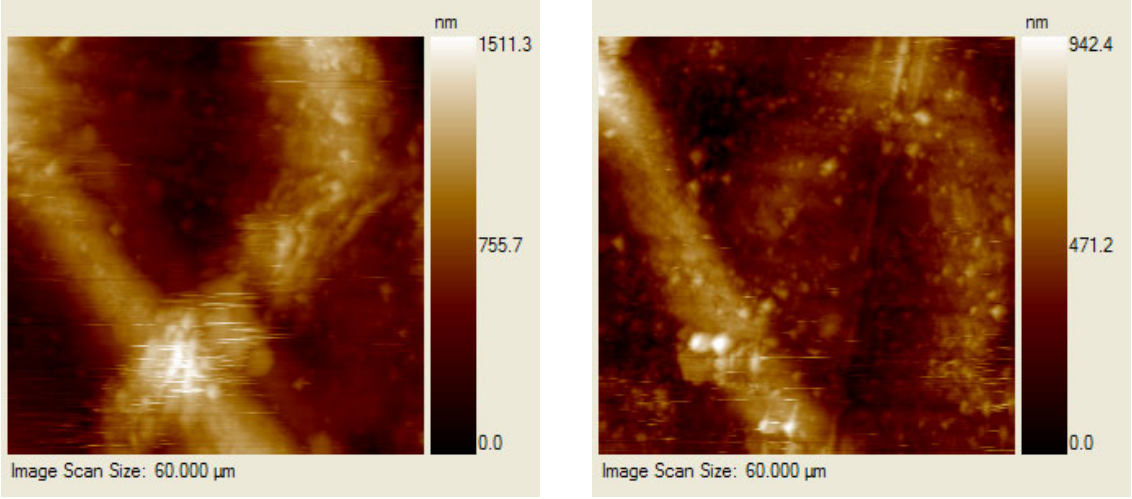

(a) (b)

Figure 5.16. Topographical representations of hierarchically-structured nano-enhanced West System with 5 wt. % CNF and embedded CMF after (a) 90 minutes sonication and (b) 6 hours sonication.

5.4.2.2 Quasi-static nanoindentation

In addition to modulus mapping, a grid of 100 quasi-static indents was made in order to gain further understanding of the role of sonication on local material properties in these hierarchically-structured nano-enhanced polymers. Table 5.4 summarizes the data plotted in Figure 5.17 and Figure 5.18.

Qualitatively, it can be seen from Figure 5.17 and Figure 5.18 that the sample sonicated for 90 minutes has large contiguous regions of high, low or average values, whereas the sample sonicated for 6 hours has a seemingly indiscriminate dispersion of smaller contiguous areas. This can be seen quantitatively in the data by looking at the standard deviation, which is approximately 50% higher for the 6 hour sonication time.

CNT wt. %	Sonication time (hrs)	Reduced Modulus (GPa)		Hardness (MPa)	
		Average	Standard Deviation	Average	Standard Deviation
5	1.5	2.20	0.24	28.70	2.97
5	6	2.15	0.31	26.20	4.24

Table 5.4. Comparison of reduced moduli and hardness in hierarchically-structured nano-enhanced West System with 5 wt. % CNF and embedded CMF after 90 minutes and 6 hours of sonication.

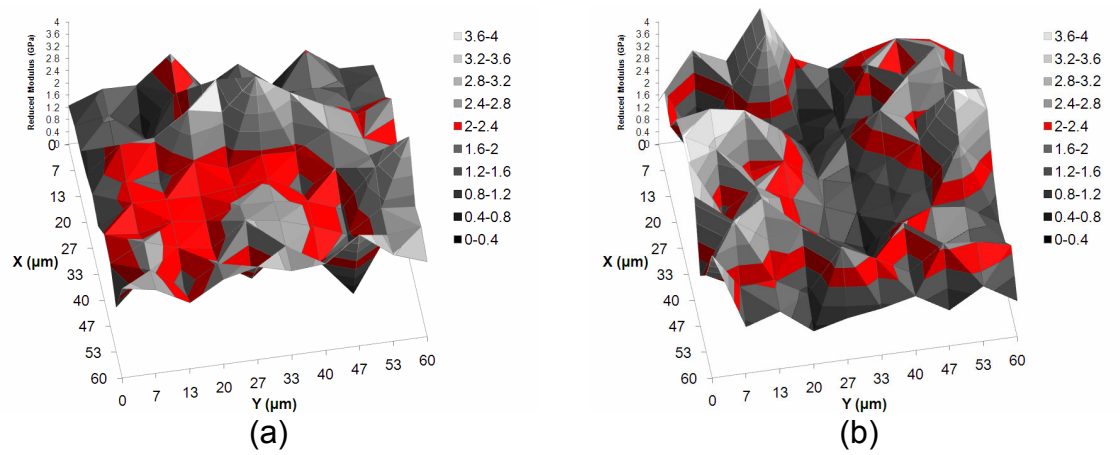

Figure 5.17. Reduced modulus of hierarchically-structured nano-enhanced West System with 5 wt. % CNF and embedded CMF after (a) 90 minutes sonication and (b) 6 hours sonication. The red bands depict regions in which the average falls.

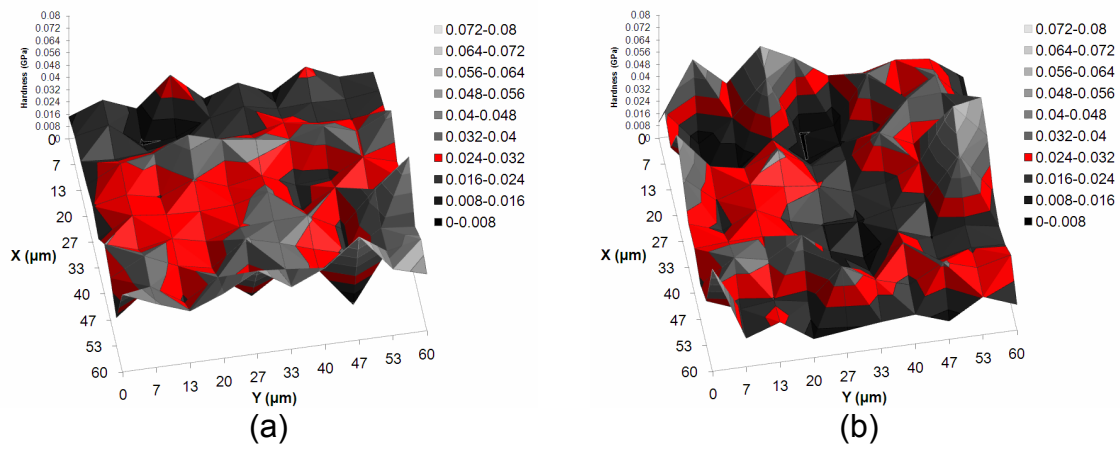

Figure 5.18. Hardness of hierarchically-structured nano-enhanced West System with 5 wt. % CNF and embedded CMF after (a) 90 minutes sonication and (b) 6 hours sonication. The red bands depict regions in which the average falls.

5.5 Summary

A new approach to multi-scale mechanical property characterization and modeling was first developed for hierarchically-structured nano-enhanced materials using PS as a model thermoplastic system and then extended to epoxies using West system as a model in order to understand their processing-structure-property relationships. Based on the characterization results and models, a method was developed for quantifying the "degree of dispersion" and "dispersion limit" for CNFs in epoxies as a function of sonication time during solvent processing which limits the development of hierarchical structure. Furthermore, the hierarchical structures that develop in the thermosets are similar to the thermoplastics, even though a different process is used for the thermosets that has lower shear force and longer processing time associated with it. The relative benefit of using microscale reinforcement in addition to nanoscale reinforcement to control the hierarchical structure and resulting mechanical properties was also characterized and modeled at different strain rates using chopped CMFs in LDPE as a model thermoplastic system and Carbon fiber veils in West system as a model thermoset system. From these models and insights, it was possible to next investigate the control of multifunctional properties of hierarchically-structured nano-enhanced polymers using additional thermal processing steps: annealing in the case of thermoplastics and then curing in the case of thermosets.

Chapter 6 Control of multifunctional properties in hierarchically-structured nano-enhanced thermoplastics through thermal processing

6.1 Modeling of annealing effects on the evolution of electrical conductivity

To understand the conductivity increase due to annealing, a model has been developed that relates the variation in conductivity to changes in connectivity between the MWCNTs/CNFs due to annealing. As a starting point, the conventional power-law relationship is used to describe the electrical conductivity σ_c as a function of the particle volume fraction β in Equation 6.1:

$$\sigma_c(\mathrm{t},\mathrm{T}) = \sigma_{\mathrm{PS}} + A\{\beta(t,T) - \beta_c\}^{\lambda} \qquad \textbf{6.1}$$

where A is the power-law coefficient, λ the power-law exponent, β is the volume fraction of interconnected particles, β_c is the critical volume fraction for percolation, and σ_{PS} is the conductivity of neat polystyrene. Note that this expression has been modified to reflect that both σ_c and β are dependent upon annealing time and temperature.

The key assumption in consideration of Figure 6.1 and Figure 6.2 is that *particle alignment decreases the effective volume fraction of interconnected particles*, which directly contributes to conductivity. This implies that the value of β is initially less than that if the particle arrangement was completely isotropic, which we denote as β_0. The effect of annealing is to randomize the particle distribution, i.e., to increase β until it approaches β_0. The variation of β with

annealing time *t* and temperature *T* is postulated to take on a stretched exponential relationship, as follows in Equation 6.2:

$$\beta = f\left(a - (a-1)e^{-(t/\tau(T))^p}\right) \qquad \textbf{6.2}$$

where τ is a time constant that varies with temperature, *f* is the total volume fraction of MWCNT or CNF reinforcement, *a* is the fraction of reinforcement that is initially percolated, and *p* is the stretching exponent. The key parameter here is the time constant τ for rearrangement of the particles, and this can be considered proportional to the relaxation time of the viscoelastic polymer matrix. Thus, much like for a polymer well above its T_g, an Arrhenius relationship can be postulated for τ as follows in Equation 6.3:

$$\tau(T) = b\exp\left(\frac{E_a}{RT}\right) \qquad \textbf{6.3}$$

where *b* is the Arrhenius coefficient, E_a the activation energy and *R* the gas constant.

Fits of this model to the data are shown in Figure 6.1 and Figure 6.2 and the constants determined from the fits are summarized in Table 6.1. The constants obtained are similar to those that have been previously reported for the percolation of polymer/MWCNT composites [Kota07a]. Note that the response of the CNFs to the viscoelastic relaxation of the polymer requires an E_a of 3.14 kJ/mol – nearly 50% greater than for the MWCNTs. This implies that a longer annealing time (or a higher temperature) is required for full recovery of conductivity in the case of the CNFs. This result may not be unexpected since the CNFs are larger and rougher than the MWCNTs, substantially increasing

their resistance to re-orientation. There is also a larger fraction of the CNFs that are percolated initially, with a value of 0.31 versus 0.11 for the MWCNTs. This would indicate that the CNFs are more resistant to alignment than the MWCNTs.

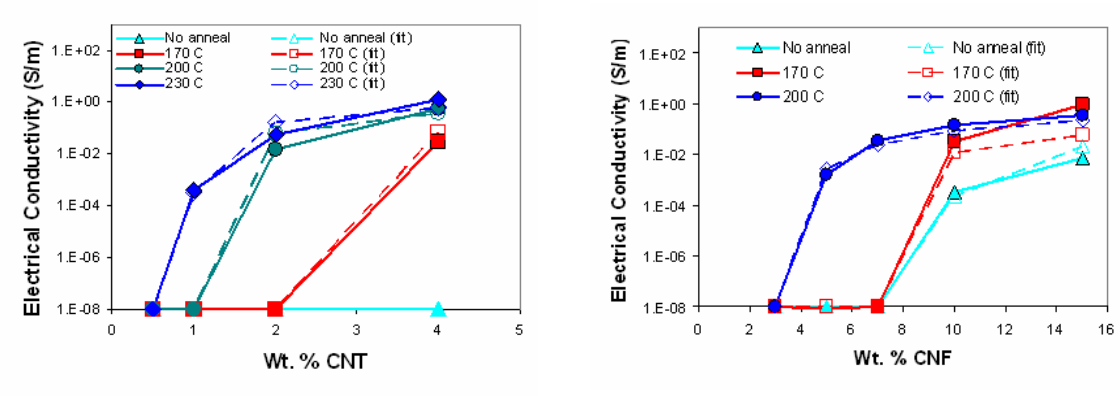

(a) (b)

Figure 6.1. Effect of annealing temperature on the conductivity of: (a) PS/CNT and (b) PS/CNF nano-enhanced polymers. Samples were annealed for 30 min each. Note the significant increases in conductivity due to annealing. The conductivity of non-conductive samples is reported as 10^{-8} S/m since that is the lowest available detection limit for this laboratory. Fits from a model of the time- and temperature-dependent electrical conductivity recovery behavior can also be seen. [Cipr08]

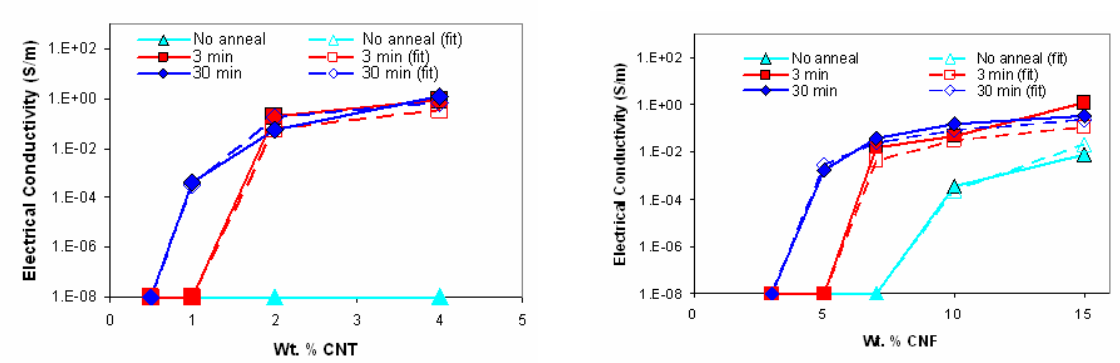

(a) (b)

Figure 6.2. Effect of annealing time on the conductivity of: (a) PS/MWCNT nano-enhanced polymers annealed at 230°C and (b) PS/CNF nano-enhanced polymers annealed at 200°C. Fits from a model of the time- and temperature-dependent electrical conductivity recovery behavior can also be seen. [Cipr08]

Constant	CNF	MWCNT
β_c	3	0.68
σ_{PS}	10^{-8} S/m	10^{-8} S/m
A	15 S/m	70 S/m
λ	1.6	1.2
a	0.31	0.11
p	-0.3	-0.3
b	1.7×10^{23}	1.8×10^{15}
E_a	3.14 kJ/mol	2.17 kJ/mol

Table 6.1. Constants determined from fitting a time- and temperature-dependent model to the data for electrical conductivity recovery due to melt annealing.

In addition to the electrical conductivity data, dynamic rheological testing was completed to determine the effects of annealing on the mechanical properties of the nano-enhanced polymers, specifically G'/G", or the inverse of the tan(δ). The results of this testing can be seen in Figure 6.3, and it should be noted that the shift in value corresponds to a reduction in percolation threshold [Kota07c].

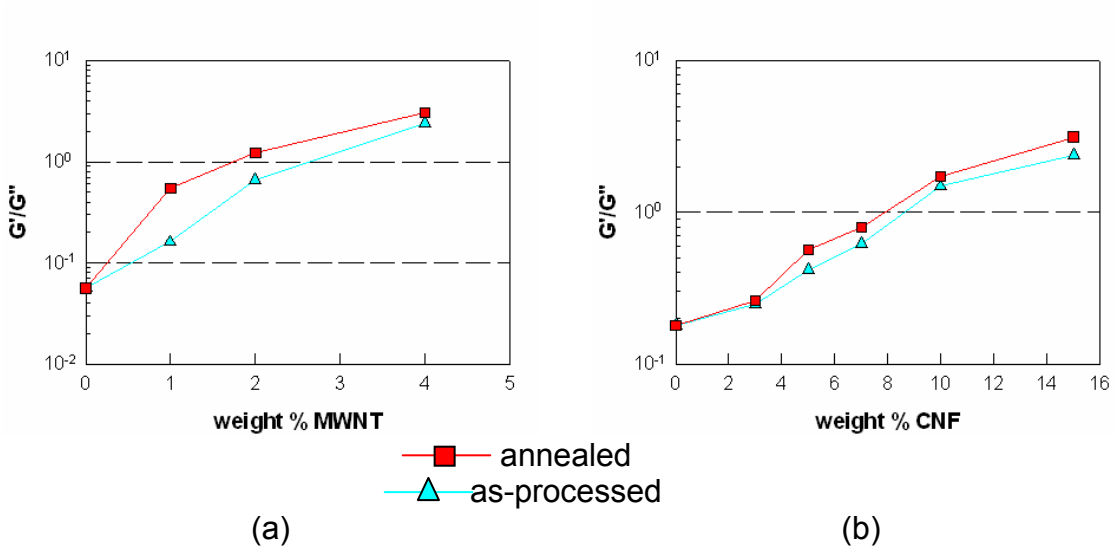

Figure 6.3. Effect of annealing on nano-enhanced polymer firmness G'/G"
(a) PS/MWCNT annealed at T = 230°C for 30 mins and
(b) PS/CNF annealed at T = 230°C for 30 mins. [Cipr08]

6.2 Multi-scale characterization of annealing effects on mechanical properties of PS-CNF nano-enhanced polymers

In order to determine the effects of annealing on PS-CNF nano-enhanced polymers, both annealed and as-processed (i.e. un-annealed) material was characterized with the microtensile tester, as well as with modulus mapping and quasi-static nanoindentation in the nanoindenter. The PS-CNF composites were annealed at 150°C for 2 hours in a vacuum oven at 400 mmHg vacuum.

6.2.1 Microtensile testing

Microtensile testing was completed to determine the tensile properties of the annealed samples. The tensile strengths, tensile moduli, and strain to failure can be seen in Figure 6.4. From this figure, the annealed samples have lower tensile strengths, tensile moduli and strains to failure. This is not unexpected, since the relaxation of fiber orientation should make the material less anisotropic and reduce the tensile properties in the original direction of fiber orientation. In fact, the reduction appears to be 50% of the increase due to the CNF loading that was measured before annealing.

In order to gain a better quantitative understanding of the reduction, the tensile modulus can be compared to the Rule-of-Mixtures (ROM) upper and lower bounds. These are represented by dashed lines in Figure 6.4 (red for upper and green for lower). Clearly, the relaxation behavior is somewhere in between the upper and lower bounds. This is not unexpected for a random fiber

distribution, since there is an equal probability of having fibers in the direction of loading as in the transverse direction. Therefore, it would appear that the micro tensile modulus results are consistent with the relaxation of the structure that was observed in confocal microscopy and quantitatively indicates a nearly random fiber distribution. Furthermore, unlike the orders of magnitude increase in electrical conductivity, the relaxation mechanism will only reduce the mechanical benefits of CNF reinforcement in half but with a tradeoff of more isotropic properties.

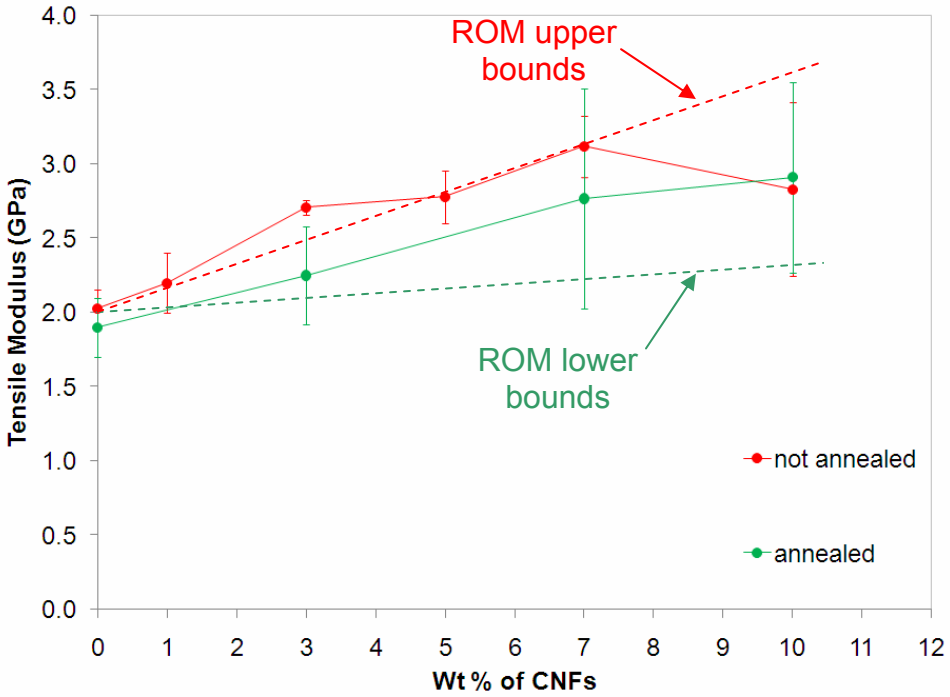

(a)

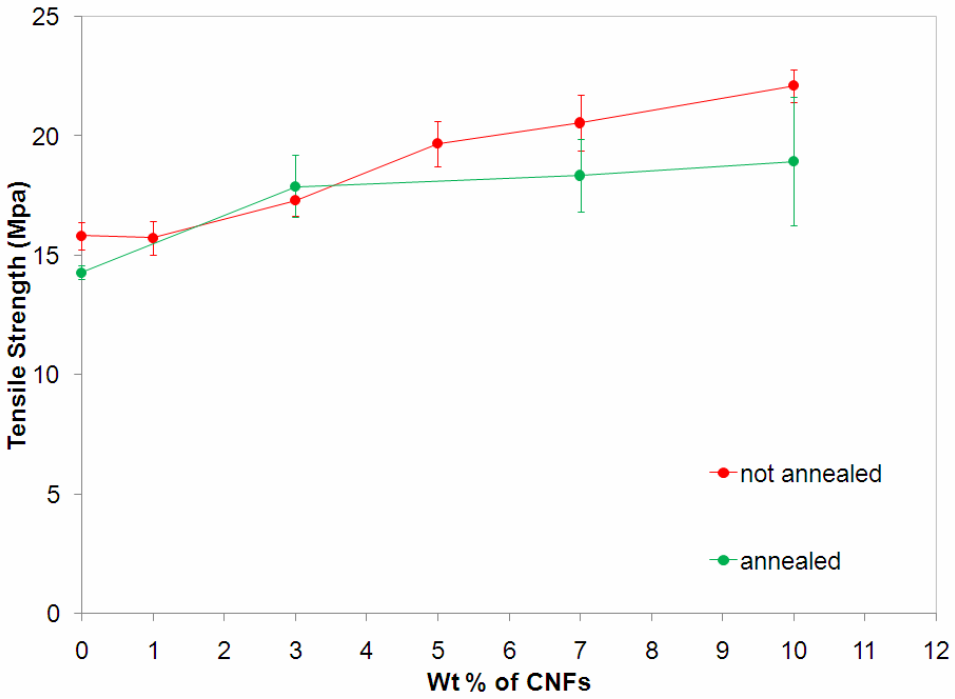

(b)

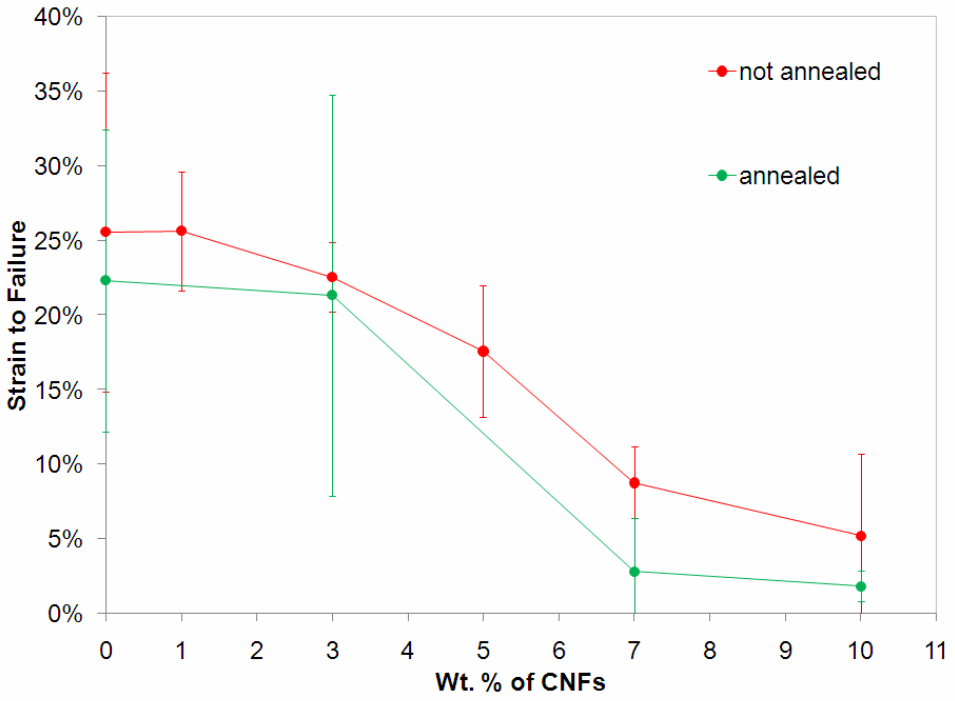

(c)

Figure 6.4. Comparison of properties for annealed and as-processed PS-CNF nano-enhanced polymers. (a) tensile modulus, (b) tensile strength and (c) strain to failure. Dashed lines on (a) represent the upper bounds (red) and lower bounds (green) associated with ROM predictions.

6.2.2 Nanomechanical characterization

6.2.2.1 Modulus mapping

Insight into the relaxation and fiber orientation at the nanoscale was obtained through a mapping of nanomechanical properties using the nanoDMA mode of the nanoindenter. In Figure 6.6, Figure 6.8 and Figure 6.10, the difference in complex modulus can be seen. The annealed 7 wt. % sample shows a slight global decrease in complex modulus. In the 10 wt. % sample, however, a distinctly lower complex modulus can be seen globally. Average values for the complex moduli were obtained by extracting the data from the modulus maps. In order to minimize the effects of perturbations in the moduli from topographical features, each horizontal line was averaged, and then the average of all lines was calculated. This isolates the variation of the moduli to one dimension. A summary of this extracted data can be seen in Table 6.2 and Figure 6.5.

PS-CNF wt. %	Annealing Condition	Complex Modulus (GPa)	
		Average	Standard Deviation
0	None	1.04	0.19
0	2 hr @ 150 C	0.89	0.14
7	None	1.32	0.08
7	2 hr @ 150 C	1.18	0.11
10	None	1.55	0.13
10	2 hr @ 150 C	0.99	0.06

Table 6.2. Comparison of complex moduli in both annealed and as-processed PS-CNF nano-enhanced polymer materials.

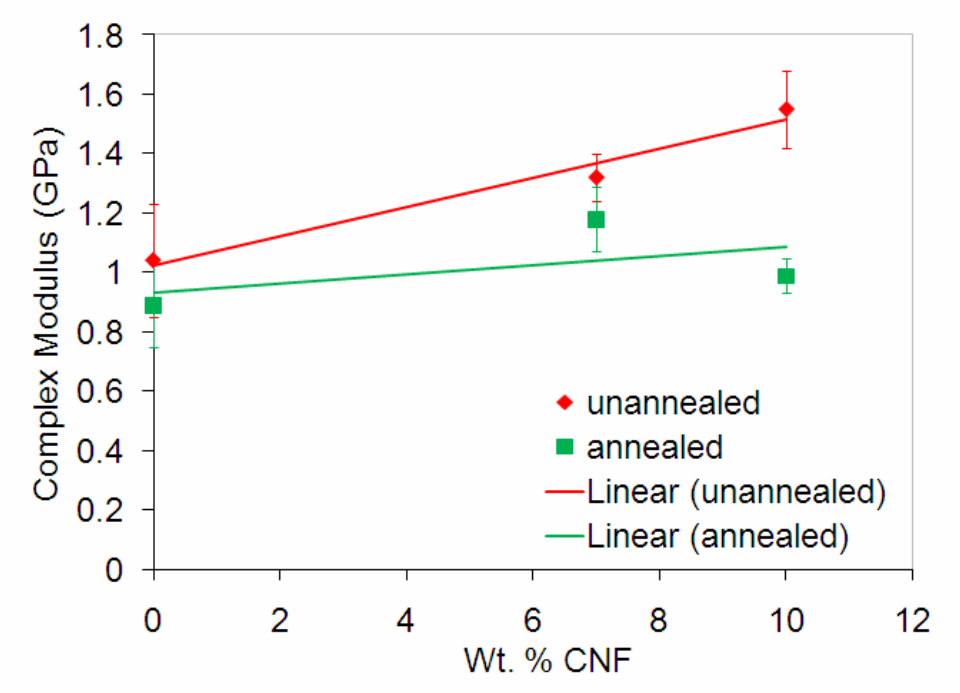

Figure 6.5. Comparison of complex moduli in both annealed and as-processed PS-CNF nano-enhanced polymer materials.

Variations in properties obtained through modulus mapping can occur from roughness or features on the surface being scanned. Figure 6.7, Figure 6.9 and Figure 6.11 depict the surface topography of the same annealed and as-processed samples. It can be seen that there are some fluctuations in properties correspond to the positions of the largest protrusions or cavities in the surface that affect the quantitative accuracy of the complex modulus values relative to the microtensile measurements. However, qualitatively it does indicate that locally there are an increased number of areas which are less stiff which does quantitatively translate into relative changes consistent with the microtensile measurements. Thus, modulus mapping provides direct evidence of localized relaxation of the fiber orientation at the nanoscale, and that at this scale the relaxation may not always be uniform.

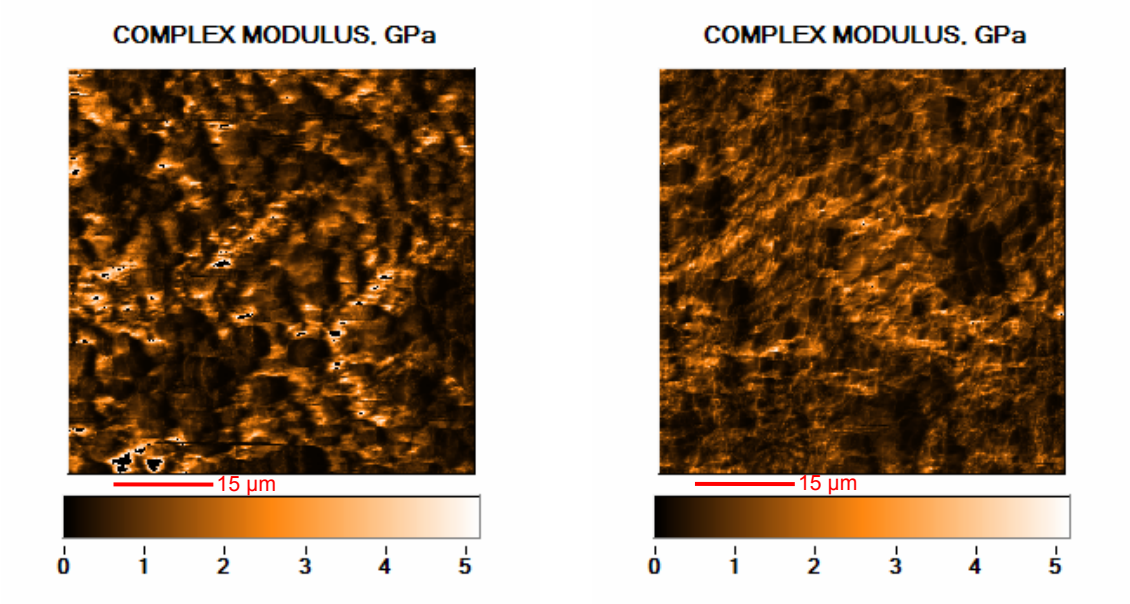

(a) (b)

Figure 6.6. Complex modulus from 60 µm modulus maps of (a) annealed and (b) as-processed neat PS.

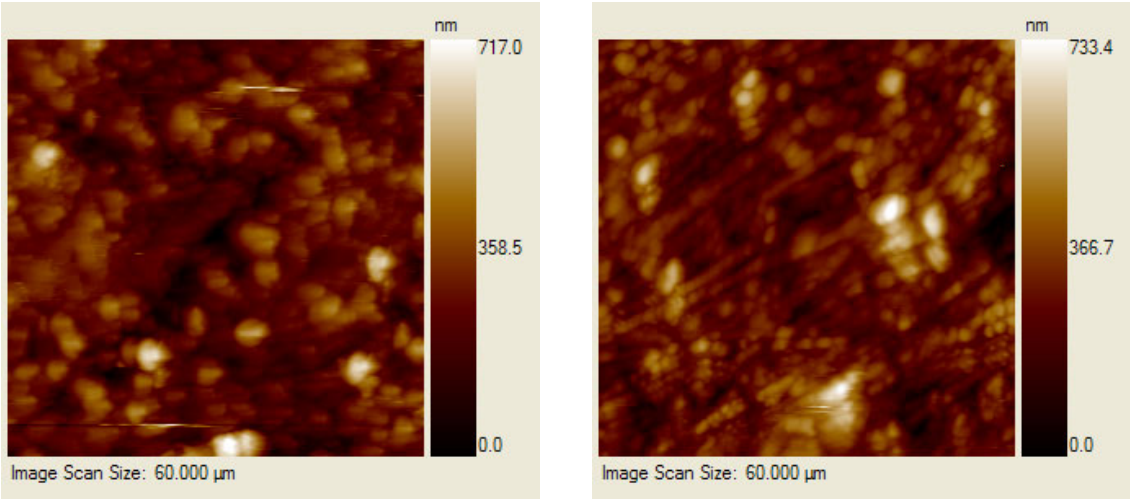

(a) (b)

Figure 6.7. Topographical representation showing surface geometry of (a) annealed and (b) as-processed neat PS.

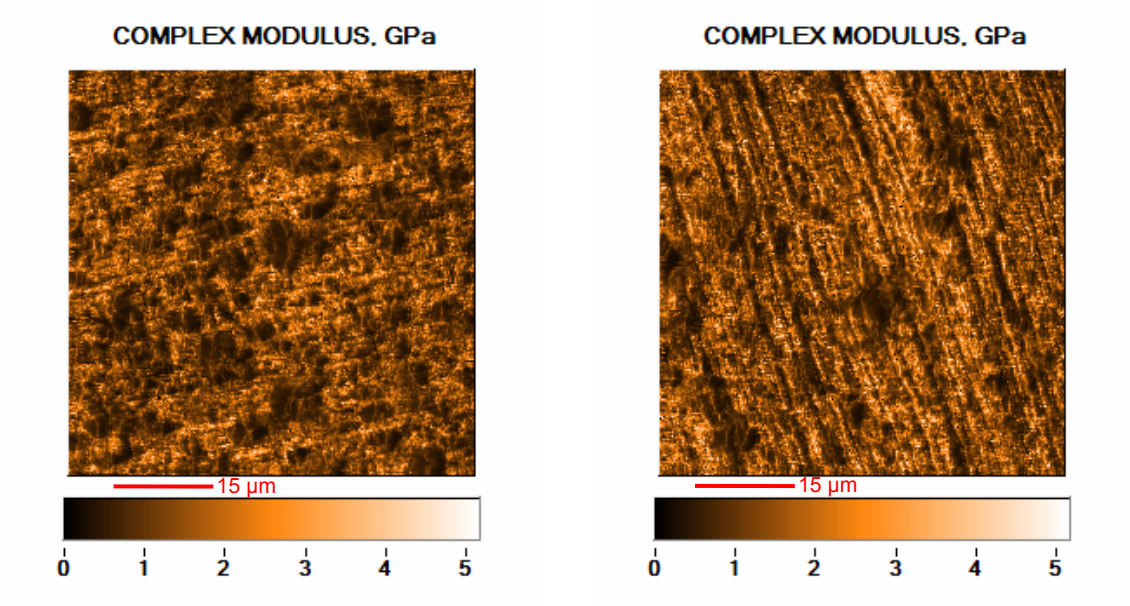

(a) (b)

Figure 6.8. Complex modulus from 60 µm modulus maps of (a) annealed and (b) as-processed PS with 7 wt. % CNF.

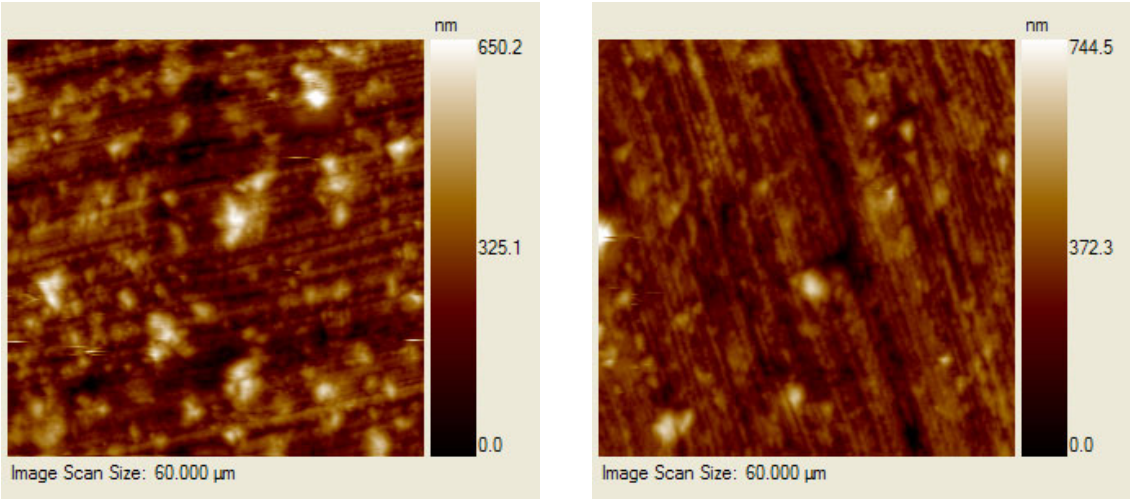

(a) (b)

Figure 6.9. Topographical representation showing surface geometry of (a) annealed and (b) as-processed PS with 7 wt. % CNF.

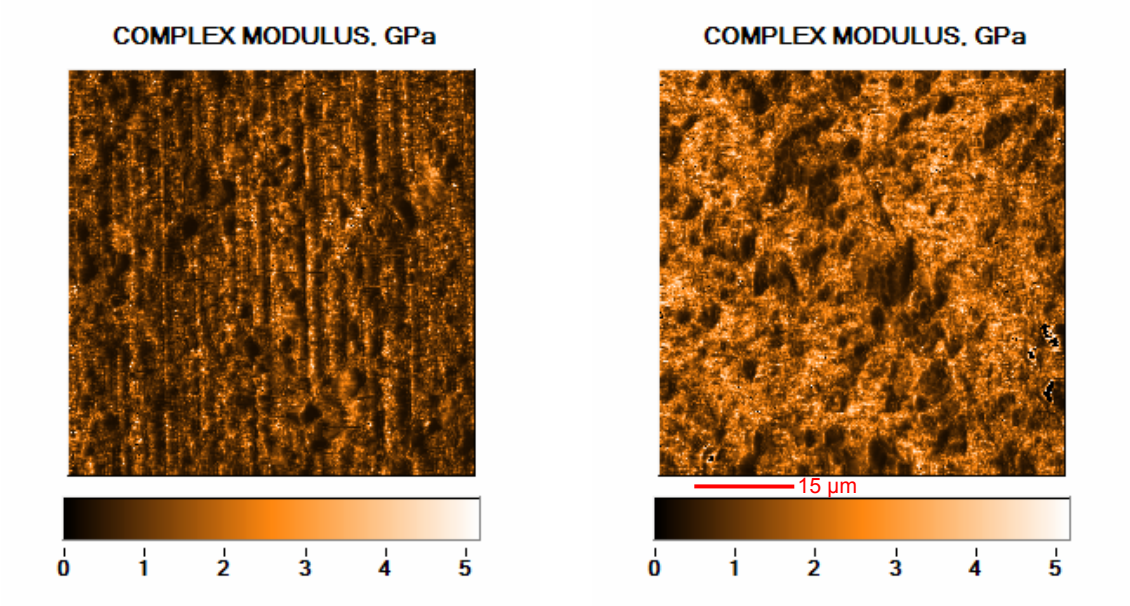

(a) (b)

Figure 6.10. Complex modulus from 60 µm modulus maps of (a) annealed and (b) as-processed PS with 10 wt. % CNF.

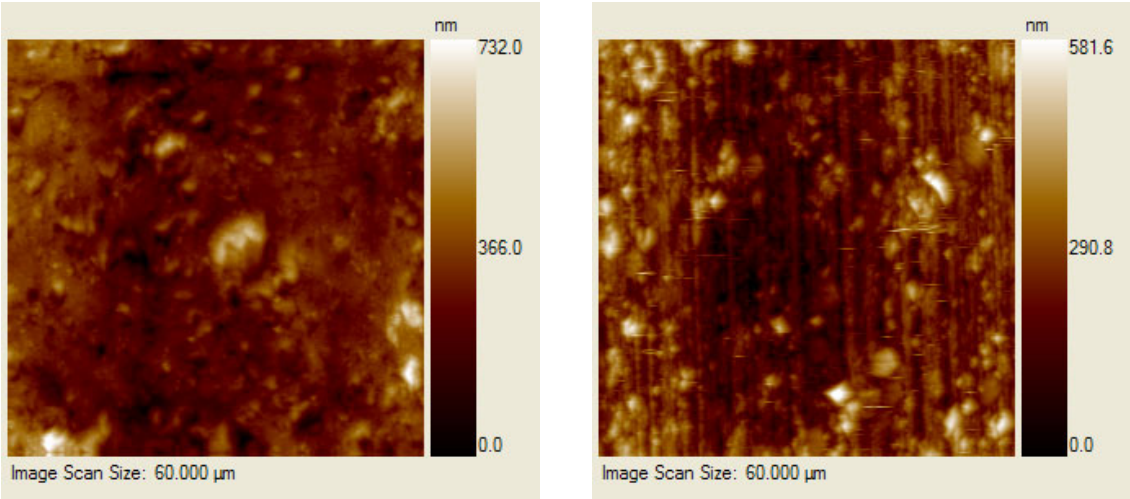

(a) (b)

Figure 6.11. Topographical representation showing surface geometry of (a) annealed and (b) as-processed PS with 10 wt. % CNF.

6.2.2.2 Quasi-static nanoindentation

In addition to modulus mapping using nanoDMA, a series of 100 quasi-static indents arranged in a 10 × 10 grid over a 60 μm × 60 μm area was also made on these materials in order to obtain more quantitatively accurate measurements that were not as affected by surface roughness. The same averaging method applied to the modulus mapping data was used to analyze the quasi-static indentation data. These results are summarized in Table 6.3. Additionally, the modulus can be visualized for neat PS as well as, 7 wt. % and 10 wt. % PS-CNF in Figure 6.12. The areas of high reduced modulus correspond to expected locations of agglomerations.

Quantitatively, the results in Figure 6.12 indicate that the agglomerations can become very stiff, reaching levels that are almost 3 times the average. However, the average value is about 50% greater than the microtensile measurements. It is possible that the 60 micron area over which these measurements were obtained were at higher average stiffness than the bulk of the composite. This is not unexpected since agglomerate sizes in the melt-processed composites can be on the order of 20-50 micron.

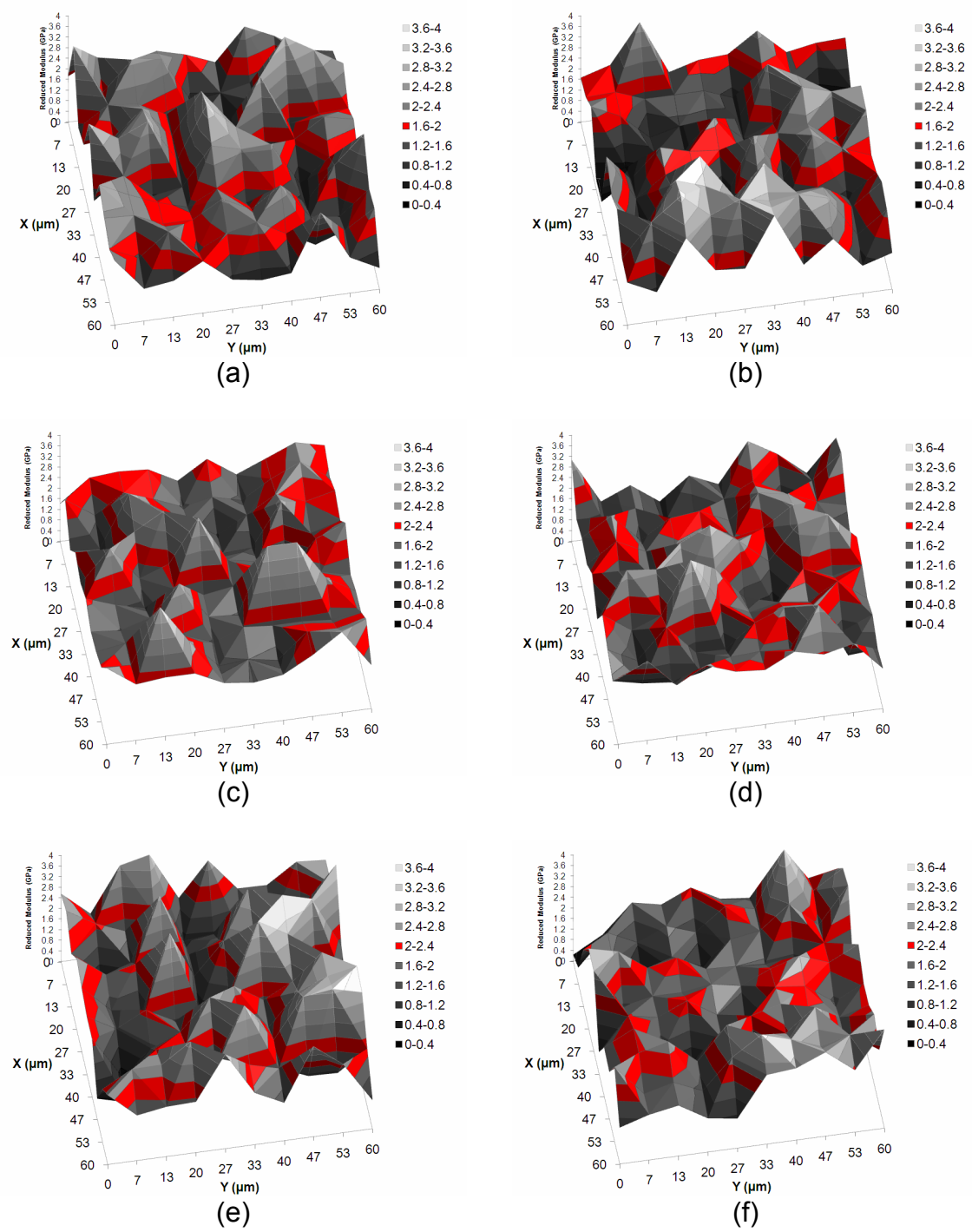

Figure 6.12. Reduced modulus maps from a series of 100 quasi-static nanoindents for (a) 0% % PS-CNF not annealed (b) 0 wt. % % PS-CNF annealed (c) 7 wt. % % PS-CNF not annealed (d) 7 wt. % % PS-CNF annealed (e) 10 wt. % % PS-CNF not annealed (f) 10 wt. % % PS-CNF annealed. The red bands depict regions in which the average falls.

Qualitatively, it would appear that there is not much difference in the features obtained using the 10 × 10 indent map over a 60 micron region. Thus, these results indicate that at this resolution (6 micron per indent) that there is nothing distinctive about the features in the samples at the nanoscale before and after annealing that would be consistent with the reorientation of the fibers responsible for the macroscale tensile effects and the changes previously observed in confocal microscopy and quantified through FFT [Cipr08]. Furthermore, as with the microtensile testing results they indicate that the modulus becomes more insensitive to wt. % CNF as the fibers become less oriented in the direction of loading, consistent with a lower ROM prediction.

Also, quasi-static hardness maps can be seen for the 0, 7 and 10 wt. % CNF in Figure 6.13 which shows similar variations between the annealed and as-processed, consistent with the reduced modulus maps. Averages for the hardness maps can be seen in Table 6.3. These results indicate that as the 10 wt. % CNF specimen is annealed, the hardness approaches that of the 7 wt. %; similar to what happens with the modulus. Once again, a lower ROM prediction would indicate that loss of orientation of the reinforcement in the direction would substantially reduce the differences between the composites as a function of wt. % CNF.

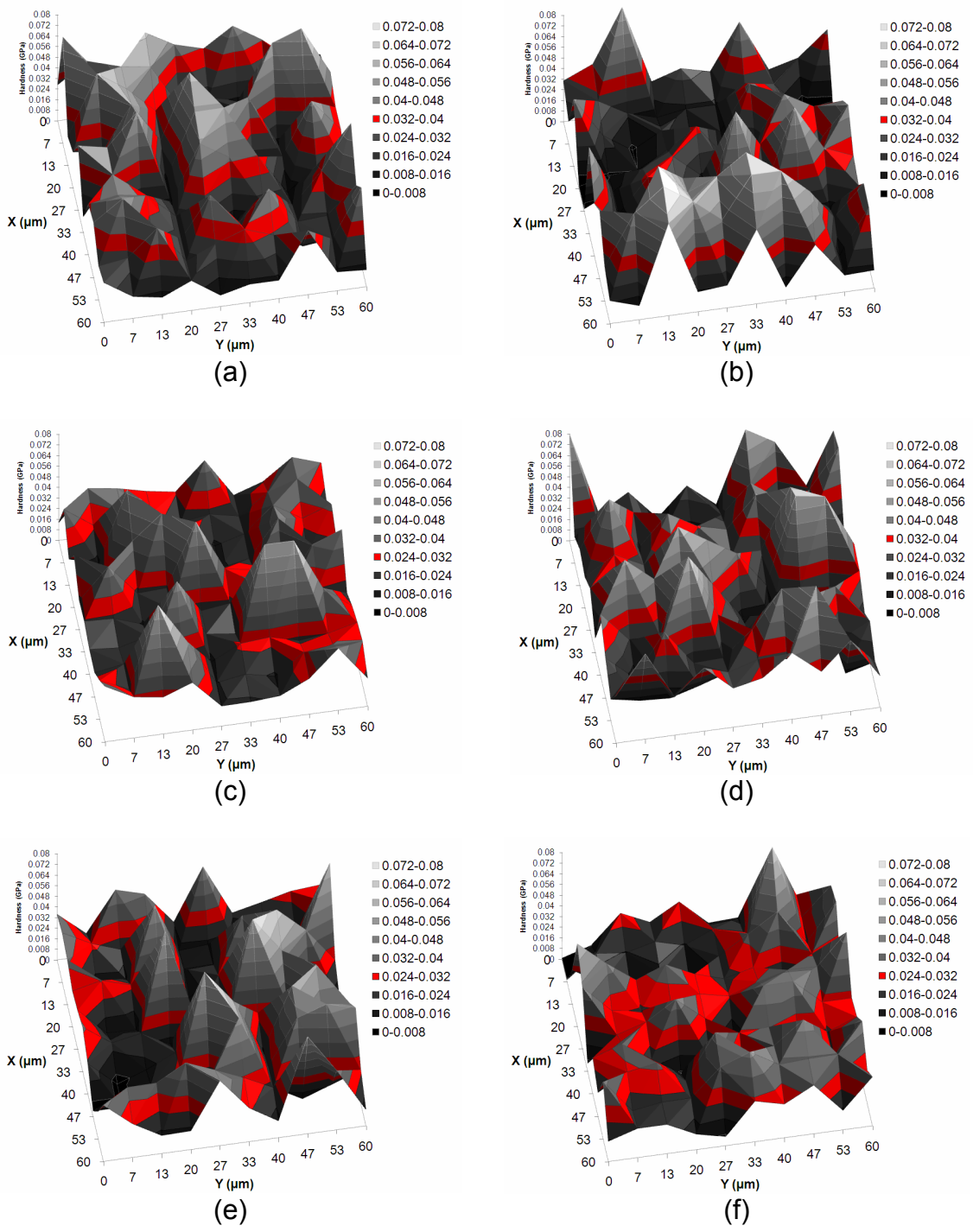

Figure 6.13. Hardness maps from a series of 100 quasi-static nanoindents for (a) 0% % PS-CNF not annealed (b) 0 wt. % % PS-CNF annealed (c) 7 wt. % % PS-CNF not annealed (d) 7 wt. % % PS-CNF annealed (e) 10 wt. % % PS-CNF not annealed (f) 10 wt. % % PS-CNF annealed. The red bands depict regions in which the average falls.

PS-CNF wt. %	Annealing Condition	Reduced Modulus (GPa)		Hardness (MPa)	
		Average	Standard Deviation	Average	Standard Deviation
0	None	1.89	0.31	34	5.1
0	2 hr @ 150 C	1.93	0.19	32	8.3
7	None	2.10	0.22	31	6.2
7	2 hr @ 150 C	2.01	0.24	34	6.6
10	None	2.18	0.33	30	6.3
10	2 hr @ 150 C	2.00	0.33	28	6.3

Table 6.3. Comparison of reduced moduli and hardness in both annealed and as-processed PS-CNF nano-enhanced composite materials.

6.3 Summary

A model of effects of an additional thermal processing step on the change in multifunctional properties due to viscoplastic relaxation of alignment in the nanostructure of hierarchically-structured nano-enhanced thermoplastics has now been developed. The effect of the structural relaxation was first characterized on the electrical properties, then on mechanical properties. The models used to gain an enhanced understanding of the effects of viscoplastic relaxation can lend insight into the control of multifunctional properties in hierarchically-structured nano-enhanced thermoplastic polymers using an additional thermal processing step. As stated in the previous chapter, it was also desirable to extend similar control of multifunctional properties to thermoset polymers using curing as an additional thermal processing step on a model filled adhesive, in this case Hysol 9309.2, with CNTs that is discussed in the next chapter.

Chapter 7 Curing effects in hierarchically-structured nano-enhanced adhesive with microfibers

7.1 Macroscale dynamic mechanical analysis and modeling of curing kinetics

Insight into the effects of an additional thermal processing step on hierarchically-structured nano-enhanced thermosets was obtained by varying the cure time in a model filled adhesive, in this case Hysol 9309.2, with CNTs. Experiments were first obtained using DMA and DSC to characterize the evolution of thermal properties due to cure time. For this instance, single-walled CNTs were used to nano-enhance the Hysol adhesive due to their processing compatibility with the Hysol fillers. Results as a function of cure at 80°C for up to 96 hours can be seen in Figure 7.1a for T_g and tan(δ). The T_g results in Figure 7.1a are consistent between the two measurement techniques and indicate an almost continuous increase in T_g for the CNT reinforced filled epoxies, while the unreinforced filled epoxy remains nearly constant. Thus, it appears that the CNT reinforcement is changing the crosslinking process. Furthermore, it appears that the effect of the CNT reinforcement is to increase the T_g of the epoxy, which would indicate that the crosslinking process is changed such that the interaction between the CNT reinforcement and the epoxy molecules actually acts as an additional crosslinking process.

In order to understand the effect of cure time on the resulting T_g, the following Arrhenius model of the curing kinetics was used:

$$T_g(t) = \left(1 - \exp\left(-\left(\frac{t}{\tau}\right)^p\right)\right)\left(T_{g\infty} - T_{g0}\right) + T_{g0} \qquad \textbf{7.1}$$

where T_{g0} is the glass transition temperature of the resin, $T_{g\infty}$ is the glass transition after infinite cure time, τ is a time constant and n is the Arrhenius exponent. The resulting fits can be seen in Figure 7.1b, and the values of the various parameters can be seen in Table 7.1. To account for the effects of the CNTs, different constants were used in Equation 7.1 to obtain a best fit. From these fits, it can be seen that the effect of the CNTs is to affect the evolution of the crosslinking by decreasing the exponent p from 1 to 0.5 for the CNT filler and to increase the time constant to 2 hr for the 0.2 wt. % CNTs and 0.75 hr for the 0.5 wt. % CNTs. Meanwhile, the glass transition temperature initially increases by 3°C for the 0.2 wt. % CNTs and 5°C for the 0.5 wt. % CNTs, while at infinity the increases are 16°C for the 0.2 wt. % CNTs and 14°C for the 0.5 wt. % CNTs. This increase usually is associated with a greater degree of crosslinking that reduces the molecular weight between crosslinks.

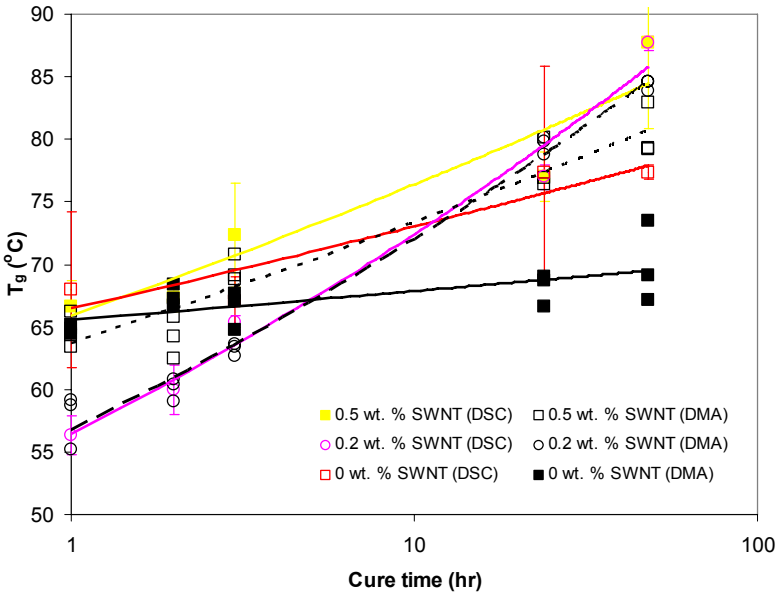

(a)

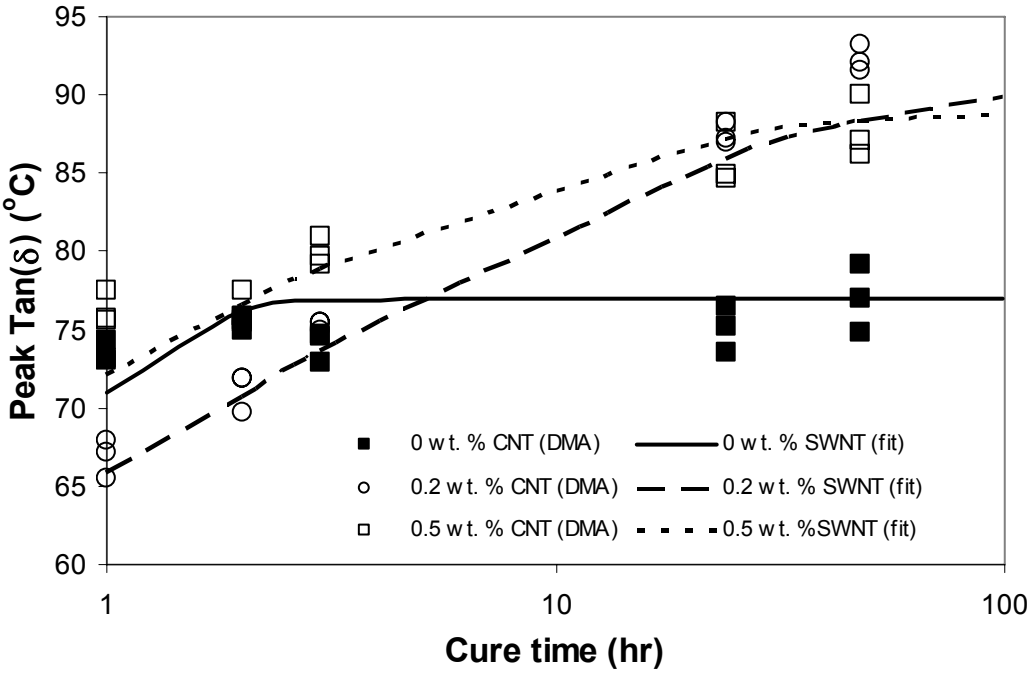

(b)

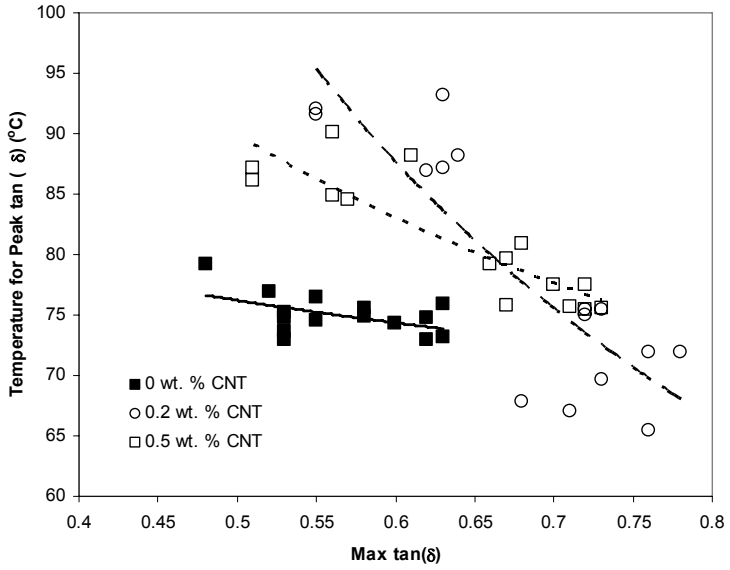

(c)

Figure 7.1. (a) Variation of Tg with cure time measured with DMA and DSC indicating constant variations for CNT reinforced filled epoxies due to change in the crosslinking process, (b) fit of Arrhenius model to the DMA data, and (c) Variation of temperature for peak tan(δ) with maximum value of tan(δ) indicating changes in relationship between evolution of mechanical and thermal properties.

Parameter	0 wt. % CNT	0.2 wt. % CNT	0.5 wt. % CNT
τ	0.5	2	1
p	1	0.5	0.5
$T_{g\infty}$	77	91	89
T_{g0}	33	36	38

Table 7.1. Parameters for Arrhenius model and corresponding fit values.

For the variation in the peak value of tan(δ) with the temperature for the peak, seen in Figure 7.1c, there is an indication that the CNT reinforcement has a significant effect on both thermal and mechanical properties that causes the variation to become much steeper and extend to much higher values of tan(δ). The increase in tan(δ) is most likely due to the frictional effects from percolated CNTs as well as a change in the adhesion between the CNTs and epoxy matrix. The increase in the glass transition temperature itself is most likely due to the increased thermal stability from the CNTs once they adhere with the matrix.

For the pure epoxy, there appears to be structural independence between the evolution of thermal and mechanical behavior. This would indicate that the damping characteristics are not depending on the curing kinetics. Since the Hysol is inherently an epoxy with a copolymer blend and microscale fillers, it is possible that the decrease in tan(δ) could also be due to increased adhesion between the fillers and epoxy matrix or the copolymer. Typically, tan(δ) reflects the damping due to molecular mobility, thus it would be reasonable to assume

that this is the case since it would not as substantially affect T_g because it is more dependent on the crosslinking within the epoxy matrix.

Adding CNTs appears to have even more significant effects on tan(δ), likely because of the substantially higher surface area of the CNTs relative to the inherent microscale fillers of the epoxy. The specific surface area of the SWNTs is on the order of 400 m^2/g, whereas the microscale silica fibers and titanium dioxide particles have specific surface areas on the order of 0.1 m^2/g. Furthermore, the increase in surface area also appears to have more of an effect on the simultaneous evolution of thermal and mechanical properties.

7.2 Microtensile testing

Tensile modulus as a function of cure time and the resulting strength and percentage of elongation at the break of the epoxies obtained from small scale test specimens can be seen in Figure 7.2. These results indicate an increase in the strength and stiffness with cure time for the epoxies filled with CNT, with a decrease in ductility that follows a power law fit. However, the unfilled epoxies indicate no change in strength and stiffness with a slight increase in ductility, which is consistent with the absence of change in observed T_g.

Using the same type kinetic model as was used for T_g, it is possible to understand the evolution of the strength and stiffness due to the CNT reinforcement. This is consistent with the previous observation of simultaneous increases in T_g and tan(δ) when the CNTs are added. Thus, it was assumed that the mechanical properties can evolve with the same exponents and time

constants, but different initial and final values of the mechanical properties. The fits using the values in Table 7.2 can also be seen in Figure 7.2. Thus, it would appear that the curing results in an increase of 36% and 27% in the strength and stiffness respectively using 0.2 wt. % CNT, and 31% and 23% in the strength and stiffness respectively using 0.5 wt. % CNT.

parameter	0 wt. % CNT	0.2 wt. % CNT	0.5 wt. % CNT
σ_{u0} (MPa)	23	27	25
$\sigma_{u\infty}$ (MPa)	36	49	47
E_0 (MPa)	1100	1300	1250
E_∞ (MPa)	1500	1875	1825

Table 7.2. Parameters for Arrhenius model and corresponding fit values.

The mechanism responsible for the change in ductility may not be the same one responsible for the change in the peak tan(δ) observed in Figure 7.1, which is most likely an increase in adhesion at the filler-epoxy matrix interface. Instead, it may be due to a change in the copolymer reinforcement of the epoxy matrix which typically results in an increase in impact toughness. For the CNT-filled epoxy, the decrease in ductility would be more consistent with an increase in the adhesion between the CNTs and epoxy matrix. In fact, it would appear that the increase in ductility of the neat epoxy matrix is more than offset by the increase in adhesion with the CNTs.

SEM micrographs from a cryomicrotomed specimen of filled epoxy with CNT filler, as seen in Figure 7.3, revealed attraction of the CNTs to the glass fibers in the filled epoxy. These nano reinforcements which acted like “Velcro” at

the fiber-matrix interface to increase the interfacial adhesion which subsequently increases the strength. Furthermore, 0.5 wt. % CNT specimens exhibited higher levels of ductility relative to the 0.2 wt. % specimens, probably due to the increased density of CNTs at the fiber-matrix interface that may adversely affect adhesion and could be responsible for the lower strength and stiffness as well.

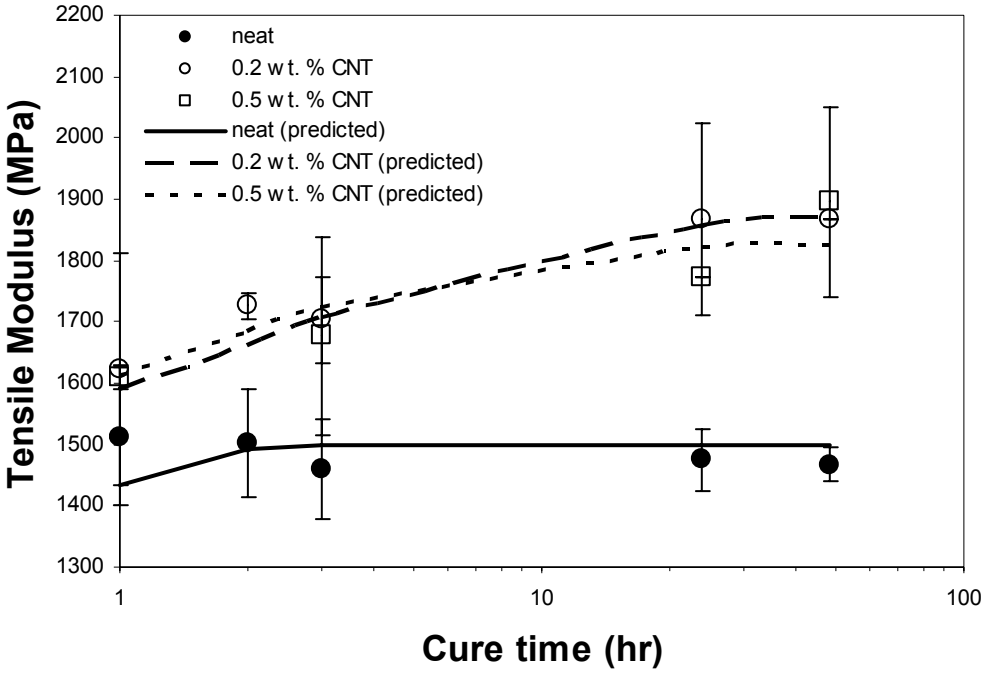

(a)

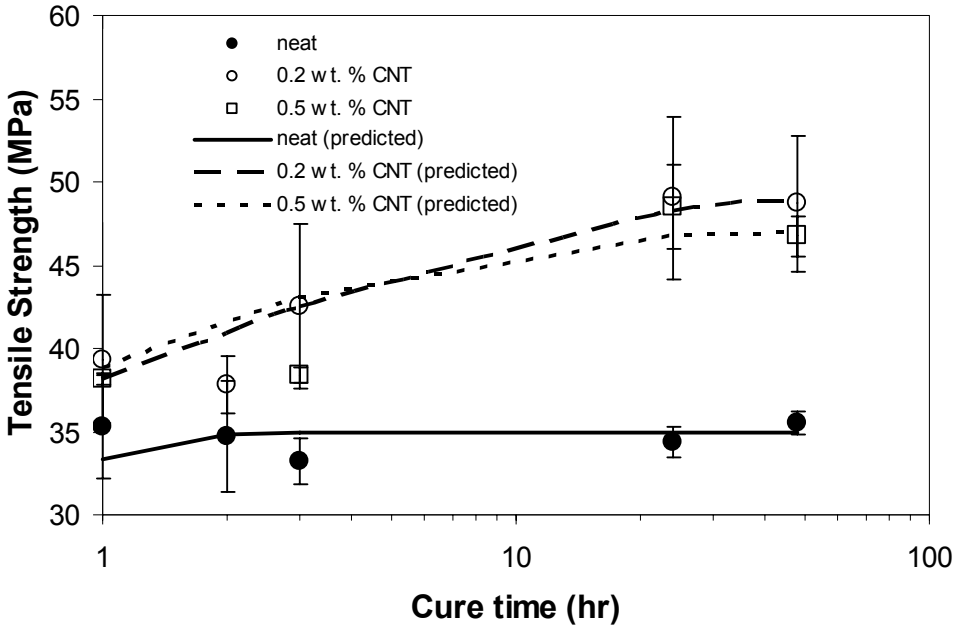

(b)

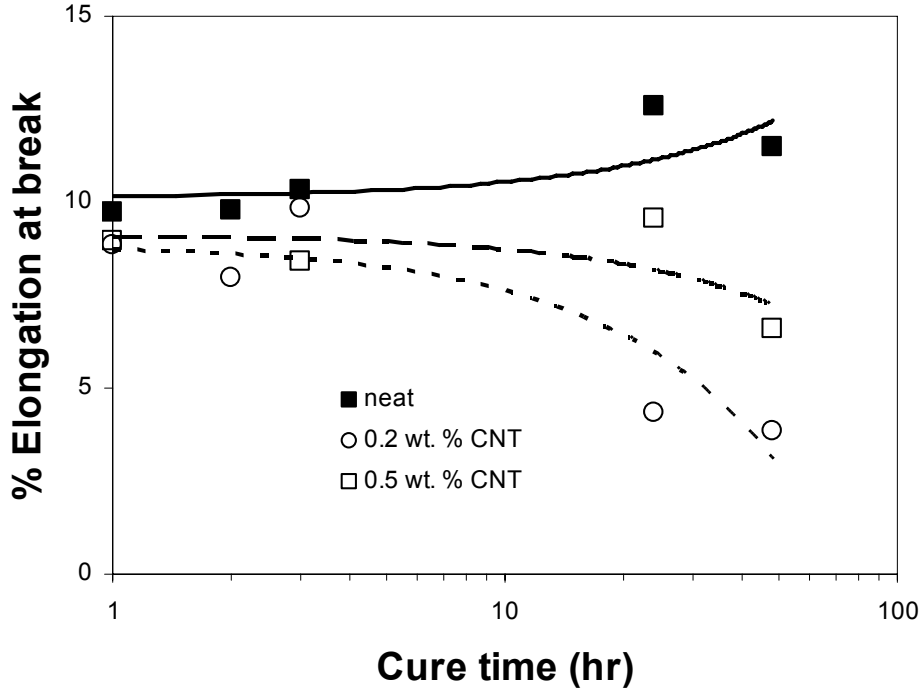

(c)

Figure 7.2. The variation in (a) tensile modulus, (b) strength, and (c) % elongation at break with cure time for the epoxy with and without CNT reinforcement indicating a substantial increase in strength and stiffness with cure time.

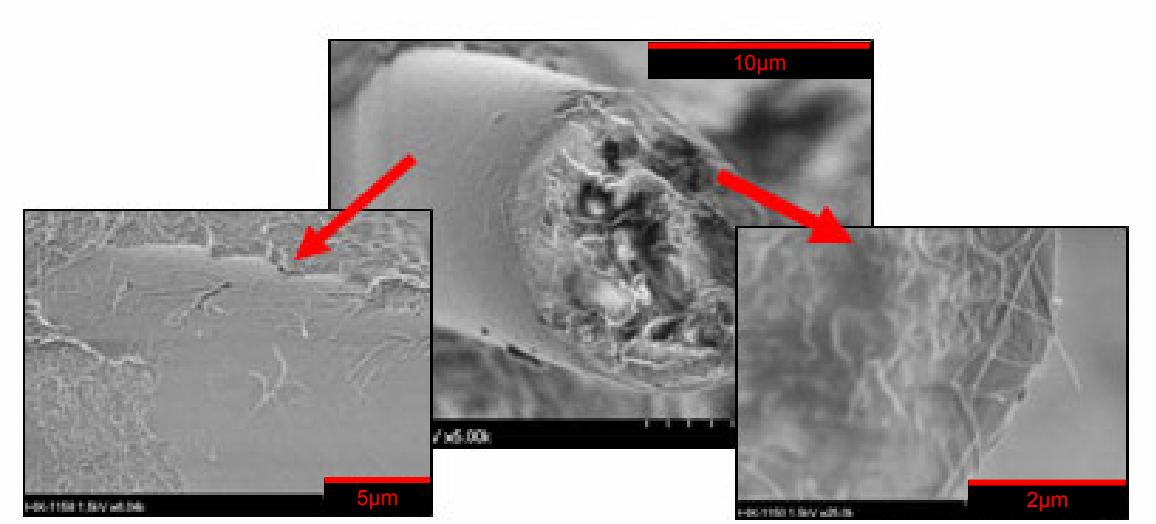

Figure 7.3. SEM micrographs of CNT reinforced filled epoxy indicating the attraction of CNT to silica fibers acting like Velcro that increase and improve interfacial adhesion for increased strength relative to ductility of the epoxy. The specimen was prepared by a 'freeze-fracture" method where the sample is exposed to liquid nitrogen to make the material brittle, then quickly snapped for cross-sectional views.

7.3 Nanomechanical characterization

In addition to point measurements, property maps were obtained to discern the variation due to the complex microstructure of the Hysol 9309.2. Maps were obtained in one of two ways: (a) modulus mapping at 3 µN dynamic load and 125 Hz, and (b) quasi-static at 300 µm load. The modulus mapping is limited in the load capacity because it drags the indenter across the surface, similar in principle to contact AFM, and therefore, obtains information that is more related to the surface of the material (e.g., surface features and property variations). However, it is very fast, taking only 20 minutes. The quasi-static nanoindentation is much slower, taking approximately one hour per 10 points. However, it can be used at much higher loads to diminish surface effects and sample only property variations due to microstructure. Results of the complex

modulus map from nanoDMA as well as the reduced modulus and hardness from quasi-static nanoindentation were obtained over 60 micron areas.

7.3.1 Quasi-static nanoindentation

Property mapping was completed for the nano-enhanced Hysol 9309.2 with several different time periods of post cure at 80°C. Figure 7.4 shows maps of reduced modulus for neat Hysol 9309.2 and 0.2 wt. % CNT with 1, 3 and 24 hours of post cure, Figure 7.5 shows hardness maps for the same materials and Figure 7.6 has the topographical representations of the same materials. A summary of these properties can be seen in Table 7.3.

CNT wt. %	Cure time (hrs)	Reduced Modulus (GPa)		Hardness (MPa)	
		Average	Standard Deviation	Average	Standard Deviation
0	1	2.13	0.16	34	3.5
0	3	2.03	0.21	41	6.9
0	24	2.30	0.19	49	4.9
0.2	1	2.08	0.25	37	6.5
0.2	3	2.26	0.10	50	5.0
0.2	24	2.46	0.23	53	9,5

Table 7.3. Comparison of reduced moduli and hardness in neat and 0.2 wt. % CNT Hysol 9309.2 after 1, 3, and 24 hours of cure at 80°C.

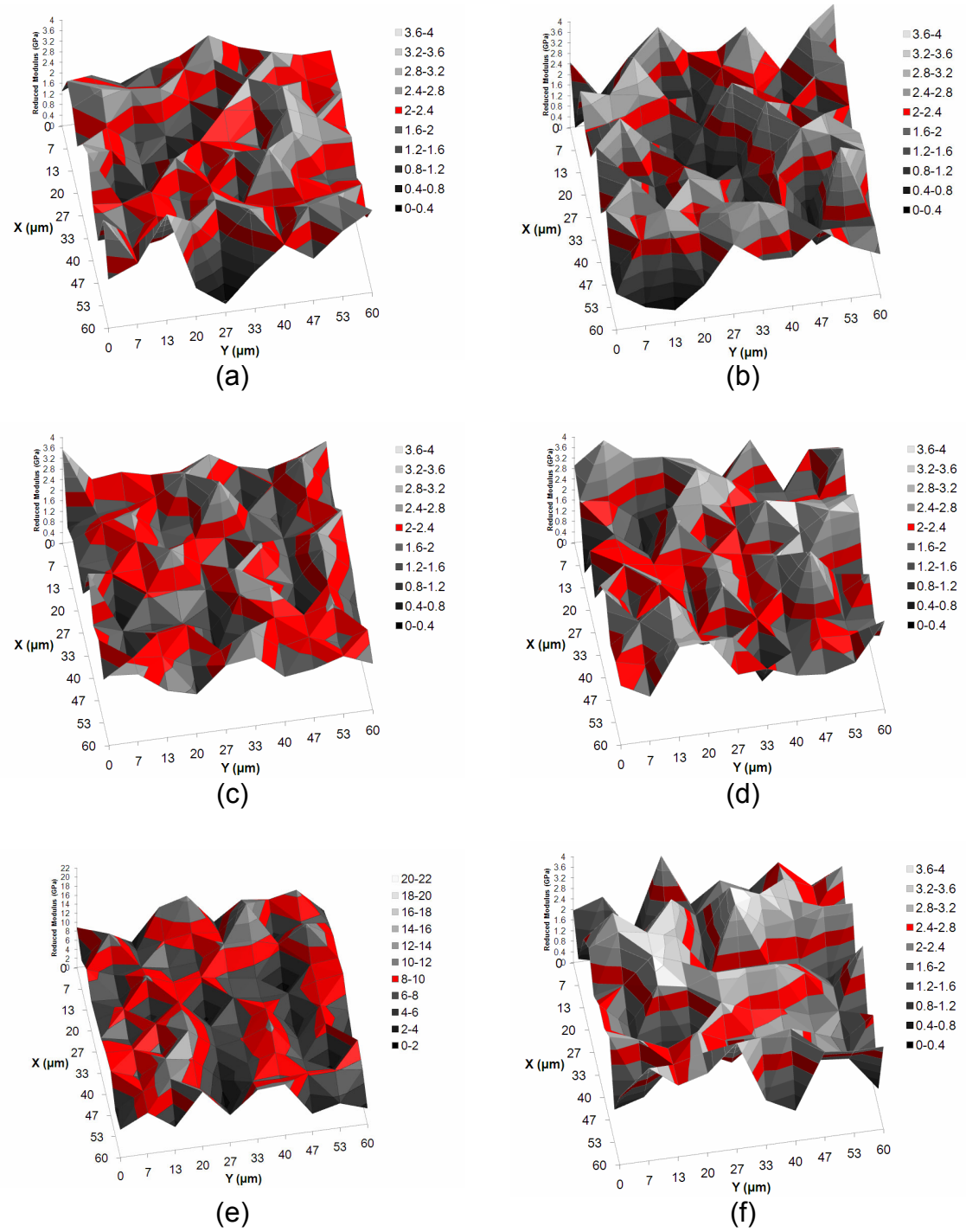

Figure 7.4. Maps of reduced modulus obtained from quasi-static measurements at 300 μN on (a) neat material with 1 hour 80°C cure, (b) 0.2 wt. % material with 1 hour 80°C cure, (c) neat material with 3 hour 80°C cure, (d) 0.2 wt. % material with 3 hour 80°C cure, (e) neat material with 24 hour 80°C cure, (f) 0.2 wt. % material with 24 hour 80°C cure. The red bands depict regions in which the averages fall.

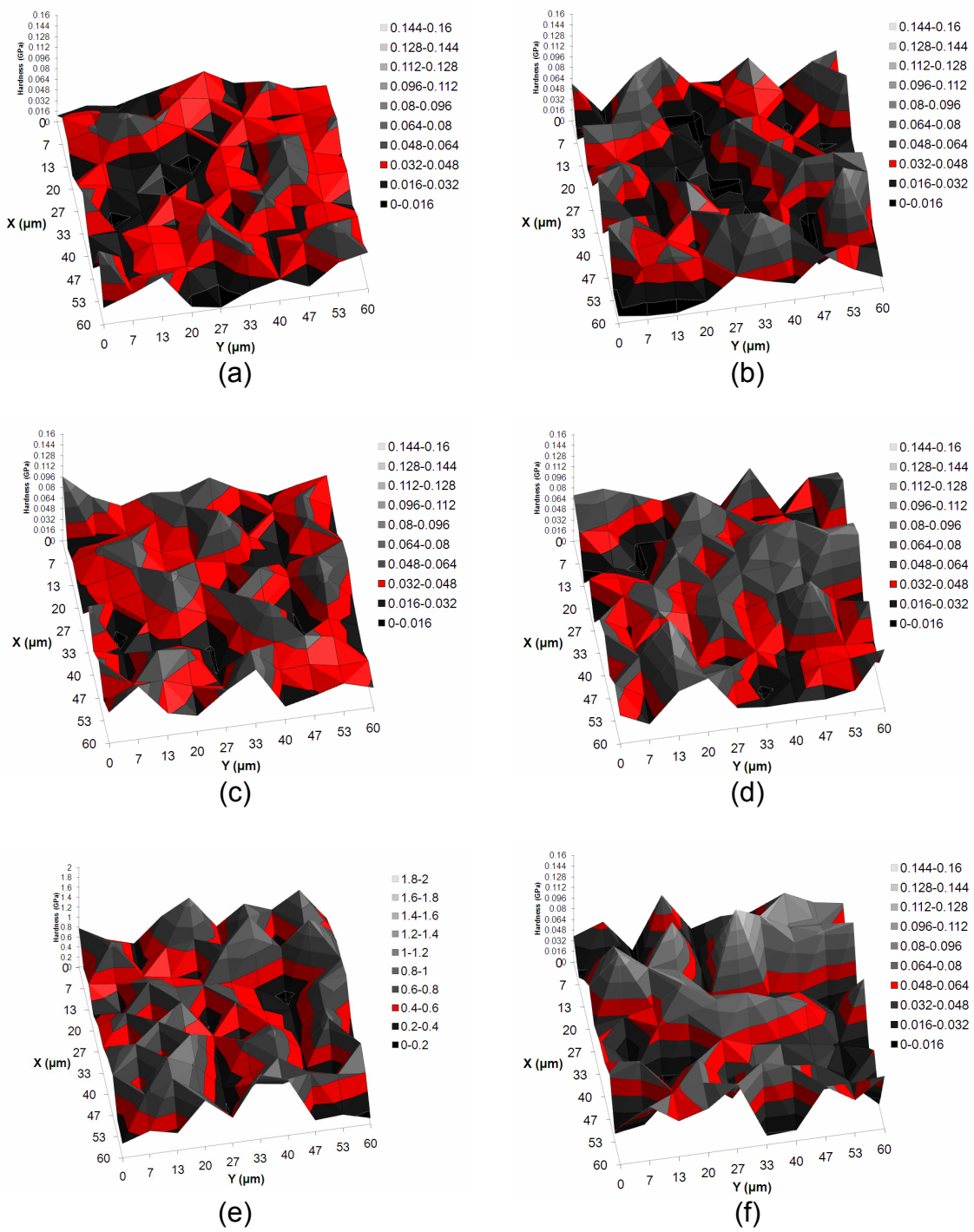

Figure 7.5. Maps of hardness obtained from quasi-static measurements at 300 μN on (a) neat material with 1 hour 80°C cure, (b) 0.2 wt. % material with 1 hour 80°C cure, (c) neat material with 3 hour 80°C cure, (d) 0.2 wt. % material with 3 hour 80°C cure, (e) neat material with 24 hour 80°C cure, (f) 0.2 wt. % material with 24 hour 80°C cure. The red bands depict regions in which the averages fall.

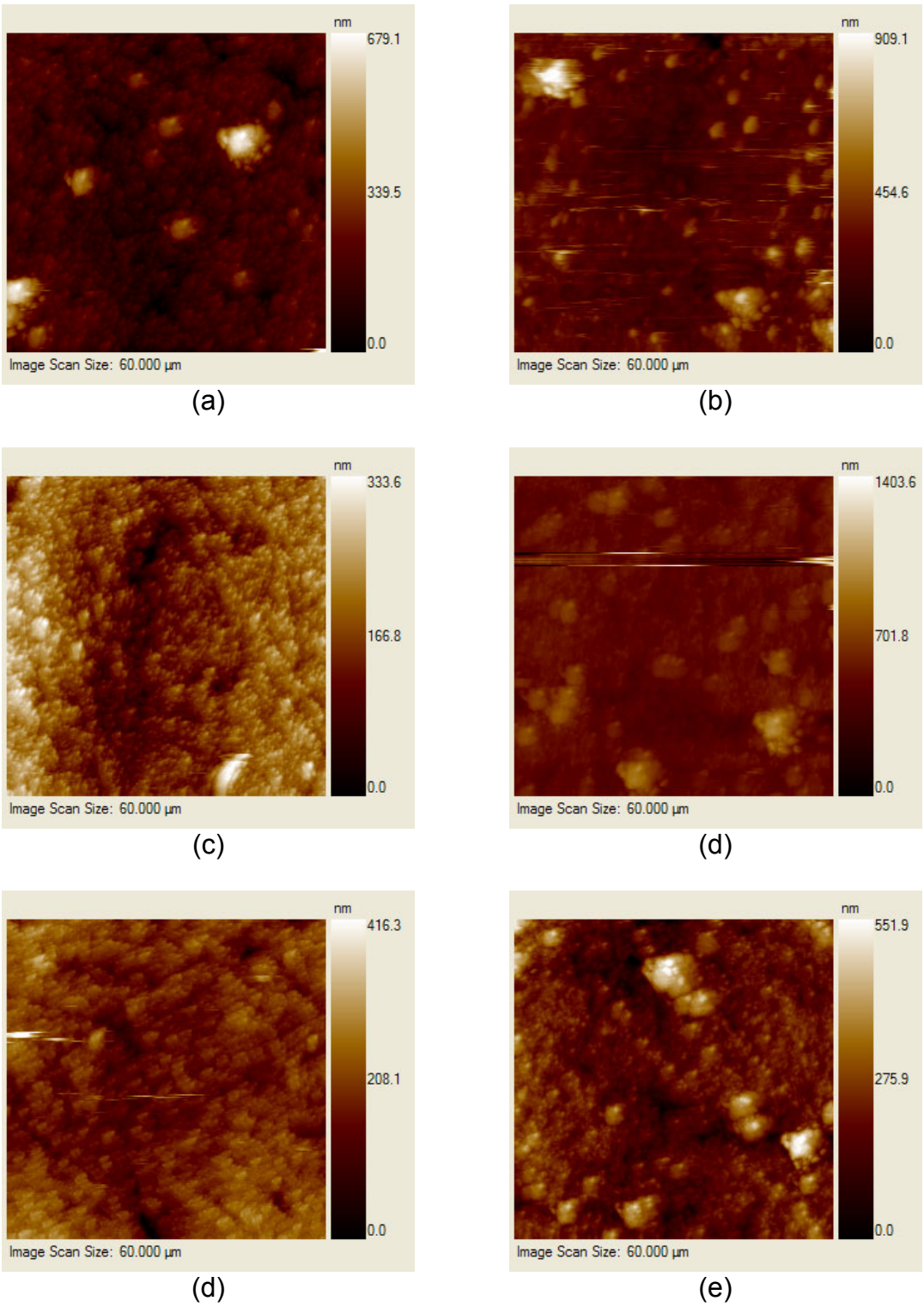

Figure 7.6. Topographical representations of (a) neat material with 1 hour 80°C cure, (b) 0.2 wt. % material with 1 hour 80°C cure, (c) neat material with 3 hour 80°C cure, (d) 0.2 wt. % material with 3 hour 80°C cure, (e) neat material with 24 hour 80°C cure, (f) 0.2 wt. % material with 24 hour 80°C cure.

7.3.2 Modulus mapping

Modulus mapping was completed on these specimens to complement the quasi-static property mapping. A summary of the data can be seen below in Table 7.4, and the complex modulus and tan(δ) maps can be seen in Figure 7.7 and Figure 7.8 respectively, with their corresponding topographical representations in Figure 7.9. From these maps, it can be seen that the changes in complex modulus and tan(δ) at the nanoscale with curing time are similar to those seen in the microtensile tests. However, the effects seem to be greater at the larger length scales. This may be due to the fact that there is an additional benefit on the mechanical properties obtained from the "Velcro-like" adhesion mechanism through the interaction of the CNTs with the microscale reinforcement that is enhanced with curing. However, the nanoscale data does indicate through tan(δ) that the epoxy is becoming more "elastic" due to the CNT reinforcement independent of curing. This is most likely due to the percolation effects that were previously seen in the nano-enhanced thermoplastics.

CNT wt. %	Cure time (hrs)	Complex Modulus (GPa)		Tan(δ)	
		Average	Standard Deviation	Average	Standard Deviation
0	1	1.38	0.10	0.19	0.02
0	3	1.39	0.10	0.18	0.02
0	24	1.49	0.12	0.18	0.03
0.2	1	1.76	0.11	0.13	0.02
0.2	3	1.88	0.16	0.10	0.02
0.2	24	1.90	0.14	0.11	0.02

Table 7.4. Comparison of complex moduli and tan(δ) in neat and 0.2 wt. % CNT Hysol 9309.2 after 1, 3, and 24 hours of cure at 80°C.

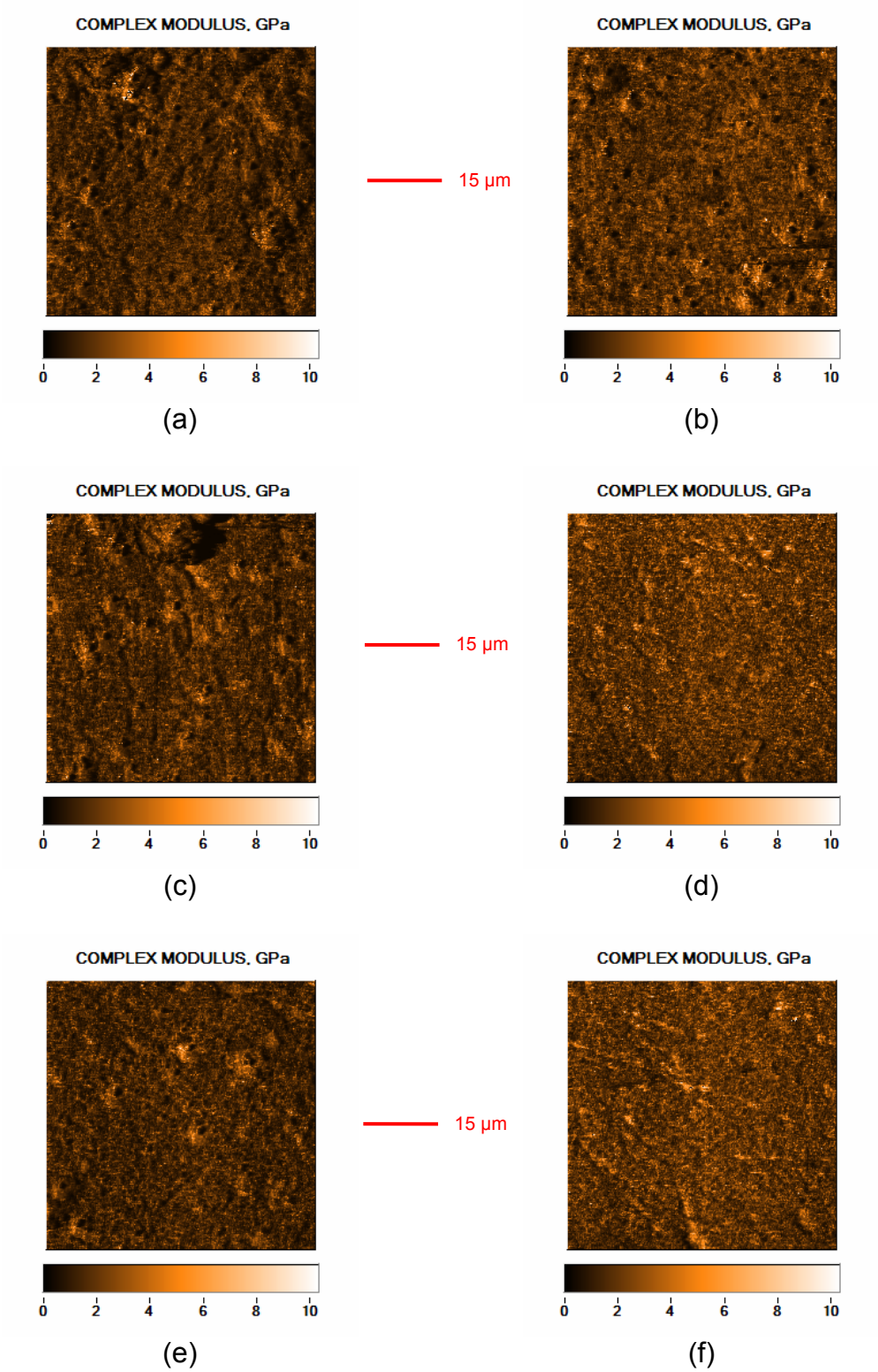

Figure 7.7. Complex modulus maps of Hysol 9309.2 with (a) 0 wt. % 1 hr post cure, (b) 0.2 wt. % 1 hr post cure, (c) 0 wt. % 3 hrs post cure, (d) 0.2 wt. % 3 hrs post cure, (e) 0 wt. % 24 hrs post cure and (f) 0.2 wt. % 24 hrs post cure.

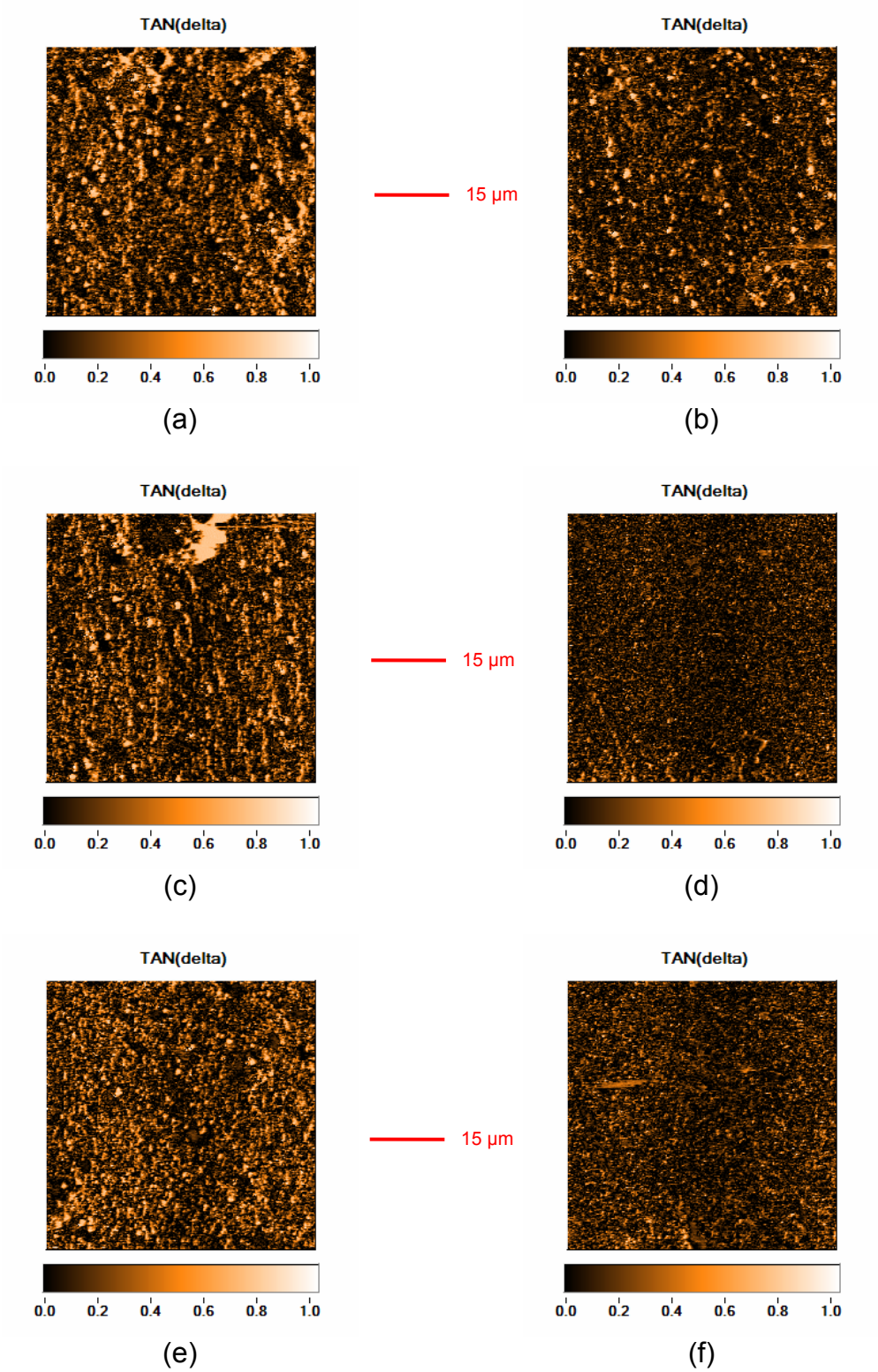

Figure 7.8. Tan(δ) maps of Hysol 9309.2 with (a) 0 wt. % 1 hr post cure, (b) 0.2 wt. % 1 hr post cure, (c) 0 wt. % 3 hrs post cure, (d) 0.2 wt. % 3 hrs post cure, (e) 0 wt. % 24 hrs post cure and (f) 0.2 wt. % 24 hrs post cure.

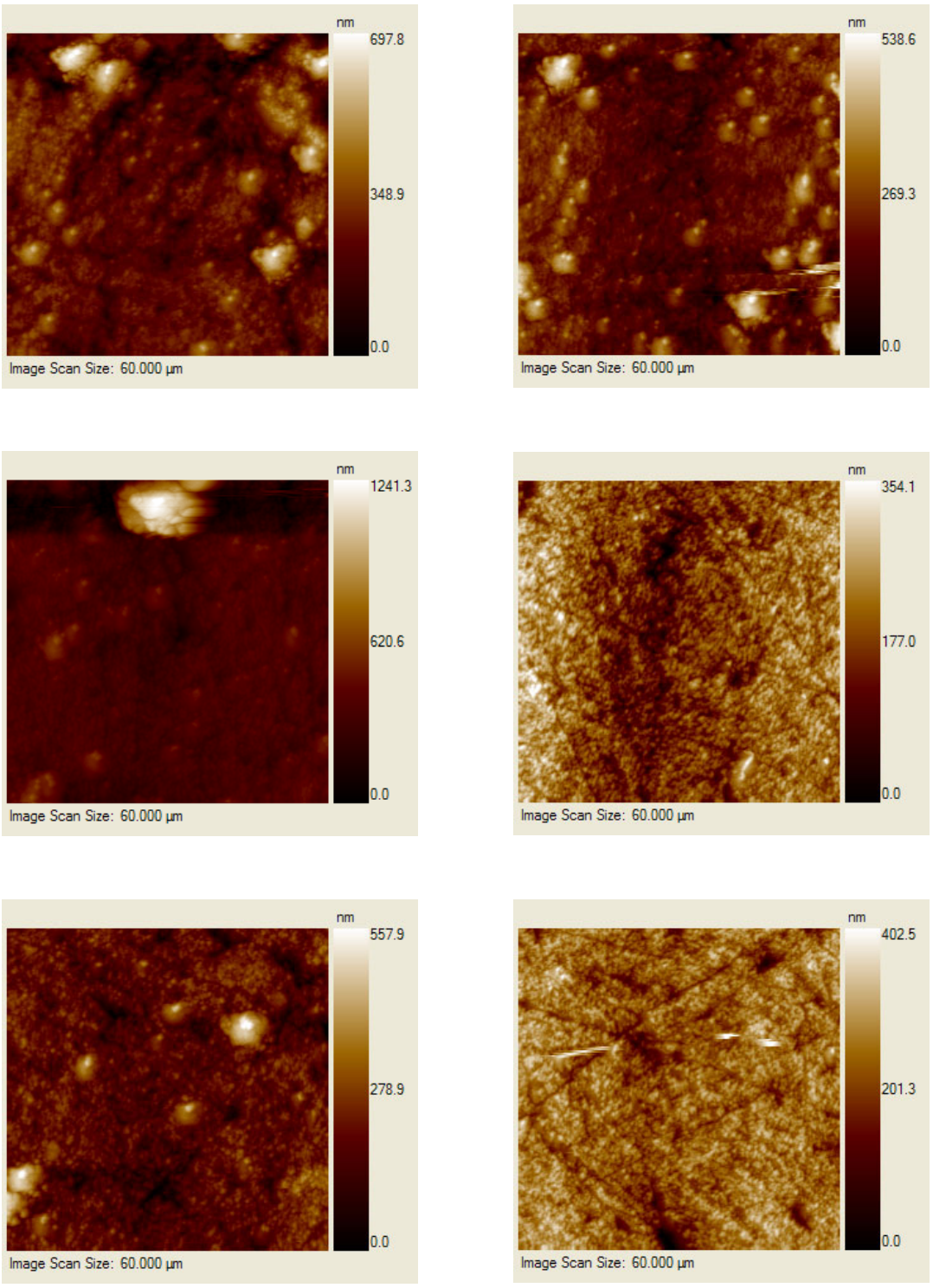

Figure 7.9. Topographical representations of Hysol 9309.2 with (a) 0 wt. % 1 hr post cure, (b) 0.2 wt. % 1 hr post cure, (c) 0 wt. % 3 hrs post cure, (d) 0.2 wt. % 3 hrs post cure, (e) 0 wt. % 24 hrs post cure and (f) 0.2 wt. % 24 hrs post cure.

The effects of CNTs on the development of adhesion associated with the kinetics of epoxy curing have been characterized and modeled. In addition, a new adhesion mechanism responsible for the increase in strength and stiffness due to the "Velcro-like" interaction of CNTs with microscale reinforcement was identified and quantified. The effects of the CNT reinforcement on the evolution of mechanical properties in the epoxy during curing were distinguished from the new adhesion mechanism through nanomechanical characterization.

7.4 Summary

The effect of an additional thermal processing step, cure time, in hierarchically-structured nano-enhanced thermosets on thermal and mechanical properties has been characterized with the multi-scale characterization approach using Hysol as a model filled adhesive with CNTs. A kinetics model of the curing process was applied to understand the changes in the time constant and exponent associated with the addition of CNTs to the adhesive. Thus, the multi-scale characterization and modeling approach provided better understanding of the processing-structure-property relationships of several hierarchically-structured nano-enhanced polymers. Using these same characterization methods, it was next possible to study and model the properties of a model natural hierarchically-structured material, palmetto wood, in order to provide a connection between biological and synthetic hierarchically-structured materials that can serve as a basis for biological inspiration.

Chapter 8 Multi-scale mechanical characterization of a model natural hierarchically-structured material: palmetto wood

A macroscale cross-section of the palmetto wood can be seen in Figure 8.1. From this cross-section, it can be seen that a thin layer of approximately 1-2 mm of hard bark covers a 2-3 cm thick layer of soft, loose fiber fill. Below the loose fiber fill is the core of the palmetto wood.

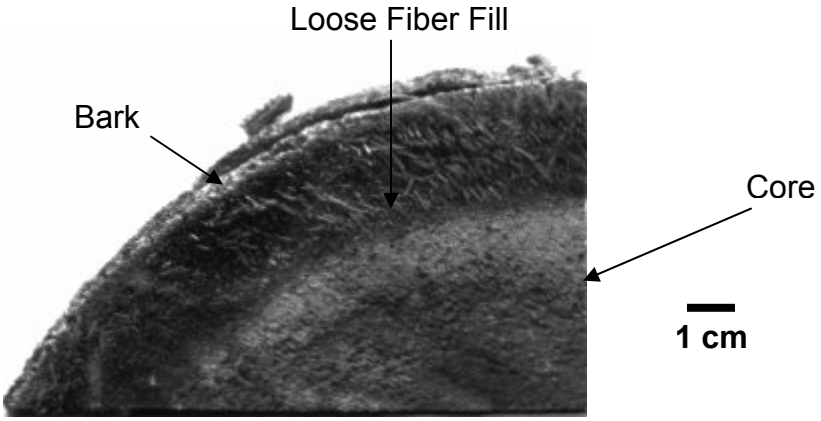

Figure 8.1. Cross-section of palmetto wood showing macroscale structure consisting of bark, fiber fill and the core. Image obtained with a digital camera.

To determine the multi-scale structure of the core, optical microscopy was first performed to bridge the milliscale and microscale. These results can be seen in Figure 8.2. Small fibers can be seen at the milliscale that are randomly distributed but aligned with the axis of the tree and with a gradient of high concentration at the outer surface of the core and decreasing as the center of the core is approached. There are also regions of optically dark wood separated by optically light wood. The core is composed of a porous cellulose matrix reinforced with irregularly shaped fibers of approximately 300-500 microns in

diameter. Finally, within the fibers are small capillaries that are roughly 20-60 microns in diameter.

Details of the microfibers can be seen in Figure 8.3. The contrast in the image was obtained by straining the wood. The strain enabled the softer inner portion of the layers to be compressed by an approximately 1 micron thick hard outer layer that resulted in bulging and surface gradients that enhanced Differential Imaging Contrast. Each microfiber consists of 3 to 5 rings that are approximately 10 microns in thickness.

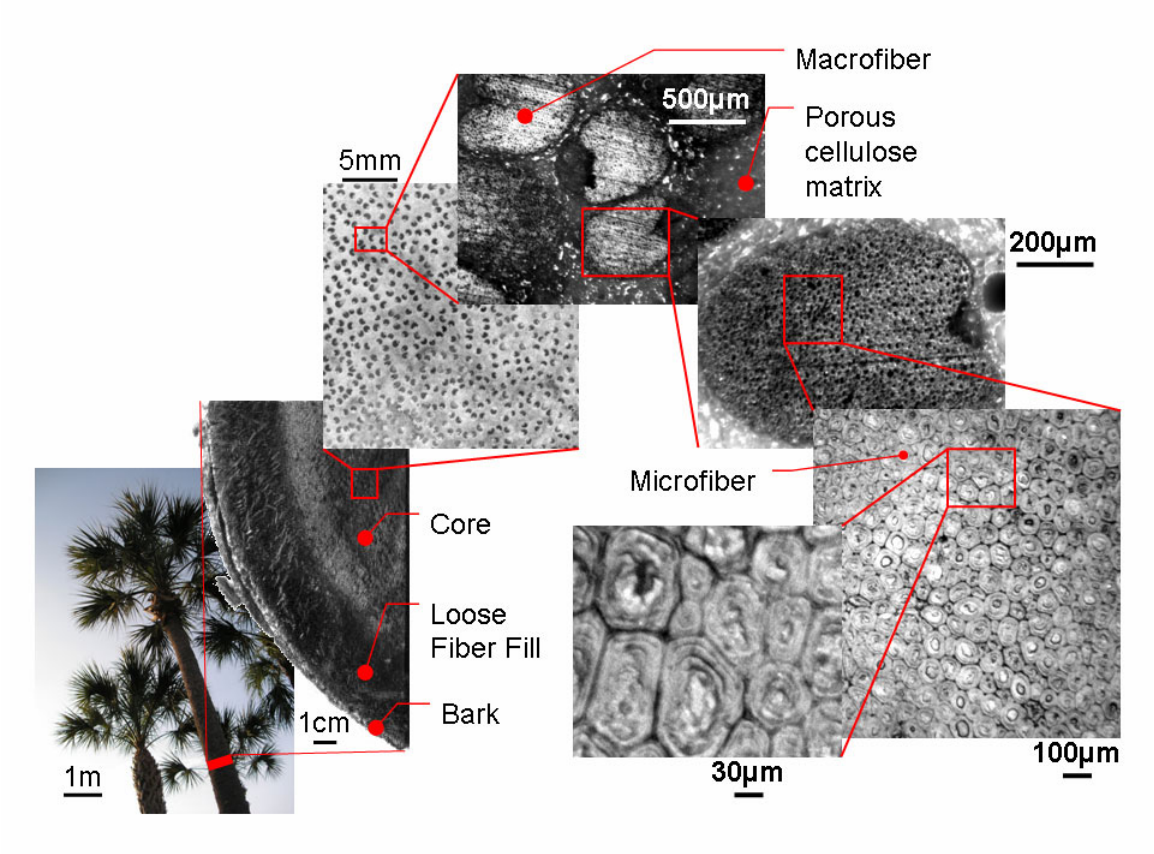

Figure 8.2. Hierarchical structure of palmetto wood from macroscale to microscale. Images obtained with a digital camera or through optical microscopy.

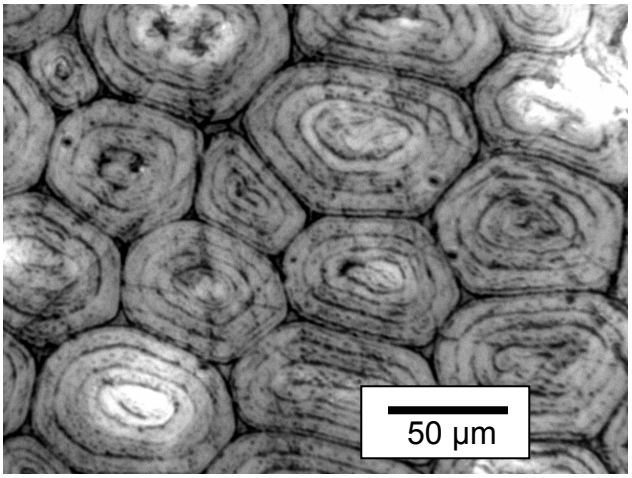

Figure 8.3. Microfibers in the core of the wood. The contrast between the layers was obtained by straining the wood. Image obtained through optical microscopy.

8.1 Pycnometric characterization of porosity

To understand the volume of the core that was composed of free volume in the capillaries, gas pycnometry measurements were obtained. These measurements can be seen in Table 8.1 for an optically dark and optically light piece of wood. The bulk density of the wood is 0.25 g/cc for the dark and 0.30 g/cc for the light. Furthermore, the true density is also higher for the light wood – 1.49 g/cc versus 1.41 g/cc for the dark wood. This results in a volume fraction of porosity of 0.79 for the dark and 0.83 for the light. When the samples are moist, the density is almost identical at approximately 1.08 g/cc. Thus, it would appear that the darker cellulose matrix has a lower true density but less porosity than the lighter matrix, and that the microstructure is designed to produce a uniform wet density.

% Macrofibers	Bulk density (g/cc)	True density (g/cc)	Volume Fraction Porosity	Wet density (g/cc)
12%	0.25	1.41	0.79	1.09
20%	0.30	1.49	0.83	1.08

Table 8.1. Pycnometry measurements of dark and light sections from the core of the palmetto wood.

8.2 Dynamic failure resistance characterization using Charpy impact

Instrumented Charpy impact tests were conducted on dry specimens from both the light and dark regions of the core, as seen in Figure 8.4. This enabled determination of the effects of the difference in the matrix material on the impact failure energy. Results from the Charpy impact tests can be seen in Table 8.2. The dark wood had a Charpy Impact Energy Density of 10.80 J/cm^2 while the light wood was 16.59 J/cm^2, an increase of 54%. However, if the specific energy density is calculated using the porosity, the differences drop to only 27% with the dark wood being 434 J-m/kg and the light wood 552 J-m/kg. Thus, it appears that the lower true density of the dark wood results in lower impact energy density despite the lower volume fraction of porosity. This tends to indicate that the dark porous cellulose is fundamentally weaker than the light porous cellulose. These results indicate an increase in Charpy Impact Energy of approximately 60% for the light wood and 33% for the specific energy. Note how the fibers break in these higher loading rate tests, as can be seen in Figure 8.5.

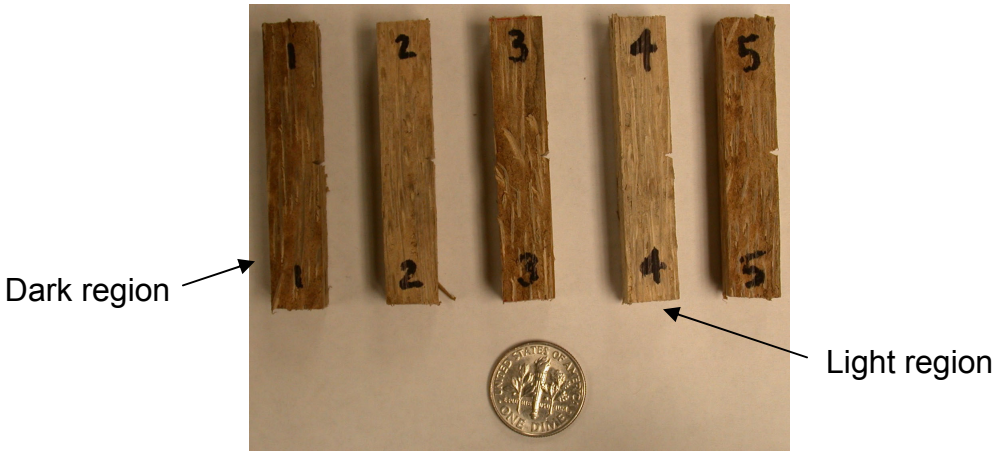

Figure 8.4. Charpy impact specimens from light and dark regions of the core.

Figure 8.5. Dynamic failure response from Charpy impact test.

% Macrofibers	Charpy Impact Energy Density (J/cm^2)	Specific Charpy Impact Energy Density (J-m/kg)
12%	10.80	434
20%	16.59	552

Table 8.2. Instrumented Charpy impact data from dark and light regions of palmetto wood.

8.3 Static failure characterization using three-point bend

Specimens obtained along the axis of the palmetto that were used for Charpy Impact testing were also tested statically without notches in a three point bend test with a separation between loading points of 62.5 mm. The results can be seen in Figure 8.6. Summary of the results can be seen in Table 8.3.

These results are very similar to those obtained from the Charpy Impact Test. However, the bend energy density is about 1/10th that of the Charpy Impact Test. Also, it appears that the stiffness is similar to the static tensile test ranging from 700 MPa for the dark wood to 1200 MPa for the light, an increase of 70%. The yield strength is much greater in bending though, ranging from 6.9 MPa for the dark wood to 10.0 MPa for the dark wood, while the flexural strength ranges from 12.31 MPa for the dark wood to 22.89 MPa for the light. The percent elongation before failure is also about 3 to 5 times higher in bending than tension. The differences may be explained by the failure of the palmetto seen in Figure 8.7. There is significant localized plastic deformation where the central load is applied, which indicates that the yield strength is indicative of the hardness of the specimen. When failure initiates, it occurs along one of the large microfiber bundles instead of fiber pullout in the tensile test. These fibers are at an angle to the axis of the specimen, so the loading is indicative of the peel strength of the fiber rather than the fiber pullout in the tensile test. Furthermore, it is the stable propagation of the debonding at an angle to the specimen axis that enables the specimen to sustain higher loads post-failure and increase the bend energy density.

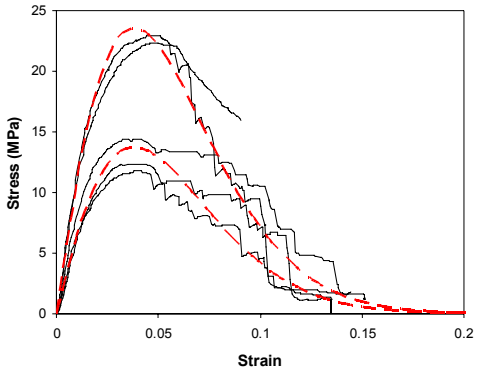

Figure 8.6. Quasi-static three point bend tests conducted on specimens obtained along the axis of the palmetto wood.

% Macrofibers	Bend Modulus (MPa)	Max Yield Strength (MPa)	Max Flexural Strength (MPa)	Bend Energy Density (J/m^2)	% Elongation
12%	700	6.9	12.31	1.04	4.9
20%	1200	10.0	22.89	1.65	6.0

Table 8.3. Summary of quasi-static mechanical properties determined from three point bend testing.

Figure 8.7. Quasi-static three point bend test specimen after failure indicates peeling of the microfiber bundles away from the specimen due to fiber-matrix debonding.

8.4 Characterization of microfiber reinforcement using microtensile testing

Several microfiber samples from the bark (Figure 8.8) ranging in diameter from 80-160 μm were tested on a Microtensile test frame with a load cell capacity of 250 g. The results of a representative fiber can be seen in Figure 8.9. From these results, it would appear that the fiber has a modulus ranging from 4.4-6.9 GPa. The elongation at break of the fiber ranges from 3.2-6.5% with a 0.2% yield stress of 70-120 MPa and an ultimate tensile strength of 95-180 MPa. The properties of the palmetto microfiber are remarkably similar to those of standard polymer microfibers with similar cross-sectional area. Summary of the variation of the properties with diameter can be seen in Table 8.4. Their properties are also similar to the 500 micron microfibers that were tested in the bark, tending to indicate that the fundamental reinforcing behavior in the 500 micron fibers is independent of length scale.

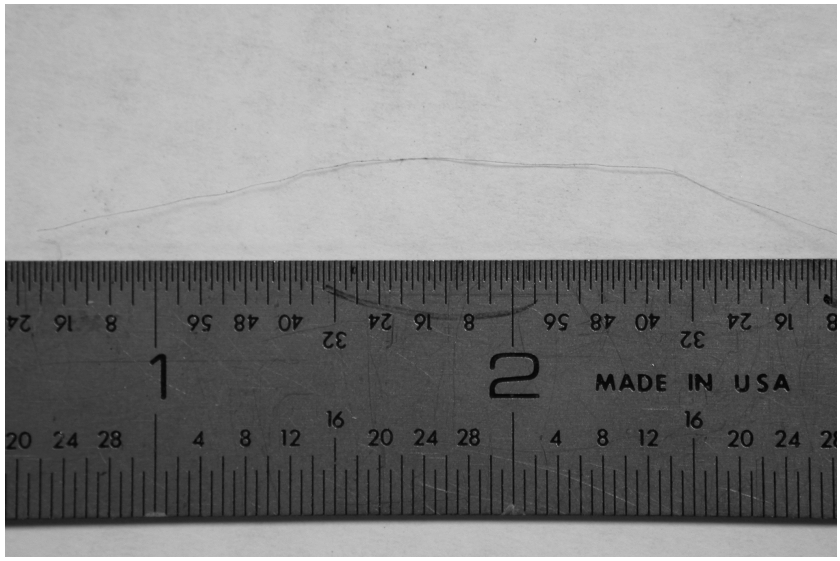

Figure 8.8. 80 μm microfiber from bark.

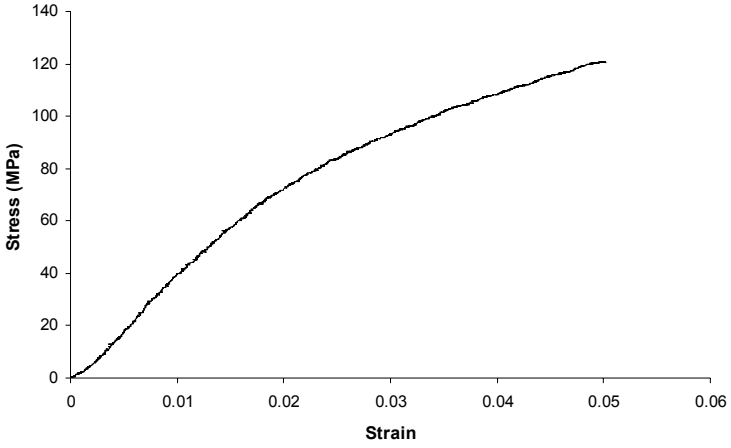

Figure 8.9. Representative microtensile data from 60μm microfiber from bark.

Fiber Diameter (μm)	Modulus (GPa)	0.2% Yield Strength (MPa)	Ultimate Tensile Strength (MPa)	% Elongation
160	4.40	70	95	3.2
145	4.69	80	112	4.2
110	5.33	90	167	4.6
80	6.90	120	180	4.2

Table 8.4. Summary of quasi-static tensile properties for microfibers.

8.5 Nanoscale characterization

8.5.1 Modulus mapping

Modulus mapping of a cross-sectioned and polished macrofiber from the core of the palmetto tree was accomplished with the nanoindenter. From this data, the complex modulus of the walls of the microfibers that make up the macrofiber can be determined. The higher modulus material in the center of the microfibers in Figure 8.10a is an artifact of mounting and polishing. A topographical image of the microfibers can be seen in Figure 8.11.

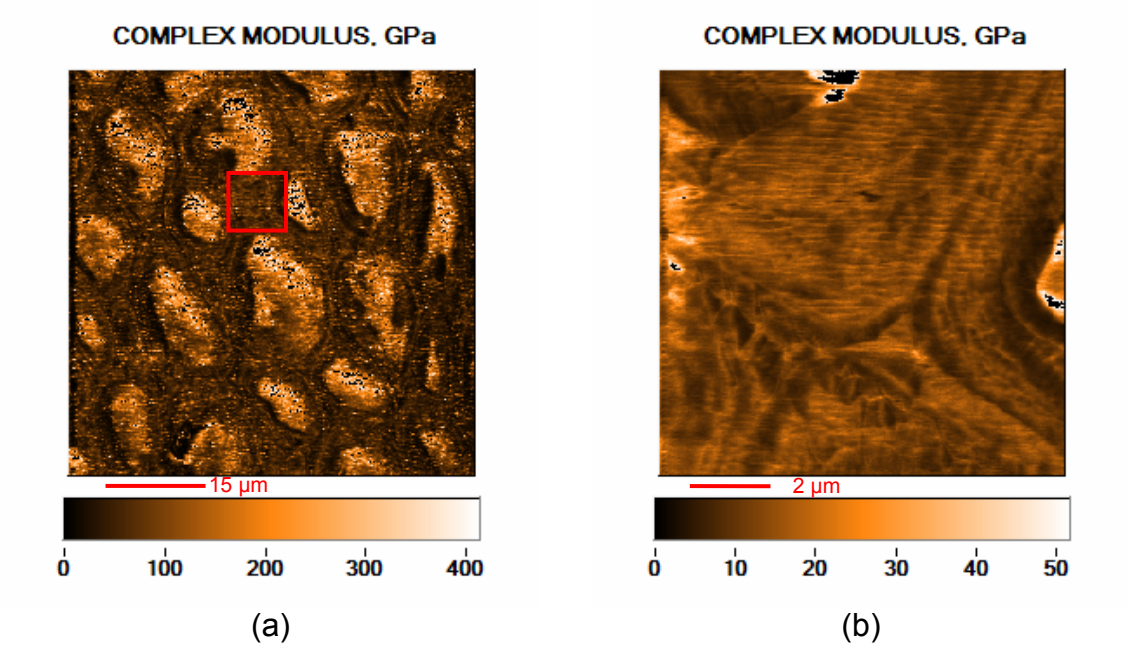

Figure 8.10. (a) 60 µm modulus map of the cross section of a palmetto macrofiber. (b) 10 µm modulus map centered on the red box in (a).

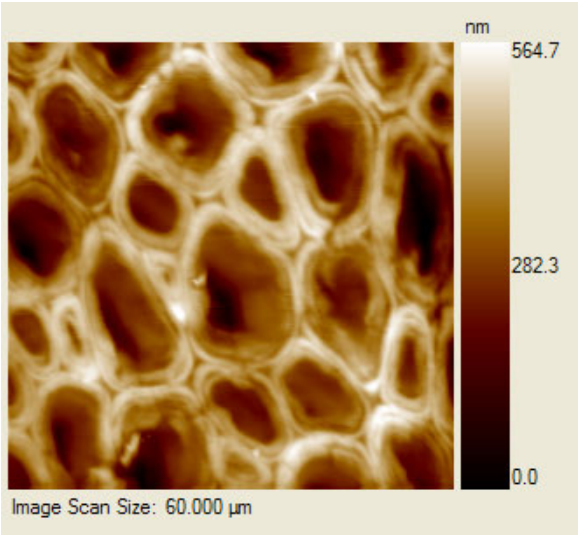

Figure 8.11. Topographical representation of the cross section of a palmetto macrofiber

The walls of the microfibers have a complex modulus, which usually correlates well with the Young's Modulus, of 11.70 GPa. This was determined by extracting the complex modulus data along a line in the modulus map that

appears to be only on the walls of the microfibers, as can be seen in Figure 8.12. The standard deviation of the data over these 256 data points is 2.39 GPa. In addition, the storage modulus (*E'*) – representing the elastic portion of the complex modulus – was extracted along the same line. The average storage modulus was 11.25 GPa, with a standard deviation of 2.21 GPa. Since this value is close to the complex modulus, it indicates that the material is highly elastic in nature rather than viscoelastic.

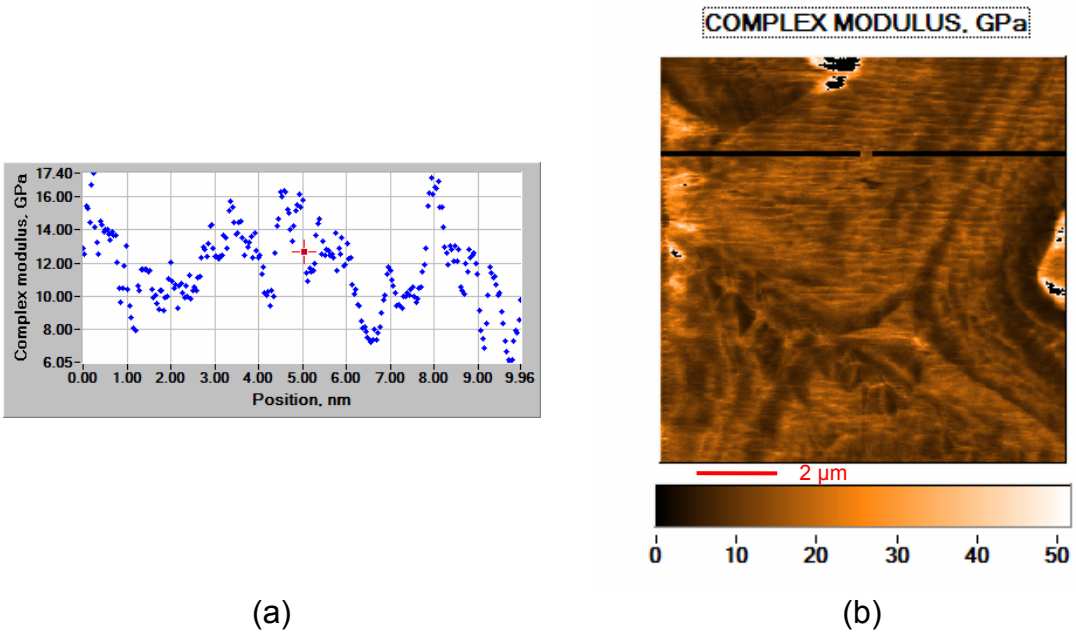

Figure 8.12. (a) Graph of complex modulus data extraction along the line shown in (b).

8.5.2 Quasi-static nanoindentation

In addition, three nanoindents were made on the walls of the microfibers. Pre- and post-indent images can be seen in Figure 8.13. A close up image of a nanoindent can be seen in Figure 8.14. From these nanoindents, the reduced

modulus and hardness of the walls of the microfiber can be determined. The average reduced modulus is 11.44 GPa with a standard deviation of 0.44 GPa, and the average hardness is 375.2 MPa with a standard deviation of 26.6 MPa. The value obtained for the reduced modulus is extremely close to the values obtained for both the complex and storage moduli from modulus mapping, which indicates that the properties obtained from the nanoDMA are quantitatively accurate measurements of the elastic behavior of the microfibers at the nanoscale. The moduli values for each method of nanomechanical measurement are summarized in Table 8.5.

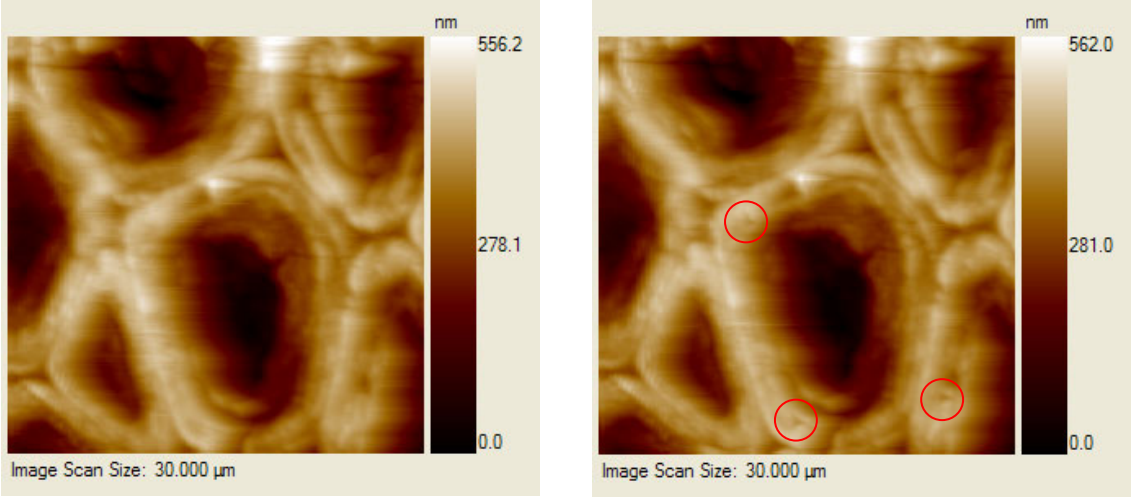

(a) (b)

Figure 8.13. (a) Pre-indent topographical image of microfibers.
(b) Post-indent topographical image with nanoindents circled in red.

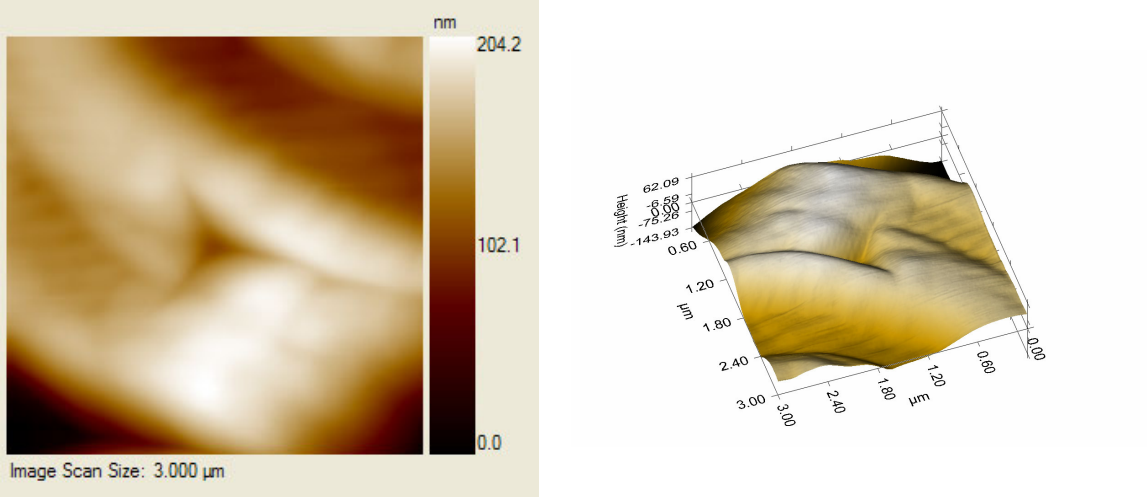

(a) (b)

Figure 8.14. (a) Topographical and (b) 3 dimensional images of a close up view of a nanoindent made in the wall of a microfiber.

Nanomechanical Measurement	Modulus (GPa)	Hardness (MPa)
NanoDMA (Storage Modulus)	11.25 ±2.21	N/A
NanoDMA (Complex Modulus)	11.70 ±2.39	N/A
Quasi-static Nanoindentation	11.44 ±0.44	375.2 ±26.6

Table 8.5. Summary of mechanical properties of microfiber from nanoindentation measurements

8.5.3 Determination of porosity

During the polishing process, epoxy was deposited in the pores of the microfibers. This is seen in Figure 8.10a as the areas of higher complex modulus. From this, the average porosity of the macrofiber can be determined. By manipulating the image to obtain a binary color distribution through a threshold process, the walls and pores of the microfibers can be distinguished. Because of the binary nature of the image, the average color value of the image

will give the average porosity over the image. Using ImageJ version 1.41o, the image is cropped, converted into 8-bit grayscale color depth, and adjusted with a threshold to obtain the image seen in Figure 8.15.

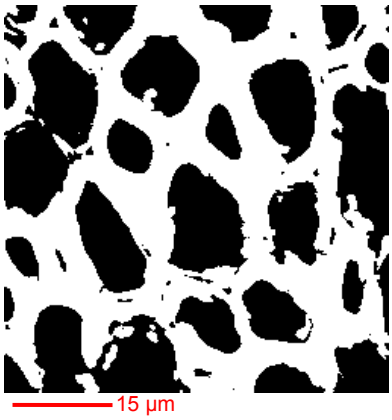

Figure 8.15. Processed image used to obtain porosity.

The taking a value of 255 for each white pixel and 0 for each black pixel, the average value of the image can be determined. This value corresponds to the porosity of the macrofiber. In this case, over an area of 65,024 pixels, the average value is 124.1, which corresponds to a porosity of 48.7%.

8.6 Multi-scale modeling of mechanical behavior of palmetto wood

The nanoindentation of the individual microfibers and tensile testing of the macrofiber can now be used to develop a multi-scale model of the mechanical behavior of palmetto wood. Based on the measured porosity, it is reasonable to assume that a linear ROM model can be applied to the nanoscale properties of the microfiber to obtain the microscale properties of the macrofiber. Thus, a

predicted modulus of approximately 5.88 GPa would be expected. This value is near the high end of the range of moduli obtained for the macrofibers, which was 4.40 GPa for a 160 micron diameter macrofiber to 6.90 GPa for an 80 micron diameter macrofiber.

Typically, the hardness of a material, H, can be related to the yield strength, Y, as follows in Equation 8.1 [Masu06]:

$$\frac{H}{Y} = \frac{2}{3}\left(1 + \ln\left(\frac{E\cot(\theta)}{3Y}\right)\right) \qquad \textbf{8.1}$$

where E is the Young's Modulus and θ is the half-angle of the indenter, which is 65.35° for a Berkovich. The resulting strength would be 172 MPa for the microfiber. Therefore, using the same linear ROM model on the microfiber hardness would yield a strength of 86 MPa for the macrofiber. This is on the low end of the range of 0.2% yield strengths for the macrofiber, which was 70 MPa for a 160 micron diameter macrofiber to 120 MPa for an 80 micron diameter macrofiber. Thus, it would appear that the bundles of microfibers are effectively translating their properties from the nanoscale up to the microscale in the macrofiber via a linear ROM relationship.

To extend the multi-scale mechanical model to the macroscale, it is necessary to analyze the macroscale behavior of the three-point bend specimens in more detail. When failure initiates, it occurs as a debond along the macrofiber-cellulose interface. These fibers are at an angle to the axis of the specimen, so the loading is indicative of the peel strength of the macrofiber-cellulose interface rather than the fiber pullout strength. Furthermore, it is the stable propagation of the debond at an angle to the specimen axis that enables higher post-failure

loads and increased bend energy density due to fiber-bridging. In general, the failure response in bending can be described through Weibull failure statistics as follows in Equation 8.2 [Zhou01]:

$$\sigma = E\varepsilon \exp\left[-\left(\frac{\varepsilon}{\varepsilon_o}\right)^{\beta}\right] \qquad \textbf{8.2}$$

where the stress, σ, varies with the strain, ε, the scaling Weibull parameters ε_o and β, and the elastic modulus, E. Fits to the experimental data can be seen in Figure 8.6. These results indicate that E depends on % macrofibers varying from 700 to 1200 MPa as previously indicated in Table 8.3, and the Weibull parameters are 0.05 and 1.5 for ε_o and β respectively. Therefore, it appears that the physical distribution of macrofiber reinforcement enables the palmetto tree to modify the distribution of stiffness throughout its core without altering the inherent failure mechanism defined by the constants in Equation 8.2.

Now that the macroscale mechanical behavior has been established, it is possible to relate the microscale properties of the macrofiber to the macroscale properties of the palmetto wood. Once again, applying a linear ROM analysis to the predicted macrofiber properties based on the vol. % macrofibers in the palmetto wood, a modulus of 706 MPa would be expected for 12 vol. % while 1180 MPa for 20 vol. %. These correlate exactly to the moduli obtained from the analysis in Equation 8.1. Furthermore, it would appear the Weibull parameter of 0.05 for ε_o correlates well with the 3.2 to 4.2% failure strains for the macrofibers. However, the yield strengths of 6.9 MPa for 12 vol. % and 10.0 MPa for 20 vol. % at the macroscale are approximately 40% lower than expected from a linear

ROM prediction from the microscale properties, which would indicate yield strengths of 10.32 to 17.2 MPa. So, it would appear that the multi-scale elastic behavior has a strong correlation with a linear ROM prediction of modulus, while the strength appears to have a slightly weaker correlation. This may not be unexpected, since the macroscale yield mechanism is not purely due to macrofiber yielding. Instead, it is possible that there is interfacial debonding that is limiting the yield strength of the palmetto wood. The bond strength still produces approximately 60% of the predicted value, which is quite substantial. Thus, the limiting factor in translating the nanoscale properties of the microfibers to the macroscale properties of the palmetto wood appear to be the interfacial bond strength for the macrofibers, rather than other factors such as the strength of the macrofibers or the interfacial strength of the microfibers themselves.

This multi-scale model is the first quantitative insight into the relationship between the hierarchical structure of natural materials, in this case palmetto wood, and the properties of those materials. It can serve as a guide to understanding how the synthetic hierarchically-structured materials described in this dissertation can be developed in order to optimize properties, such as strength-to-weight and stiffness-to-weight ratios. In particular, the work indicating the Velcro-like behavior of CNTs at the interface of microfibers may be one mechanism that can enable the synthetic hierarchically-structured materials to overcome the interfacial strength limitations of the macrofibers in the palmetto wood.

8.7 Prototype biologically-inspired hierarchically-structured polymer composite

In order to demonstrate the multi-scale mechanical benefits of the hierarchical structure in Palmetto wood, a prototype biologically-inspired hierarchically-structured polymer composite was created using the nano-enhanced polymers investigated in this dissertation. To create the hierarchically-structured polymer composite, pairs of 700 μm thick unidirectional (0 degree) carbon-fiber/epoxy composites from CST, Inc. (Tehachapi, CA) were bonded together in a hot-press using the extruded nano-enhanced polymers with 10 wt. % CNF and with 0 wt. % CNF (cross-sectional micrograph of the 0 wt. % CNF bond line can be seen in Figure 8.16). The resulting laminated structure formed a very thin bond line (~100-200 μm).

Mechanical properties of the hierarchically-structured polymer composite were characterized in the same three-point bend test use for the Palmetto wood at strain rates of approximately 3×10^{-4}/sec. In addition to the hierarchically-structured polymer composite, a single unidirectional composite layer was tested as well as two unidirectional composite layers that were bonded with the polymer without nano-enhancement and without any bonding. Results of the three-point bend tests seen in Figure 8.17 indicated that the hierarchical structure formed from the nano-enhanced polymer increases flexural strength of the laminated unidirectional and cross-ply composite structures by approximately 38% over the pure polymer, however the strength is still about 25% less than the single unidirectional layer. The stiffness of the bonded composites is also very similar

to the single unidirectional layer, indicating good shear load transfer across the interlaminar polymer nano-enhanced polymer. The maximum flexural energy density also changes from 11.75 mJ/mm^3 to 14.80 mJ/mm^3 for the polymer nano-enhanced polymer bonded specimen and 5.75 mJ/mm^3. So, the nano-enhanced polymer appears to increase the maximum flexural energy density of the laminated composite by approximately 25% over a single layer and approximately 150% over the pure polymer. Results for no bond line (i.e., two unidirectional carbon-fiber/epoxy layers on top of each other) are also shown for comparison in Figure 8.17.

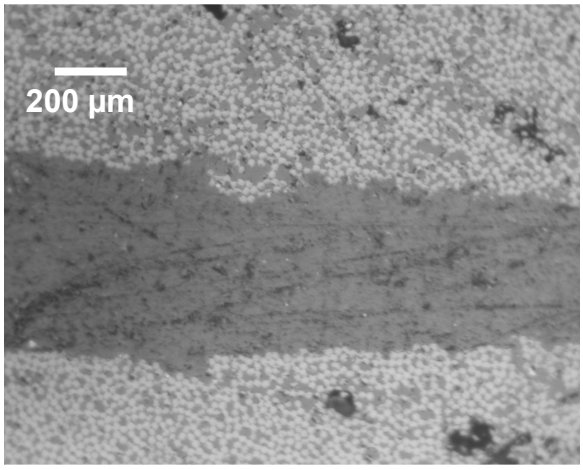

Figure 8.16. Optical micrograph of laminated unidirectional composite with 10 wt. % CNF bond line.

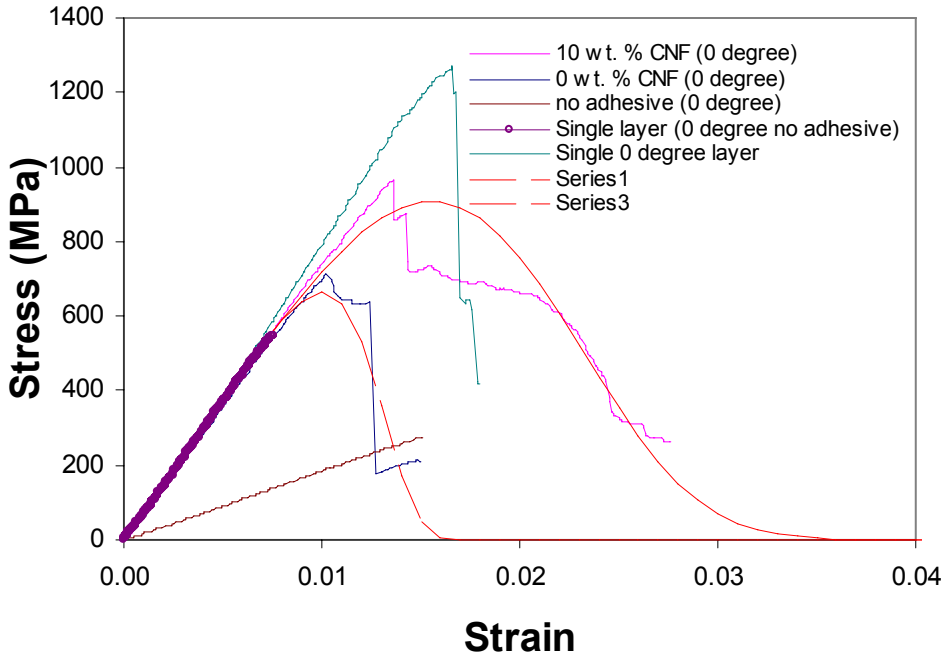

Figure 8.17. Three-point bend tests on laminated unidirectional (0 degree) and cross-ply carbon-fiber/epoxy composite structures bonded with 0 and 10 wt. % CNF polymer nano-enhanced polymers.

Partial delamination also occurred during testing of the specimens bonded using the polymer with and without the nano-enhancement. This can be seen in the data as a step drop in stress followed by a continued strain increase, and sometimes even an increase in stress. An example of this partial delamination on a sample of 10 wt. % CNF/LDPE laminate can be seen in Figure 8.18. However, it can also be seen in Figure 7.15 that the drop was more precipitous for the polymer without the nano-enhancement. Using Equation 8.2, the effects of the nano-enhancement could be quantified. The modulus was determined to be 75 GPa both with and without the nano-enhancement. However, the Weibull parameters for the polymer without nano-enhancement are 0.013 and 8 for ε_o and β respectively while the nano-enhancement increases ε_o to 0.022 and decrease β to 4. Thus, the hierarchical structure formed by the nano-enhanced

polymer appears to stabilize failure of the polymer composite in the same way that the hierarchical structure benefits the mechanical behavior of Palmetto wood. Therefore, these tests validate the benefits of using Palmetto wood as biological inspiration for creating synthetic hierarchically-structured polymer composites using the nano-enhanced polymers developed and characterized in this dissertation.

Figure 8.18. Laminated 10 wt. % specimen after 3-point bend testing. Note delamination on left. Image taken with a digital camera.

8.8 Summary

The hierarchical structure of palmetto wood has now been characterized at multiple length scales for the first time. The macroscale mechanical behavior of palmetto wood was also characterized at multiple length scales using the multi-scale characterization approach, and a multi-scale structure-property model was developed similar to the one used for the synthetic hierarchically-structured nano-enhanced polymers. Thus, it was possible to establish a connection between biological and synthetic hierarchically-structured materials. Furthermore, using the structure of the palmetto wood and the multi-scale models describing its mechanical behavior, it was possible to fabricate a prototype biologically-inspired hierarchically-structured polymer composite in order to demonstrate enhanced resistance to mechanical failure.

Chapter 9 Scientific and technical contributions and future work

9.1 Scientific and technical contributions

There have been many significant scientific and technical contributions made in this dissertation that have elucidated on the processing-structure-property relationships of hierarchically-structured polymer composites that will enable them to be tailored for multifunctional structures. The main contribution was the ability to draw connections from a multi-scale biological system – palmetto wood – that enabled the development of a biologically inspired synthetic material based on the linear ROM model that applies to all of the synthetic and natural systems that were studied. Specific details of further contributions will now be discussed.

9.1.1 Characterization of combinatorially-processed nano-enhanced polymers for hierarchically-structured polymer composites

There were two specific contributions made in this dissertation that help to characterize nano-enhanced polymers that are made through a combinatorial approach involving graded compositions of formulations produced using twin screw extrusion.

1. A method was developed using pycnometry to characterize the gradient architecture, which was validated by TGA measurements
2. A microtensile testing approach was developed to rapidly determine the variation of mechanical properties with composition from the gradient architecture

For the first, the pycnometry measurements were found to have reasonable accuracy but were much easier and faster to obtain than TGA. For the second, it was possible to quickly and easily establish the trends in the mechanical reinforcement due to CNFs using sub-scale ASTM standard specimens machined from the gradient architecture and then tested. The results were extrapolated to obtain an effective modulus of 15 GPa for the CNFs that were used to develop multi-scale models of mechanical properties in hierarchically-structured nano-enhanced polymers. Furthermore, this modulus is consistent with previous observations of reduced benefits from nanoscale reinforcement due to "spring-like" effects attributed to geometric imperfections in the reinforcement. The contributions of this work resulted in a journal paper that is to appear in *Journal of Composite Materials*.

9.1.2 Multi-scale characterization and modeling of hierarchically-structured polymer composites

There were many contributions made that have impacted the understanding of the structure-property relationship of hierarchically-structured polymer composites across different length scales.

1. New mechanical property models for hierarchically-structured materials were developed based on multi-scale characterization techniques
2. A method was developed for quantifying the "degree of dispersion" and "dispersion limit" for CNFs as a function of sonication time

during solvent processing which limits the development of the hierarchical structure

3. The enhancement of mechanical properties through the combination of microscale and nanoscale ingredients was characterized and modeled
4. The relative benefit of microscale reinforcement versus nanoscale reinforcement at different strain rates was characterized and modeled

The first contribution involved the use of a nanomechanical testing approach based on nanoindentation that enabled the individual moduli of microscale features in the hierarchical structure to be isolated from the nano-reinforced matrix system. From these measurements, it was possible to develop a multi-scale model that assumes load transfer across the microscale features and the nano-reinforced matrix system in a linear ROM formulation. This model enables the effective modulus of the nanofiber reinforcement to be obtained through extrapolation of the data previously obtained via the combinatorial approach. The resulting predictions obtained with this multi-scale model were validated using the microtensile measurements from the combinatorial approach. These results also were used to predict what the modulus would be for a perfectly dispersed nano-enhanced polymer, and determined to not be substantially different from that obtained with the hierarchically-structured nano-enhanced polymer.

The second contribution utilized the multi-scale model to develop a method for quantifying the “degree of dispersion” as a function of sonication time for solvent processed composites to be quantified and an associated time constant to be identified. Furthermore, it was determined that there was a “dispersion limit” of approximately 3 to 3.5 wt. % CNFs which limited the development of the hierarchical structure using solvent processing and was found to be similar to the thermoplastics even though lower shear forces and longer processing times are associated with it.

The third contribution involved the combination of a CMF mat with a nano-enhanced epoxy. Depending on the dispersion of CNFs in the nano-enhanced epoxy, different hierarchical structures were formed through the combination. At lower levels of dispersion, the CMF mat acted as a “filter” to trap CNF agglomerates that enhanced the properties at the interface of the CMF with the epoxy. However, if the degree of dispersion was increased too much or there were too many agglomerates, there was a reduction of this benefit or the mat would become “clogged”.

The final contribution was made through quasi-static and dynamic compression testing of hierarchically-structured polymer composites fabricated using a mixture of CMFs and CNFs. These results indicated that the effects of the nanoscale reinforcement were not as great as those of the microscale reinforcement for similar volume fractions. These effects were differentiated using a ROM model similar to the multi-scale model which represented the hierarchically-structured polymer composite as an interpenetrating-phase

composite consisting of the CMF-reinforced polymer and a CNF-reinforced polymer. The predicted behavior for the hierarchically-structured polymer composite matched the experimental measurements at both high and low strain rates. Furthermore, it was possible to isolate the strain-rate effects on the polymer from that obtained by the additions of the CMF and CNF reinforcement. A journal paper is currently being completed on all three contributions.

9.1.3 Control of multifunctional properties through thermal processing

There were two processing-related contributions made to the control of multifunctional properties in hierarchically-structured polymer composites fabricated from thermoplastics.

1. A model of effects of thermal processing on the change in electrical conductivity due to viscoplastic relaxation of alignment in the nanostructure of the composite was developed
2. The effect of the structural relaxation on mechanical properties was characterized using the microtensile testing approach

For the first, the model was able to identify changes in the energy associated with the structural relaxation mechanism when CNFs or CNTs are used. For the second, the level of reduction in the tensile mechanical properties due to a decrease in anisotropy from a more random orientation of the fibers was identified. This reduction was found to produce about half of the benefit that was derived from having oriented fibers. Furthermore, this reduction could also be

identified at the nanoscale via nanoindentation measurements. This work was published in the journal *Polymer*.

9.1.4 Curing characterization of nano-enhanced adhesives with microfiber reinforcement

Two contributions were made to the fundamental mechanical characterization of hierarchically-structured polymer composites by adding CNTs to microfiber-reinforced thermoset polymers (i.e., nano-enhanced adhesives).

1. The effects of CNTs on the development of adhesion associated with the kinetics of epoxy curing were characterized and modeled
2. A new adhesion mechanism responsible for the increase in strength and stiffness due to the "Velcro-like" interaction of CNTs with microscale reinforcement was identified and quantified
3. The effects of the CNT reinforcement on the evolution of mechanical properties in the epoxy during curing were distinguished from the new adhesion mechanism through nanomechanical characterization

The first contribution was obtained through direct evidence from macroscale DMA that the curing behavior of the polymer matrix was being impacted by the presence of the CNTs through changes in the glass transition temperature and to apply the curing kinetics model to explain this effect. From these results, it was possible to modify a model of the kinetics of curing effects to account for the development of adhesion between the polymer matrix and the reinforcement which resulted in an increase in the time constant and exponent associated with

the evolution of the thermal and mechanical properties. The second contribution was made through microtensile measurements and micrographs of the composite which indicated increases in the strength and stiffness of the composite due to enhanced load transfer between the polymer matrix and microfiber reinforcement due to a “Velcro-like” adhesion mechanism created by the interaction of the CNTs with the microfibers. The final contribution was able to distinguish the effects of the CNT reinforcement on the epoxy from the new adhesion mechanism through property mapping at the nanoscale. These results also indicated an increase in the “elastic” behavior of the epoxy that is similar to the percolation effects observed in nano-enhanced thermoplastics. A journal paper is currently being completed on these contributions.

9.1.5 Characterization and multi-scale modeling of mechanical properties for a natural hierarchically-structured composite

Another set of contributions were made through microstructural and mechanical characterization of palmetto wood, which is a natural hierarchically-structured composite that can serve as biological inspiration for tailoring the design of the hierarchically-structured polymer composites that were processed in this dissertation.

1. The hierarchical structure of palmetto wood has been characterized
2. The macroscale mechanical behavior of palmetto wood was characterized at multiple length scales and a multi-scale model was developed

3. The effects of macrofiber reinforcement on the mechanical behavior of palmetto wood has been determined to be strain rate independent
4. A prototype biologically-inspired hierarchically-structured polymer composite was fabricated and the benefits on mechanical behavior were characterized

The first contribution was made through optical microscopy, which indicated a graded distribution of macrofibers formed from microfibers and held together by a porous cellulose matrix. The second involved characterizing the macroscale mechanical behavior through three-point bend testing of palmetto wood at the macroscale, microtensile testing of a macrofiber, and then nanomechanical characterization of microfibers. It was then possible to develop a multi-scale model of the mechanical behavior using Rule-of-Mixtures formulations and probabilistic failure mechanisms, which indicated that the volume fraction of macrofibers only affected the stiffness of the palmetto wood. The third was to determine that the effects of macrofiber reinforcement on the macroscale mechanical behavior did not change with strain rate. Finally, the knowledge obtained from the Palmetto wood was used to create a prototype biologically-inspired hierarchically-structured polymer composite which exhibited a significant increase in resistance to failure and stability during failure. A journal paper is currently being completed on these contributions.

9.2 Future work

During the course of this line of research, some interesting issues have been uncovered that affect the development of hierarchically-structured nano-enhanced polymers which need further investigation. A list of these issues follows:

1. Characterize the mechanical properties of the extruded nano-enhanced polymers in both axial and transverse directions. This will provide a better understanding of the nanoscale filler alignment on the mechanical properties of the nano-enhanced polymers. To accomplish this task, it will be necessary to redesign the tensile specimens to further reduce the size scale or to develop a completely new test specimen geometry, such as a "+"-shaped specimen, that can be used in biaxial tension to determine the differences in the mechanical response in each direction that can be used to obtain information on the relative rather than absolute changes in properties.
2. Process and characterize the properties of hierarchically-structured composites using other fillers such as MWCNTs and SWNTs. In the present work, the composites were made using only one type of nanoscale filler to enhance properties. By studying multi-component and multi-scale systems with different nano-scale fillers, an understanding of how the aspect ratios and differing electrical

properties of these nanoscale fillers will affect changes in the resulting hierarchically-structured composites.

3. Process and characterize hierarchically-structured nano-enhanced composites with other polymer systems. Polymers, such as Nylon or ABS, are qualified for different applications. They may also offer better interfacial adhesion between the polymer matrix and the CNFs resulting in better mechanical properties.

4. Process and characterize composites of polymers with CNTs and/or CNFs functionalized both at the ends and the sidewalls. The end and sidewall functionalization can be utilized to cross-link the CNTs and/or CNFs with one another, thereby creating a continuous mesh-like structure. The functionalization can also be used to improve adhesion between the nanoscale filler and the polymer matrix. This could potentially result in ultra-strong nano-enhanced composites with impressive electrical and thermal conductivity.

5. Process and characterize hierarchically-structured laminated composites employing other polymer systems and micro- and nanoscale fillers. Using different micro- and nanoscale constituents, and looking to palmetto wood for inspiration, novel hierarchically-structured laminated composites can be created to take advantage of the information acquired in the characterization of the palmetto wood.

6. Nanoindentation approaches for hierarchically-structured polymer composites. Due to the inherent inhomogeneities present in hierarchically structured materials, nanoindentation presents a challenge. Determining a standard method to characterize these materials at the nanoscale will be a great help for future research endeavors.
7. Characterize hierarchically-structured nano-enhanced polymers at the nanoscale using smaller indenter tips, such as a 90° cube-corner tip which can have a tip radius under 40nm. These smaller radius tips allow for much higher resolution in imaging and property mapping since the plastic deformation is kept to a much smaller volume. This would enable property mapping of areas smaller than 10 μm.

References

[Abda07] M. Abdalla, D. Dean, D. Adibempe, E. Nyairo, P. Robinson, G. Thompson, 2007. “The effect of interfacial chemistry on molecular mobility and morphology of multiwalled carbon nanotubes epoxy nanocomposite,” *Polymer*, Vol. **48**, Iss. 19, pp. 5662-5670.

[Abou91] J. Aboudi. 1991. Mechanics of Composite Materials, Elsevier, Amsterdam.

[Ajay03] P.M. Ajayan, L.S. Schadler and P.V. Braun. 2003. Nanocomposite Science and Technology, Wiley-VCH: Weinheim.

[Alig07] I. Alig, D. Lellinger, S.M. Dudkin, P. Pötschke, 2007. “Conductivity spectroscopy on melt processed polypropylene–multiwalled carbon nanotube composites: Recovery after shear and crystallization,” *Polymer*, Vol. **48**, Iss. 4, pp. 1020-1029.

[Alla02] A. Allaoui, S. Bai, H.M. Cheng, J.B. Bai, 2002. “Mechanical and electrical properties of a MWNT/epoxy composite,” *Composites Science and Technology*, Vol. **62**, Iss. 15, pp. 1993-1998.

[Amis02] E.J. Amis, X.D. Xiang and J.C. Zhao, 2002. “Combinatorial materials science: What's new since Edison,” *MRS Bulletin*, Vol. **27**, pp. 295-297.

[Andr02] R. Andrews, D. Jacques, M. Minot, T. Rantell, 2002. “Fabrication of Carbon Multiwall Nanotube/Polymer Composites by Shear Mixing,” *Macromolecular Materials and Engineering*, Vol. **287**, pp. 395-403.

[Baer92] E. Baer, A. Hiltner, R. Morgan. 1992, “Biological and synthetic hierarchical composites,” *Physics Today*, Vol. **45**, pp. 60-67.

[Bala06] A.C. Balazs, T. Emrick and T.P. Russell, 2006. “Nanoparticle Polymer Composites: Where Two Small Worlds Meet,” *Science*, Vol. **314**. no. 5802, pp. 1107-1110.

[Barb02] R.L. Barbour, 2002. South Carolina’s Revolutionary War Battlefields, Pelican Publishing Company, Gretna, LA.

[Bart07] F. Barthelat, 2007. “Biomimetics for next generation materials,” *Philosophical Transactions of the Royal Society A*, Vol. **365**, pp. 2907–2919.

[Baug02] R.H. Baughman, A.A. Zakhidov, W.A. de Heer, 2002. “Carbon Nanotubes - the Route Toward Applications,” *Science*, Vol. **297**, No. 5582, pp. 787-792.

[Beno01] J-M. Benoit, B. Corraze, S. Lefrant, W.J. Blau, P. Bernier, O. Chauvet, 2001. “Transport properties of PMMA-Carbon Nanotubes composites,” *Synthetic Metals*, Vol. **121**, pp. 1215-1216.

[Berv05] M. Bervas, 2005. “Engineered nanocomposites as high-energy density positve electrode materials for rechargeable lithium batteries,” Dissertation (Ph. D.) - Rutgers University, 2005.

[Bier02] M.J. Biercuk, M.C. Llaguno, M. Radosavljevic, J.K. Hyun, A.T. Johnson, and J.E. Fischer, “Carbon nanotube composites for thermal management*,” Applied Physics Letters*, Vol. **80**, pp. 2767-2769.

[Boko07] L. Bokobza, “Multiwall carbon nanotube elastomeric composites: A review,” *Polymer*, Vol. **48**, pp. 4907-4920 (2007).

[Breu04] O. Breuer and U. Sundararaj, 2004. “Big returns from small fibers: A review of polymer/carbon nanotube composites,” *Polymer Composites*, Vol. **25**, pp. 630-645.

[Bruc02a] H.A. Bruck, J.J. Evans and M.L. Peterson, 2002. “The Role of Mechanics in Biological and Biologically Inspired Materials,” *Experimental Mechanics*, Vol. **42**; Part 4, pp. 361-371.

[Bruc02b] H.A. Bruck, D. Casem, R.L. Williamson and J.S. Epstein, 2002. “Characterization of short duration stress pulses generated by impacting laminated carbon-fiber/epoxy composites with magnetic flyer plates,” *Experimental Mechanics*, Vol. **42**, Iss. 3, pp. 279-287.

[Carl03] L.A. Carlsson, D.F. Adams, R.B. Pipes, 2003. Experimental Characterization of Advanced Composite Materials. CRC Press.

[Cipr08] B.H. Cipriano, A.K. Kota, A.L. Gershon, C.J. Laskowski, T. Kashiwagi, H.A. Bruck, S.R. Raghavan, 2008. “Conductivity Enhancement of Carbon Nanotube and Nanofiber-based Polymer Nanocomposites by Melt Annealing”, *Polymer*, Vol. **49**, Iss. 22, pp. 4846-4851.

[Cole06] J.N. Coleman, U. Khan and Y.K. Gun'ko, 2006. “Mechanical reinforcement of polymers using carbon nanotubes,” *Advanced Materials*, Vol. **18**, pp. 689-706.

[Cost05] M.L. Costa, S.F.M. de Almeida, M.C. Rezende, 2006. “Hygrothermal effects on dynamic mechanical analysis and fracture behavior of polymeric composites,” *Materials Research*, Vol. **8**, No. 3, pp. 335-340.

[Dalm05] F.Dalmas, L. Chazeau, C. Gauthier, K. Masenelli-Varlot, R. Dendievel, J.Y. Cavaille, L. Forro, 2006. “Multiwalled carbon nanotube/polymer nanocomposites: Processing and properties,” *Journal of Polymer Science Part B: Polymer Physics*, Vol. **43**, Iss. 10, pp. 1186-1197.

[Dalt03] A.B. Dalton, S. Collins, E. Munoz, J.M. Razal, V.H. Ebron, J.P. Ferraris, J.N. Coleman, B.G. Kim, R.H. Baughman, 2006. “Super-tough carbon-nanotube fibres,” *Nature*, Vol. **423**, pp. 703.

[Davi99] M.E. Davis, 1999. “Combinatorial Methods: How will they Integrate into Chemical Engineering,” *AICHE Journal*, Vol. **45**, pp. 2270-2272.

[Dela99] M.L. De la Chapelle, C. Stéphan, T.P. Nguyen, S. Lefrant, C. Journet, P. Bernier, E. Munoz, A. Benito, W.K. Maser, M.T. Martinez, G.F. De la Fuente, T. Guillard, G. Flamant, L. Alvarez, D. Laplaze, 1999. “Raman characterization of singlewalled carbon nanotubes and PMMA-nanotubes composites,” *Synthetic Metals*, Vol. **103**, pp. 2510-2512.

[Du03] F.M. Du, J.E. Fischer, K.I. Winey, 2003. “Coagulation method for preparing single-walled carbon nanotube/poly(methyl methacrylate) composites and their modulus, electrical conductivity, and thermal stability,” *Journal of Polymer Science B: Polymer Physics*, Vol. **41**, pp .3333-3338.

[Du04] F.M. Du, R.C. Scogna, W. Zhou, S. Brand, J.E. Fischer, K.I. Winey, 2004. “Nanotube Networks in Polymer Nanocomposites: Rheology and Electrical Conductivity,” *Macromolecules*, Vol **37**, Iss. 24, pp. 9048-9055.

[Du05] F.M. Du, J.E. Fischer, K.I. Winey, 2005. “Effect of nanotube alignment on percolation conductivity in carbon nanotube/polymer composites,” *Physical Review B*, Vol **72**, Iss. 12, 121404, 4 pp.

[Eide04] N. Eidelman and C.G. Simon Jr. 2004. “Characterization of combinatorial polymer blend composition gradients by FTIR microspectroscopy,” *Journal of Research of the National Institute of Standards and Technology*, Vol. **109**, pp. 219-231.

[Engs00] J.R. Engstrom and W.H. Weinberg, 2000. “Combinatorial Materials Science: Paradigm Shift in Materials Discovery and Optimization,” *AICHE Journal*, Vol. **46**, pp. 2-5.

[Esaw07] A.M.K. Esawi, M.M. Farag, 2007. “Carbon nanotube reinforced composites: Potential and current challenges,” *Materials & Design*, Vol. **28**, Iss. 9, pp. 2394-2401.

[Ferg98] D.W. Ferguson, E.W.S. Bryant, H.C. Fowler, 1998. “ESD Thermoplastic Product Offers Advantages for Demanding Electronics Applications,” *Proceedings of SPE ANTEC*, p. 1219 (1998).

[Gall04] F.M. Gallant, H.A. Bruck, A.K. Kota, 2004. “Fabrication of particle-reinforced polymers with continuous gradient architectures using twin screw extrusion process,” *Journal of Composite Materials*, Vol. **38**, Iss. **21**, pp. 1873-1893.

[Gall06] F.M. Gallant, H.A. Bruck, S.E. Prickett, M. Cesarec, 2006. “Graded polymer composites using twin-screw extrusion: a combinatorial approach to developing new energetic materials,” *Composites A*, Vol. **37**, pp. 957-969.

[Gilm03] J.W. Gilman, S. Bourbigot, J.R. Shields, M. Nyden, T. Kashiwagi, R.D. Davis, D.L. Vanderhart, W. Demory, C.A. Wilkie, A.B. Morgan, J. Harris, R.E. Lyon, 2003. “High Throughput Methods for Nanocomposite Materials Research: Extrusion: NMR Characterization and Flammability Property Screening,” *Journal of Materials Science*, Vol. **38**, pp. 4451-4460.

[Gilm04] J.W. Gilman, P.H. Maupin, R.H. Harris Jr., S. Bellayer, A.J. Bur, S.C. Roth, M. Murariu, A.B. Morgan, J.D. Harris, 2004. “High Throughput Methods for Nanocomposite Materials Research: Extrusion and Visible Optical Probes,” *Polymeric Materials: Science and Engineering*, Vol. **90**, pp. 717-718.

[Gojn04] F.H. Gojny, M.H.G. Wichmann, U. Kopke, B. Fiedler, K. Schulte, 2004. “Carbon nanotube-reinforced epoxy-composites: enhanced stiffness and fracture toughness at low nanotube content,” *Composites Science and Technology*, Vol. **64**, Iss. 15, pp. 2363-2371.

[Gojn05] F.H. Gojny, M.H.G. Wichmann, U. Kopke, B. Fiedler, K. Schulte, 2005. “Influence of different carbon nanotubes on the mechanical properties of epoxy matrix composites - A comparative study,”

Composites Science and Technology, Vol. **65**, Iss. 15-16, *20th Anniversary Special Issue*, pp. 2300-2313.

[Gojn06] F.H. Gojny, M.H.G. Wichmann, B. Fiedler, I.A. Kinloch, W. Bauhofer, A.H. Windle, K. Schulte, 2006. "Evaluation and identification of electrical and thermal conduction mechanisms in carbon nanotube/epoxy composites," *Polymer*, Vol. **47**, Iss. 6, pp. 2036-2045.

[Gree99] D.W. Green, J.E. Winandy, and D.E. Kretschmann, 1999. "Mechanical Properties of Wood", Wood Handbook – Wood as an Engineering Material, Forest Products Laboratory, USDA, Madison WI.

[Hodg00] J.M. Hodgkinson (Editor). 2000. Mechanical Testing of Advanced Fibre Composites. CRC Press, Woodhead Publishing, Ltd.

[Hysi_a] Hysitron, Inc. TriboIndenter® Users Manual. NRL-M-021 v1.0. 10025 Valley View Road, Minneapolis, MN 55344.

[Hysi_b] Hysitron, Inc. Modulus Mapping Users Manual. NRL-M-011 v3.0. 10025 Valley View Road, Minneapolis, MN 55344.

[Hysi_c] Hysitron, Inc. nanoDMA® Users Manual. NRL-M-013 v3.0. 10025 Valley View Road, Minneapolis, MN 55344.

[Jin04] H. Jin, 2004. "New Metrological Techniques for Mechanical Characterization at the Microscale and Nanoscale," Ph.D. dissertation, University of Maryland, College Park, MD.

[Jone98] R.F. Jones, M.R. Jones, D.V. Rosato. 1998. Guide to Short Fiber Reinforced Plastics. Hanser Gardner Publications.

[Kash02] T. Kashiwagi, E. Grulke, J. Hilding, R. Harris, W. Awad, J. Douglas, 2002. "Thermal Degradation and Flammability Properties of Polypropylene-Carbon Nanotube Composites," *Macromolecular Rapid Communications* Vol. **23**, pp. 761-765.

[Kepp08] K.L. Kepple, G.P. Sanborn, P.A. Lacasse, K.M. Gruenberg, W.J. Ready, 2008. "Improved fracture toughness of carbon fiber composite functionalized with multi walled carbon nanotubes," *Carbon*, Vol. **46**, Iss. 15, pp. 2026-2033.

[Khar04] S.B. Kharchenko, J.F. Douglas, J. Obrzut, E.A. Grulke, K.B. Migler, 2004. "Flow-induced properties of nanotube-filled polymer materials," *Nature Materials*, Vol. **3**, pp. 564-568.

[Kim03] J. Kim, P.K. Liaw, H. Wang. January 2003. "The NDE Analysis of Tension Behavior in Nicalon/SiC Ceramic Matrix Composites," *JOM-e: A Web-Only Supplement to JOM*.

[Kota07a] A.K. Kota, B.H. Cipriano, A.L. Gershon, M. Duesterberg, D. Powell, S.R. Raghavan and H.A. Bruck, 2007. "Electrical and Rheological Percolation in Polystyrene/MWCNT composites," *Macromolecules*, Vol. **40**, pp. 7400-7406.

[Kota07b] A.K. Kota, B.H. Cipriano, M. Duesterberg, D. Powell, S.R. Raghavan and H.A. Bruck, 2007. "Formation of an Interpenetrating Phase Composite by Percolation of Multi-Walled Carbon Nanotubes (MWCNTs) in Polystyrene Characterized Using Rheological Properties and Electrical Conductivity," submitted to *Nature Materials*.

[Kota07c] A, Kota, B.H. Cipriano, M. Duesterberg, D, Powell, S.R. Raghavan, and H.A. Bruck, 2007. "Quantitative Characterization of the Formation of an Interpenetrating Phase Composite in Polystyrene from the Percolation of Multiwalled Carbon Nanotubes," *Nanotechnology*, Vol. **18**, 505705, 7 pp.

[Kota07d] A.K. Kota, 2007. "Processing - Structure - Microstructure - Property Relationships in Polymer Nanocomposites," Ph.D. dissertation, University of Maryland, College Park, MD.

[Kota08a] A.K. Kota, L. Murphy, T. Strohmer, D.I. Bigio, H.A. Bruck, and D. Powell, 2008. "Combinatorial Development of Polymer Nanocomposites using Transient Processing Conditions in Twin Screw Extrusion", *AICHE Journal*, Vol. **54**, pp. 1895-1900.

[Kota08b] A.K. Kota, R. Kerzner, D.I. Bigio**,** H.A. Bruck, and D. Powell, 2008. "Characterization of Processing Effects in HIPS-CNF composites using Thermogravimetric Analysis", *Polymer Engineering and Science*, Vol. **48**, pp. 1120-1125.

[Kuba06] R.M. Kubacki. 2006. "Molecularly Engineered Variable Dielectric Nanocomposites to Embed Precision Capacitors On-Chip," Proceedings of the 56th Electronic Components and Technology Conference, pp. 161-166.

[Kuma02] S. Kumar, H. Doshi, M. Srinivasarao, J. O. Park, D.A. Schiraldi, "Fibers from polypropylene/nano carbon fiber composites," *Polymer*, Vol. **43**, pp. 1701-1703.

[Lee05] S. Lee. 2005. Encyclopedia of Chemical Processing. CRC Press.

[Loza01] K. Lozano, J. Bonilla-Rios, E.V. Barrera, 2001. "A study on nanofiber-reinforced thermoplastic composites (II): Investigation of the mixing rheology and conduction properties," *Journal of Applied Polymer Science*, Vol. **80**, Iss. 8, pp. 1162-1172.

[Mahf06] H. Mahfuz, A. Adnan, V.K. Rangari, M.M. Hasan, S. Jeelani, W.J. Wright, S.J. DeTeresa, 2006. "Enhancement of strength and stiffness of Nylon 6 filaments through carbon nanotubes reinforcement," *Applied Physics Letters*, Vol. **88**, p. 083119.

[Mall97] P.K. Mallick, 1997. Composites Engineering Handbook. Marcel Dekker, Inc., New York, NY.

[Maso97] J.J. Mason, 1997. "On the Application of Dynamic Fracture Mechanics to Continuous Fiber Reinforced Composite Materials," *Annual Report to the Office of Naval Research, 27 May 1997.*

[Masu06] H. Masuda, K. Higashitani, H. Yoshida. 2006. Powder technology handbook. CRC Press.

[McNa05] T. McNally, P. Pötschke, P. Halley, M. Murphy, D. Martin, S.E.J. Bell, G.P. Brennan, D. Bein, P. Lemoine, J.P. Quinn, 2006. "Polyethylene multiwalled carbon nanotube composites," *Polymer*. Vol. **46**, Iss. 19, pp. 8222-8232.

[Meye06] M.A. Meyers, A.Y.M. Lin, Y. Seki, P.Y. Chen, B.K. Kad, S. Bodde, 2006. "Structural Biological Composites: An Overview," *JOM Journal of the Minerals, Metals and Materials Society*. Vol. **58**, no. 7, pp. 35-41.

[Moni06] M. Moniruzzaman, K.I. Winey, 2006. "Polymer nanocomposites containing carbon nanotubes," *Macromolecules*. Vol. **39**, pp. 5194-5205.

[Nyde02] M. Nyden, J.W. Gilman, R Davis, J.R. Shields, "High-throughput Methods for Flammability Screening of Multicomponent Polymer Blends and Nanocomposites," *SAMPE* at Long Beach, CA. May 12 - 16, 2002, pp. 738-749.

[Olso97] G.B. Olson, 1997. "Computational Design of Hierarchically-structured Materials", *Science*, Vol. **277**, pp. 1237-1242.

[Pöts03] P. Pötschke, S. Dudkin, I. Alig, 2003. “Dielectric spectroscopy on melt processed polycarbonate-multiwalled carbon nanotube composites,” *Polymer*, Vol. **44**, Iss. 26, pp. 5023-5030.

[Pöts04] P. Pötschke, M. Abdel-Goad, I. Alig, S. Dudkin, D. Lellinger, 2004. “Rheological and dielectrical characterization of melt mixed polycarbonate-multiwalled carbon nanotube composites,” *Polymer*, Vol. **45**, Iss. 26, pp. 8863-8870.

[Pott97] K. Potter, 1997. Resin Transfer Moulding. Chapman & Hall, London, UK.

[Poty03] R.A. Potyrailo, R.J. Wroczynski, J.E. Pickett, M. Rubinsztajn, 2003. “High-Throughput Fabrication, Performance Testing, and Characterization of One-Dimensional Libraries of Polymeric Compositions,” *Macromolecular Rapid Communications*, Vol. **24**, pp. 123-130.

[Poty05] R.A. Potyrailo and I. Takeuchi, 2005. “Role of High-throughput Characterization Tools in Combinatorial Materials Science,” *Measurement Science and Technology*, Vol. **16**, pp. 1-4.

[Qian00] D. Qian, E.C. Dickey, R. Andrews, T. Rantell, 2000. “Load transfer and deformation mechanisms in carbon nanotube-polystyrene composites,” *Applied Physics Letters*, Vol. **76**, pp. 2868-2870.

[Rama03] R. Ramasubramaniam, J. Chen, H. Liu, 2003. “Homogeneous carbon nanotube/polymer composites for electrical applications,” *Applied Physics Letters*, Vol. **83**, Iss. 14, pp. 2928-2930.

[Safa02] B. Safadi, R. Andrews, E.A. Grulke, 2002. “Multiwalled carbon nanotube polymer composites: Synthesis and characterization of thin films,” *Journal of Applied Polymer Science*, Vol. **84**, pp. 2660-2669.

[Sand99] J. Sandler, M.S.P. Shaffer, T. Prasse, W. Bauhofer, K. Schulte, A.H. Windle, 1999. “Development of a dispersion process for carbon nanotubes in an epoxy matrix and the resulting electrical properties,” *Polymer*, Vol. **40**, Iss. 21, pp. 5967-5971.

[Sand03a] J.K.W. Sandler, A.H. Windle, P. Werner, V. Altstadt, M.V. Es, M.S.P. Shaffer, 2003. “Carbon-nanofibre-reinforced poly(ether ether ketone) fibres,” *Journal of Materials Science*, Vol. **38**, pp. 2135-2141.

[Sand03b] J.K.W. Sandler, J.E. Kirk, I.A. Kinloch, M.S.P. Shaffer, A.H. Windle, 2007. “Ultra-low electrical percolation threshold in carbon-nanotube-epoxy composites,” *Polymer*, Vol. **44**, Iss. 19, pp. 5893-5899.

[Sari95] M. Sarikaya and I.A. Aksay, (editors), 1995. Biomimetics, design and processing of materials, polymers and complex materials. American Institute of Physics, Woodbury, NY.

[Seyh07] A.T. Seyhan, F.H. Gojny, M. Tanoglu, K. Schulte, 2007. “Critical aspects related to processing of carbon nanotube/unsaturated thermoset polyester nanocomposites,” *European Polymer Journal*, Vol. **43**, Iss. 2, pp. 374-379.

[Senn03] M. Sennett, E. Welsh, J.B. Wright, W.Z. Li, J.G. Wen, Z.F. Ren, 2003. “Dispersion and alignment of carbon nanotubes in polycarbonate", *Applied Physics A - Materials Science and Processing*, Vol. **76**, pp. 111-113.

[Shaf99] M.S.P. Shaffer, A.H. Windle, 1999. “Fabrication and Characterization of Carbon Nanotube/Poly(vinyl alcohol) Composites,” *Advanced Materials*, Vol. **11**, pp. 937-941.

[Sier01] R.L. Sierakowski and S.K. Chaturvedi, 2001. Dynamic Loading and Characterization of Fiber-Reinforced Composites. Wiley-Interscience.

[Smit04] J.G. Smith Jr, J.W. Connell, D.M. Delozier, P.T. Lillehei, K.A. Watson, Y.Lin, B.Zhou, Y.P. Sun, 2004. “Space durable polymer/carbon nanotube films for electrostatic charge mitigation,” *Polymer*, Vol. **45**, Iss. 3, pp. 825-836.

[Sout09a] Southwest Nanotechnologies, Inc. 27 March 2009. <http://www.swnano.com/tech/sg.php>.

[Sout09b] Southwest Nanotechnologies, Inc. 27 March 2009. <http://www.swnano.com/tech/docs/Final_SG_65_Data_Sheet.pdf>.

[Srin91] A.V. Srinivasan, G.K. Haritos, F.L. Hedberg, 1991. “Biomimetics: Advancing Man-Made Materials Through Guidance from Nature,” *Applied Mechanics Review*, Vol. **44**, pp. 463.

[Stép02] C. Stéphan, T.P. Nguyen, B. Lahr, W. Blau, S. Lefrant, O. Chauvet, 2002. “Raman spectroscopy and conductivity measurements on polymer-multiwalled carbon nanotubes composites,” *Journal of Materials Research*, Vol. **17**, No. 2, pp. 396-400.

[Thom04] J. Thomas and M. Qidwai, 2004. “Mechanical design and performance of composite multifunctional materials,” *Acta Materialia*. Vol. **52**, pp. 2155-2164.

[Thom06] J. Thomas, *et al.*, 2006 “Multifunctional structure-plus-power concepts,” *43rd AIAA/ASME/ASCE/AHS/ASC Structures, Structural Dynamics, and Materials Conference*, April 22-25, Denver, CO.

[Veed06] V.P. Veedu, C. Cao, X. Li, K. Ma, C. Soldano, K. Swastik, P.M. Ajayan, M.N. Ghasemi-Nejhad. 2006. “Multifunctional composites using reinforced laminae with carbon-nanotube forests,” *Nature Materials.* Vol. **5**, Iss. 6, pp. 452-462.

[Vinc91] J.F.V. Vincent. 1991. Structural Biomaterials. Princeton University Press, Princeton, NJ.

[Watt01] P.C.P. Watts, W.K. Hsu, G.Z. Chen, D.J. Fray, H.W. Kroto, D.R.M. Walton, 2001. “A low resistance boron-doped carbon nanotube–polystyrene composite,” *Journal of Materials Chemistry*, Vol. **11**, pp. 2482-2488.

[Whit93] J.M. Whitney, I.M. Daniel, R.B. Pipes. 1993. Experimental Mechanics of Fiber Reinforced Composite Materials. Society for Experimental Stress Analysis; Rev. Sub. Edition.

[Xian95] X.D. Xiang, X.D. Sun, G. Briceno, Y.L. Lou, K.A. Wang, H.Y. Chang, W.G. Wallace-Freedman, S.W. Chen and P.G. Schultz, 1995. “A Combinatorial Approach to Materials Discovery,” *Science*, Vol. **268**, pp. 1738-1740.

[Yang04] Y.L. Yang, M.C. Gupta, K.L. Dudley, R.W. Lawrence, 2004. “The fabrication and electrical properties of carbon nanofiber-polystyrene composites,” *Nanotechnology*, Vol. **15**, pp. 1545-1548.

[Zhan06] B. Zhang, R.W. Fu, M.Q. Zhang, X.M. Dong, L.C. Wang, C.U. Pittman, 2006. “Gas sensitive vapor grown carbon nanofiber/polystyrene sensors,” *Materials Research Bulletin*, Vol. **41**, pp. 553-562.

[Zhou01] Y.X. Zhou, D. Z. Jiang, and Y.M. Xiz, “Tensile Mechanical Behavior of T300 and M40J Fiber Bundles at Different Strain Rates”, *Journal of Materials Science*, 36, 919-922, (2001)

[Zhou07] Y. Zhou, F. Pervin, L. Lewis, S. Jeelani, 2007, “Experimental study on the thermal and mechanical properties of multi-walled carbon

nanotube-reinforced epoxy," *Materials Science and Engineering: A*, Vols. **452-453**, pp. 657-664.

[Zhou08] Y. Zhou, F. Pervin, L. Lewis, S. Jeelani, 2008 "Fabrication and characterization of carbon/epoxy composites mixed with multi-walled carbon nanotubes," *Materials Science and Engineering: A*, Vol. **475**, Iss. 1-2, pp. 157-165.

[Zhon04] D. Zhong, K.H. Kim, I.W. Park, T. Dennin, B. Mishra, E. Levashov and J.J. Moore. 2004. "Nanocomposite Coating Systems Tailored for Specific Engineering Applications," in *Nanostructured Thin Films and Nanodispersion Strengthened Coatings*, Vol. **155**, pp. 91-102.